AFRL-RX-TY-TR-2008-4540

RESISTANCE OF MEMBRANE RETROFIT CONCRETE MASONRY WALLS TO LATERAL PRESSURE

Lee Moradi

University of Alabama at Birmingham
1075 13th Street South
Birmingham, AL 35294

APRIL 2008

Final Report for 3 September 2002 – 30 July 2007

AIRBASE TECHNOLOGIES DIVISION
MATERIALS AND MANUFACTURING DIRECTORATE
AIR FORCE RESEARCH LABORATORY
AIR FORCE MATERIEL COMMAND
139 BARNES DRIVE, SUITE 2
TYNDALL AIR FORCE BASE, FL 32403-5323

NOTICE AND SIGNATURE PAGE

Using Government drawings, specifications, or other data included in this document for any purpose other than Government procurement does not in any way obligate the U.S. Government. The fact that the Government formulated or supplied the drawings, specifications, or other data does not license the holder or any other person or corporation; or convey any rights or permission to manufacture, use, or sell any patented invention that may relate to them.

This report was cleared for public release by the Air Force Research Laboratory, Materials and Manufacturing Directorate, Airbase Technologies Division, Public Affairs and is available to the general public, including foreign nationals. Copies may be obtained from the Defense Technical Information Center (DTIC) (http://www.dtic.mil).

REPORT NUMBER AFRL-RX-TY-TR-2008-4540 HAS BEEN REVIEWED AND IS APPROVED FOR PUBLICATION IN ACCORDANCE WITH ASSIGNED DISTRIBUTION STATEMENT.

//signature//
ROBERT J. DINAN, Ph.D
Work Unit Manager

//signature//
JEREMY R. GILBERTSON, Major, USAF
Chief, Force Protection Branch

//signature//
ALBERT N. RHODES, Ph.D.
Acting Chief, Airbase Technologies Division

This report is published in the interest of scientific and technical information exchange, and its publication does not constitute the Government's approval or disapproval of its ideas or findings.

REPORT DOCUMENTATION PAGE

Form Approved
OMB No. 0704-0188

PLEASE DO NOT RETURN YOUR FORM TO THE ABOVE ADDRESS.

1. REPORT DATE *(DD-MM-YYYY)*	2. REPORT TYPE	3. DATES COVERED *(From - To)*
31-JUL-2007	Final Technical Report	03-SEP-2002 -- 30-JUL-2007

4. TITLE AND SUBTITLE

Resistance of Membrane Retrofit Concrete Masonry Walls to Lateral Pressure

5a. CONTRACT NUMBER

F08637-02-C-7027

5b. GRANT NUMBER

5c. PROGRAM ELEMENT NUMBER

62102F

6. AUTHOR(S)

Moradi, Lee

5d. PROJECT NUMBER

4915

5e. TASK NUMBER

F2

5f. WORK UNIT NUMBER

4914F24B

7. PERFORMING ORGANIZATION NAME(S) AND ADDRESS(ES)

University of Alabama at Birmingham
1075 13th Street South
Birmingham, AL 35294

8. PERFORMING ORGANIZATION REPORT NUMBER

9. SPONSORING/MONITORING AGENCY NAME(S) AND ADDRESS(ES)

Air Force Research Laboratory
Materials and Manufacturing Directorate
139 Barnes Drive, Suite 2
Tyndall Air Force Base, FL 32403-5323

10. SPONSOR/MONITOR'S ACRONYM(S)

AFRL/RXQF

11. SPONSOR/MONITOR'S REPORT NUMBER(S)

AFRL-RX-TY-TR-2008-4540

12. DISTRIBUTION/AVAILABILITY STATEMENT

Distribution Statement A: Approved for public release; distribution unlimited.

13. SUPPLEMENTARY NOTES

Ref AFRL/RXQ Public Affairs Case # 08-115. Document contains color images.

14. ABSTRACT

Mitigation techniques are currently being sought to ensure public safety in the event of intentional or accidental explosions. Building material fragmentation is a major cause of human injury during such events. Use of concrete masonry walls is a common method of building construction. Concrete masonry provides a fast inexpensive way to construct buildings of various heights; however, these walls are extremely vulnerable to blast pressure resulting in collapse, fragmentation and severe injury to occupants. Much research has been conducted using actual blast tests as well as computational methods to study the behavior of masonry walls. Blast tests examined masonry walls of various shapes and make up, as well as the use of retrofit materials to mitigate the blast damage to masonry. In the computational arena, research made use of Livermore Software - DYNamics (LS-DYNA) finite element software to simulate full-scale models of concrete masonry walls. The results were compared to the actual blast tests, but the cost of high fidelity computational models made them impractical for day-to-day design. Design tools developed by other investigators in the field have been available for the past few years; however, their accuracy remains questionable when compared to actual blast test data. The research presented in this dissertation developed resistance functions for three different scenarios of membrane retrofit unreinforced concrete masonry walls to lateral pressure. These functions were further coupled with single degree of freedom systems to predict wall response to blast loads. The analysis results were compared to field blast tests for verification. This research gives the structural engineer a practical software tool for the design of membrane retrofit masonry walls to resist lateral pressures such as wind, and various blast charges and distances.

15. SUBJECT TERMS

concrete, formwork walls, polymer, finite element, dynamic response

16. SECURITY CLASSIFICATION OF:			17. LIMITATION OF ABSTRACT	18. NUMBER OF PAGES	19a. NAME OF RESPONSIBLE PERSON
a. REPORT	b. ABSTRACT	c. THIS PAGE			Robert Dinan
U	U	U	UU	163	19b. TELEPHONE NUMBER *(Include area code)*

Reset

Standard Form 298 (Rev. 8/98)
Prescribed by ANSI Std. Z39.18

RESISTANCE OF MEMBRANE RETROFIT CONCRETE MASONRY WALLS TO LATERAL PRESSURE

James S. Davidson and Lee G. Moradi
University of Alabama at Birmingham
1075 13th Street South
Birmingham, AL 35294

A technical report submitted to:
Airbase Technologies Division
Materials And Manufacturing Directorate
Air Force Research Laboratory
Air Force Materiel Command
Tyndall Air Force Base, Fl 32403-5323
Technical POC: Dr. Robert J. Dinan

December 2007

ABSTRACT

Mitigation techniques are currently being sought to ensure public safety in the event of intentional or accidental explosions. Building material fragmentation is a major cause of human injury during such events. One of the most common methods of construction in buildings is the use of concrete masonry walls. Concrete masonry provides a fast inexpensive way to construct buildings of various heights; however, these walls are extremely vulnerable to blast pressure resulting in collapse, fragmentation, and severe injury to occupants.

Much research has been conducted using actual blast tests as well as computational methods to study the behavior of masonry walls. Blast tests examined masonry walls of various shapes and make up, as well as the use of retrofit materials to mitigate the blast damage to masonry.

In the computational arena, research made use of Livermore Software – DYNAmics (LS-DYNA) finite element software to simulate full-scale models of concrete masonry walls. The results were compared to the actual blast tests, but the cost of high fidelity computational models made them impractical for day-to-day design. Design tools developed by other investigators in the field have been available for the past few years; however, their accuracy remains questionable when compared to actual blast test data.

The research presented in this report developed resistance functions for three different scenarios of membrane retrofit unreinforced concrete masonry walls to lateral pressure. These functions were further coupled with single degree of freedom systems to

predict the wall response to blast loads. The analysis results were compared to field blast tests for verification.

This research gives the structural engineer a practical software tool for the design of membrane retrofit masonry walls to resist lateral pressures such as wind, and various blast charges and distances.

TABLE OF CONTENTS

Page

LIST OF TABLES

LIST OF FIGURES

LIST OF FIGURES - CONTINUED

LIST OF FIGURES - CONTINUED

LIST OF ABBREVIATIONS

AFB	Air Force Base
AFRL	Air Force Research Laboratory
ANFO	Ammonium Nitrate and Fuel Oil
CFRP	Carbon Fiber-Reinforced Plastics
CMU	Concrete Masonry Unit
CONWEP	Conventional Weapon Effect
ERDC	Engineering Research and Development Center
FE	Finite Element
ft	Foot
ft/sec	Foot/second
GUI	Graphical User Interface
IED	Improvised Explosive Device
in	Inch
in/sec	Inch/second
ksi	Kilo-pounds per square inch
lb	Pound
ln	Natural logarithm
LS-DYNA	Livermore Software - DYNAmics
mph	Miles per hour

LIST OF ABREVIATIONS - CONTINUED

msec	Milli seconds
P-I	Pressure-Impulse
psf	Pounds per square feet
psi	Pounds per square inch
RBS	Royal Building Systems
SBEDS	Single-Degree-of-freedom Blast Effects Design Spreadsheet
SDOF	Single-Degree-of-Freedom System
TCCMAR	Technical Coordinating Committee for Masonry Research
TNT	Trinitrotoluene
UAB	University of Alabama at Birmingham
WAC	Wall Analysis Code

LIST OF NOTATIONS

A	Area
a	Width of arching area
A_{op}	Solid surface area of wall with opening
A_r	Area of retrofit
$A_{Surface}$	Solid surface of wall with no openings
α	Wall support degree of fixity
β	Ratio of wall curvature
B_w	Factor for opening in wall
c	Radius of curvature
Δ	wall lateral displacement, inch
δ	½ of crack opening
E	elastic modulus, psi
E_c	concrete masonry elastic modulus, psi
E_r	polymer retrofit elastic modulus, psi
ε	Strain
^oF	Degree Fahrenheit
f_c	Compressive stress
f'_c	Compressive strength of mortar
f_{cr}	Compressive stress at cracking
ft	Foot

f'_m	CMU compressive strength
F_o	Maximum Blast Force (lbs)
F_{yr}	Yield strength of membrane retrofit
G	Modulus of rigidity
H	horizontal reaction force, lbs/in
h	height of wall, in
I	Moment of inertia
KLM	Effective Load Mass factor
KW	Kilowatt
l	Tributary length of membrane retrofit
M	moment
η	Arching variable
Ω	Retrofit variable
p	lateral pressure, psi
P	wall surcharge, lbs/in
P_o	Maximum Blast Pressure (psi)
PI	Incident pressure in blast (psi)
PL	Pressure load in blast (psi)
PR	Reflected pressure in blast (psi)
Φ	Wall curvature
Φ_{cr}	Wall curvature at cracking
Φ_{crG}	Wall curvature as crack grows

R	Resultant force of the compressive stresses in the wall, lbs/in
r_u	Height of arch
σ	Stress (psi)
σ_{cr}	Stress at cracking
σ_{crG}	Stress as crack grows
t	Wall thickness
T	Tension in the polymer retrofit, lbs/in
θ	Angle of incident
t_r	Polymer retrofit thickness, in
V_u	Arching force
V_{Top}	Arching force at top support
V_{Bottom}	Arching force at bottom support
x	Distance from R to the wall centerline
y	crack length, in
W	Weight of explosive (lbs)
w_i	Wall weight, lbs/in

1 INTRODUCTION

In today's society, there is an increasing risk of terrorist attacks by radical groups, political separatists, and those people who intend to injure, and even kill, innocent people. Attacks of this nature can be carried out with relative ease by anyone who has such intent. The most widely used type of device in such an attack is an Improvised Explosive Device (IED). The simplest of IEDs may consist only of a container carrying fuel, an oxidizer, and a detonation device. IEDs may be easily concealed and are commonly delivered by vehicles, in postal packages, and even on foot.

Terrorist attacks commonly target crowded facilities, such as office buildings and restaurants, not to mention military installations. Casualties and injuries sustained in such attacks often cause the disintegration and fragmentation of walls, the shattering of windows, and by non-secured objects that can be propelled at high velocities by the blast. Ensuring that the exterior walls of a structure are able to withstand a blast and not produce deadly fragments is an important part of minimizing injuries to building occupants.

Most civilian structures are constructed with lightly reinforced or unreinforced exterior walls without any consideration to blast loading (Crawford et al. 1997a). These exterior walls must therefore be strengthened to increase the resistance to blast loads. One of the most common ways to reinforce a wall for blast loading is to increase the mass of the wall. This can be achieved by applying additional concrete and steel

reinforcement. Reinforcing an existing wall with additional concrete and steel is not only time-consuming and expensive, but provides little assurance regarding the containment of deadly fragments and projectile. An expedient, efficient method for reinforcing existing concrete and masonry walls is needed.

A very common method of construction is the use of concrete masonry units (CMU) in the walls of buildings. CMUs provide a fast and inexpensive way to construct building facilities of various heights. However, CMU walls are extremely vulnerable to the high pressures induced by blast, resulting in collapse, fragmentation, and severe injury to occupants. An understanding of the structural behavior of CMU walls during blast is the key to providing mitigation techniques. Much research has been conducted using actual explosive tests as well as finite element methods to examine structural failure due to blast. The Air Force Research Laboratory (AFRL) at Tyndall Air Force Base (AFB) in Florida has been testing the effectiveness of inexpensive, lightweight polymer retrofits for protection against blast loadings. AFRL has constructed and destroyed numerous full-scale wall structures during their explosive testing. This type of testing is expensive and requires much preparation, but has been supplemented with the aid of computer models. The use of finite element models allows a variety of structures and retrofit materials to be examined with relatively low expense in a much shorter time frame.

A noteworthy effort in this area is the research performed under the direction of Dr. Jim Davidson. This research made use of LS-DYNA finite element software to simulate full-scale models of concrete masonry walls. The results were compared to the actual blast tests conducted by AFRL at Tyndall AFB. Various parameters of these

models were tuned to better match the test results, but the ultimate cost of high fidelity computational models made them impractical for the day-to-day design of retrofitted masonry walls to withstand blast loads. Design tools developed by other investigators in the field have been available for the past few years; however, they do not account for the impact of the membrane retrofit on the overall behavior of the wall.

1.1 Objectives

The overall objective of this research was to develop resistance function equations for membrane retrofit unreinforced concrete masonry walls and implement them into a Single-Degree-Of-Freedom (SDOF) model. The specific goals of the research are as follows:

- Develop a theoretical model for the static load-deflection response of the membrane retrofit concrete masonry wall resistance function.
- Develop a SDOF dynamic response model.
- Validate the model with existing test results and high-end analytical predictions.
- Find forces at wall connection points.
- Develop the initial stages of a practical software tool (Graphical User Iterface) for use by the structural engineer in the field.

1.2 Scope and Methodology

A general literature review was conducted to investigate the research performed to date on masonry walls subjected to blast. This review included the results of a number of actual blast tests conducted by AFRL on various configurations of polymer reinforced

masonry walls as well as unreinforced masonry walls. It included the research using computational finite element techniques as well as destructive and non-destructive tests. The literature review investigated the availability of software tools for the response prediction and design methodology of such systems.

This effort analyzed and documented the results of pertinent blast tests and used computational finite element analyses for verification purposes. Subsequently, the resistance function of the membrane retrofit masonry wall was developed to describe the deformation of the wall under uniformly applied loads. The study determined the inelastic behavior of the wall to develop the large deformation behavior region of the resistance function.

Using the resistance function, the study idealized the one-way masonry wall as a SDOF system and developed the required differential equation and its solution. Assuming the results of actual tests to be relatively correct, the results of the SDOF analysis were compared to field test results for verification. Methodologies were developed using the output of the SDOF analyses and offered to the structural engineer in the field for the design of membrane retrofit masonry walls to be subjected to blast.

1.3 Organization of Report

This report is organized into eight chapters. Chapter 1 is an introduction that gives an overview of the objectives, scope, methodology, and organization of the report. Chapter 2 is a review of previously published literature concerning the strength of masonry walls exposed to lateral loads, including seismic and blast, actual blast tests, and finite element modeling.

Chapter 3 presents the discussion of the full-scale explosive tests performed at Tyndall AFB and other locations to date. The test setup, test results, and a discussion of the results are also included in this chapter. Chapter 4 discusses the development of the high-fidelity finite element models using LS-DYNA for concrete masonry wall investigation. Chapter 5 discusses the development of the resistance function based on the latest techniques in the industry.

Chapter 6 discusses the development of the SDOF model using the resistant function approach. Chapter 7 uses the model discussed in Chapter 4 to develop analytical results for several wall tests. Analytical results from the SDOF and FE models are compared to actual blast test results in Chapter 7. Chapter 8 provides a discussion of the results, conclusions of the work accomplished, and recommendations on ways in which the research may be extended in the future.

2 LITERATURE REVIEW

2.1 Seismic Investigations

The largely empirical design of masonry structures does not "rely extensively on the rational application of engineering principles," which can result in the designer not fully recognizing all of the relevant design variables (Yokel and Dikkers 1971). Design variables such as loading geometry, end fixity, wall stiffness, and cross-sectional properties can have significant effects on the overall strength of masonry walls. In May of 1971, Yokel and Dikkers reported on the strength of load-bearing masonry walls based on 192 full-scale masonry wall tests previously conducted by the National Bureau of Standards and the Structural Clay Products Institute. This study used rational analysis methods, which were based upon established theory, to predict the strength of load-bearing masonry walls (Yokel and Dikkers 1971). In the same year, Yokel developed a methodology for stability and load capacity of members with no tensile strength (Yokel 1971). Eccentrically loaded compression members were examined, beginning with their elastic behavior and continuing through their cracked and rocking rigid body behavior, until ultimate load capacity was reached. Yokel developed equations for strength calculations of such compression members and verified his results with 39 full-scale tests on brick walls. The most extensive dynamic studies were performed as part of an investigation aimed at developing standards for the renovation of unreinforced masonry buildings in Los Angeles, particularly with respect to the acceptable height-to-thickness

ratio of walls (Tropical Report 08, ABK 1984; Kariotis 1985). The study investigated the one-way behavior of eight wall specimens of varying construction and geometry under a range of gravity loads and several dynamic motions at top and bottom, simulating the input motion from the ground or from a diaphragm anchorage. The study concluded that the primary concern is "dynamic stability" - the equilibrium of the cracked wall under the influence of applied loads, self weight, and inertial loads, rather than material stress levels. The results showed a close correlation with the tests and were presented in an eight-volume report produced by ABK, A Joint Venture, of which the methodology is the final report. In 1985, Priestley developed a similar methodology to examine the behavior of one-way unreinforced masonry walls under the action of lateral seismic loads (Priestley 1985). The methodology was later corrected in 1986 (Priestley and Robinson 1986), with a final publication in 1992 (Paulay and Priestley 1992). Priestley argues that the formation of cracks does not constitute wall failure, even in unreinforced masonry walls. Failure occurs only when the resultant compression force from surcharge and wall weight above the crack is displaced outside the line of action of the applied gravity loads at the top and bottom of the wall. The method determines the nonlinear load-deflection curve for a masonry wall subjected to out-of-plane loading.

In 1995, La Mendola et al. examined the stability conditions of masonry walls subjected to seismic transverse forces. The problem was translated into the analysis of a fixed free-ended prismatic column undergoing static, horizontal forces equivalent to maximum inertia actions. Hamid and Drysdale (1988) investigated fracture of masonry structures using the finite element approach. This investigation resulted in constitutive models capable of simulating the initiation and propagation of fracture under combined

normal and shear stresses in both tension-shear and compression-shear regions. The models predicted the load-carrying capacity of masonry assemblages and provided detailed information on the failure mode, ductility, and crack patterns. Drysdale et al. (1994) used a very similar approach to that employed by Yokel (1971) and Priestley and Robinson (1986) to develop resistance functions for unreinforced masonry walls under lateral loads. The approach considered arching for one-way action walls confined between rigid boundaries at their top and bottom interfaces. The results showed a significant increase in the resistance of such walls to lateral loads.

Martini (1997) investigated the one-way and two-way action of unreinforced masonry walls using the finite element method and showed excellent correlation with the approach proposed by Priestley and Robinson (1986), Paulay and Priestley (1992) and La Mendola (1995). Doherty et al. (2002) published their work on displacement-based seismic analysis for the out-of-plane bending of unreinforced masonry walls. The approach adapts a simplified displacement-based procedure and a trilinear characterization of the actual nonlinear force displacement relationship in the analysis. The results of the seismic analysis show this method to yield significantly better predictions than the force-based method.

2.2 Blast Load

The load magnitude caused by a blast is determined by many factors, including charge size, type of explosive and standoff distance. Blast is broadly classified as air blast or subsurface blast. Blast can be airburst or surface burst, depending on the distance of the burst above the ground. An air blast generates a pressure sphere traveling in the radial

direction at the speed of sound (Dharaneepathy et al. 1995). This pressure has a positive phase and a negative phase as shown in Fig. 2.2-1.

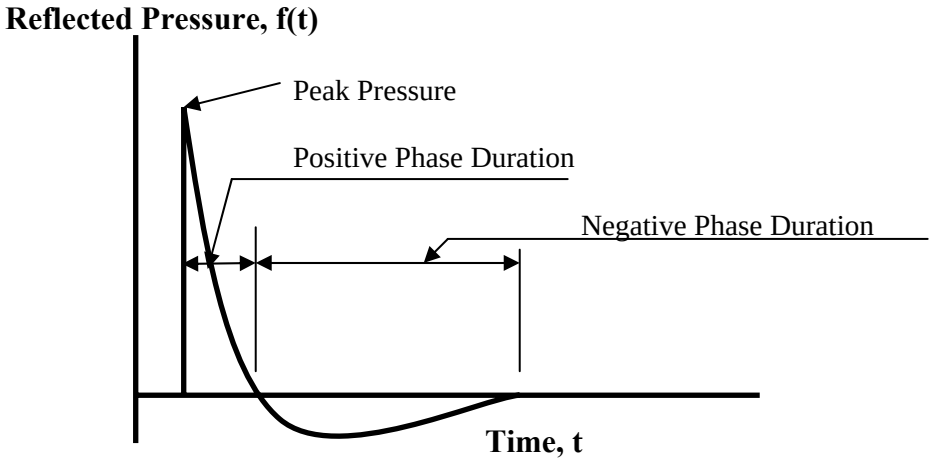

Fig. 2.2-1. Blast load waveform

The positive phase has a peak side-on pressure, and the negative phase is characterized by suction. In many studies of blast effects on structures, the negative phase is ignored (Beshara 1994). Pressure intensity depends on the location within the structure, hence the impulse depends on the standoff distance and angle of incidence. Parameters such as time of arrival, positive phase duration, wave decay coefficient, and side-on pressure depend on standoff distance. If the standoff equals the "critical blast distance," the transient dynamic response is maximum (Dharaneepathy et al. 1995).

Explosive effects do not scale linearly. For example, a 2-lb charge does not produce the same effect as a 1-lb charge at half the distance. Scaling is generally done in terms of TNT equivalence. This equivalency is affected by the charge size, confinement, nature of source, and pressure range under consideration. General important

characteristics of the blast wave, such as energy release, are measured for standard TNT tests carried out with controlled explosions. These results are then used as a benchmark to calculate data for other explosions by using the cube root scaling law, which states that "when two charges of same explosive and geometry, but different sizes, are detonated in the same atmosphere, the shock waves produced are similar in nature to the same-scaled distances" (Beshara 1994).

The point on the ground exactly below the explosion is referred to as ground zero. Pressure time history is composed of overpressure, dynamic pressure, and reflected pressure. Overpressure is a pressure that acts on the structure in the absence of such obstacles as the ground and is hydrostatic in nature. Dynamic pressure causes drag or wind-type loads on the structure and exhibits sharper pressure decay over a longer duration. Reflected pressure is generated when the shock front hits a rigid surface. The overpressure and dynamic pressure have a longer duration than reflected pressure. For conventional high explosives, the magnitude of the peak reflected pressure is higher than the peak overpressure and peak dynamic pressure. Near the ground surface, the combined effect of incident pressure and reflected pressure is considered. While studying the effect of unconfined explosions such as nuclear explosions on multistoried structures, however, peak overpressure may be more important that the reflected pressure.

Krauthammer and Otani (1997) studied the behavior and design of reinforced concrete structures subjected to blast loads and concluded that shock pressure has less of an effect on reinforced concrete structures than the lower overpressure that has a longer time duration. The function used for the load application must consider both pressures. Since the maximum dynamic pressure is very small as compared to the other two, it can

be neglected in the load calculation. This load application depends on the angle of incidence, which is the angle between the line of wave propagation and the outer normal to the element.

The U.S. Army Engineer Waterways Experiment Station developed the Conventional Weapons Effect Program (CONWEP) which provides free-field spherical and hemispherical predictions (Randers-Pehrson and Bannister 1997). The calculations consider the blast wave angle of incidence. The BRODE model implemented in DYNA3D for modeling blast pressure excludes this feature. CONWEP, on the other hand, does not combine reflected pressure and incident pressure for the calculation of the angle of incidence. Randers-Pehrson and Bannister (1997) integrated a modified CONWEP model into DYNA2D and DYNA3D by incorporating the following equation:

$$PL = PR\,(\cos 2\theta) + PI\,(1 + \cos 2\theta - 2\cos\theta) \qquad (2.2.1)$$

where PL = pressure load, PR = reflected pressure, PI = incident pressure and θ is the angle of incidence.

2.3 Retrofit Measures for Blast Loads

Masonry walls normally have adequate, predictable performance when subjected to static in-plane loading; however, masonry walls tend to perform poorly when subjected to out-of-plane loading that causes shear and flexure. The early in-depth studies arose as part of an investigation into the renovation of unreinforced masonry buildings in Los Angeles (Martini 1996). In earthquake regions, typical unreinforced masonry walls

lacked the strength and ductility to survive seismic loads. Carbon overlays were investigated as a repair and retrofit technique for masonry walls during tests of single-story masonry walls (Laursen et al. 1995). The carbon overlays were used in an attempt to enhance shear and flexural strength. The test results indicated a "significant increase in strength and deformation capacities" (Laursen et al. 1995).

Strengthening of individual structural components for seismic loading has also been the subject of numerous experimental tests. The retrofit of structural components with advanced composite materials has become popular in light of recent earthquakes. Bridge columns were the focus of an advanced composite material seismic retrofit study by Seible and Karbhari 1996. Both circular and rectangular bridge columns were retrofitted with composite jackets of glass fiber reinforcement and resin. Resin systems such as polyesters, vinylesters, and epoxies were used as the matrix of the composite materials. The composite jacket designs were determined to be as effective as steel jackets in improving deformation capacity levels of columns subjected to seismic loading.

Experimental testing of retrofit techniques has also been applied to full-scale structures. The Technical Coordinating Committee for Masonry Research (TCCMAR) constructed a full-scale five-story building and performed simulated seismic load tests on the structure. After the original test, repair and retrofit techniques were applied to damaged and undamaged components of the structure. According to Weeks et al., "the principal objective was to increase the deformation capacity of the building without increasing the flexural stiffness or strength since the latter would increase the shear demand" (Weeks et al. 1994). Carbon fiber overlays, polymer-concrete repairs, and

epoxy injection techniques were used to enhance the shear transfer in walls, beams, and floor panels. The repair and retrofit test results were compared to the results from the original test. The test results indicated "that the individual repair measures and components of the repaired five-story building performed very well" (Weeks et al. 1994). The repaired building exhibited an increase in load-carrying capacity, along with an increased capacity for deformation.

Retrofit techniques that were originally designed for seismic loading were later investigated for their use in strengthening concrete masonry structures against blast. For instance, column-jacketing techniques that have been used to improve the response of seismically loaded reinforced concrete columns have also been analyzed for their effectiveness in reducing explosive-induced damage. It has been found that multi-story reinforced concrete structures typically collapse with the failure of just a small number of outer support columns. Outer support columns tend to fail "in shear near the supports" when subjected to blast loadings (Crawford et al. 1997b). These columns can be retrofitted and strengthened by the use of steel or composite material jackets. Finite element analysis of explosively loaded columns has shown that jacketing techniques can increase the "strength and ductility of concrete".

During the summer of 1994, the United States participated in a composite retrofit material study with the Israeli Home Front Command. This study was performed to better understand the effects of blast loadings on concrete and masonry structures strengthened with composite retrofit materials. Based upon dynamic testing conducted at Tyndall AFB, two retrofit materials were selected for the first phase of the study: an autoclaved 3-ply carbon fiber composite laminate and a knitted biaxial fiberglass fabric

(Purcell et al. 1995). Phase I of the test series consisted of full-scale explosive tests against structures retrofitted with the composite materials. This phase was conducted in Qiryat Gat, Israel. Israeli civil engineers constructed the structures used in the test. Each structure had 8-inch thick wall panels that were reinforced with 3/8-inch rebar spaced 12 inches center to center. The retrofit materials were bonded to the wall surfaces in order to maximize their effects. To ensure a proper bond, the wall panels were cleaned and then primed. The carbon fiber laminate and the knitted fiberglass fabric were bonded to the wall panels using HYSOL 9460 epoxy adhesive (Purcell et al. 1995).

CONWEP software was used to calculate a standoff distance for an explosive charge of TNT (Purcell et al. 1995). This standoff distance was calculated to ensure the breaching of the wall panels. The results of the tests showed that the retrofit materials had a significant effect on the amount of wall displacement caused by the explosive charge. The knitted fiberglass fabric outperformed the carbon fiber composite during this test. In fact, the carbon fiber composite seemed to be minimally effective. The reduced performance of the carbon fiber composite can be attributed in part to a poor bond between the material and the concrete that resulted in delamination. These tests also resulted in a recommendation for the development of a finite element analysis to predict retrofitted wall response to explosive charges (Purcell et al. 1995).

In September 1995, a blast response experiment was conducted at Eglin AFB. A three-story reinforced concrete building was used to evaluate the effectiveness of externally applied reinforcement. A Kevlar fabric was used to retrofit the interior side of four wall panels facing the detonation of an explosive device. The fabric was applied to

the concrete walls, using HYSOL 9460 epoxy, in much the same way as the previous United States/Israeli test was conducted in 1994 (Taun et al. 1995).

The test structure had the following general dimensions: 40 feet wide, 40 feet deep, and 30 feet tall. The building had 10-inch thick center walls and nine 14-inch x 14-inch square sectioned columns. The floors and exterior walls were 6 inches thick. The exterior walls were approximately 7.2 feet wide and 8.5 feet tall. The walls contained number 4 rebar at 18 inches of spacing on the center. Testing of the concrete showed an average compressive strength of 4,600 psi.

One major difference between this test and the United States/Israeli test was the pre-test prediction using the DYNA-3D finite element code. Each wall panel was modeled while neglecting the contribution from the rebar for carrying tensile stress in the concrete. The behavior of the concrete was assumed to be elastic with failure in tension (Taun et al. 1995). The Kevlar material was modeled as linearly elastic and fully bonded to the concrete walls. The models were used to predict the level of failure for the retrofitted walls.

The results of the test showed that the structural response predictions by DYNA-3D were not accurate (Taun et al. 1995). The accelerations of the walls due to the blast loading were greatly underestimated, due to the absence of reliable models for concrete behavior. Three of the four retrofitted exterior walls failed completely. It was suggested that further work be done on the optimization of the layering and fiber orientation of the retrofit materials.

The lack of usable data and reliable conclusions from the experiment greatly emphasized the need for more accurate computer models. In order to obtain higher levels

of accuracy, the computer models had to become more complex so that the actual material behaviors could be simulated.

In October 1996, explosive tests were conducted to evaluate retrofit measures for conventional concrete masonry unit buildings. These tests were a continuation of the Israeli Home Front Command's research into strengthening civilian structures against terrorist threats. The tests were performed on a 5-story building and two additional test cubicles. Whiting and Coltharp, members of the U.S. Army Engineer Waterways Experiment Station research team, produced a paper concentrating on the two test cubicles and the CMU retrofit techniques (Whiting and Coltharp 1996).

The test cubicles were constructed with load-bearing CMU frames with the assumption that the walls were part of a generic 2-story building. The CMU walls were constructed with post-tensioned steel bars in ungrouted CMU void spaces. This was done to simulate the additional weight that would be present in the 2-story structure. Several mechanical/structural retrofit techniques that had been previously used for seismic retrofit of load-bearing masonry walls were selected and evaluated for effectiveness in resisting blast loadings (Whiting and Coltharp 1996). Pilasters, shotcrete, and knee bracing were the specific retrofit measures used during the tests.

Pre-test predictions were performed using SDOF applications, semi-empirical blast load calculations, and finite element analysis. The SDOF applications consisted of the SDOF Code and the Wall Analysis Code (WAC version 2). The blast load predictions and finite element analysis were performed using CONWEP and DYNA-3D, respectively. SDOF and finite element analysis were performed for each type of retrofit wall panel and a control (unretrofit) wall panel. The pre-test predictions seemed to

"compare favorably with the test results" (Whiting and Coltharp 1996). Post-test photos of the wall panels were compared to the DYNA-3D damage predictions, and it was concluded that "finite element code is the most accurate means of damage prediction" for complex masonry cross-sections (Whiting and Coltharp 1996).

In the fall of 1999, researchers at the AFRL began looking for retrofit techniques to increase the blast resistance of common exterior walls. One of the researcher's goals was to develop a retrofit technique that did not have difficult application processes and the high expense of commonly used methods for strengthening walls, such as increasing the mass with reinforced concrete. The need arose for a "lighter weight solution" that would "introduce ductility and resilience into building walls" (Knox et al. 2000). An elastomeric polymer, with a polyurea base, was chosen for use as a retrofit material based upon the results of material testing performed at Tyndall AFB. The material was selected based on its strength, flammability, and cost. The application method for this material was a relatively straightforward spray-on process, as shown in Fig. 2.3-1.

Fig. 2.3-1. Application of spray-on polymer

Proof-of-concept tests were performed using blast-loaded masonry walls and lightweight structures retrofitted with the polymer material. The material was easily sprayed onto the interior and exterior wall surfaces while control over the application thickness was monitored. The proof-of-concept tests showed that the masonry and the lightweight structure walls experienced large deflections without breaching, and that no debris entered the interior of the test structures. The lightweight structure used in the proof-of-concept tests stayed intact, but the structure experienced severe ceiling crushing, which needed to be mitigated.

The successful proof-of-concept tests performed by the AFRL quickly led to the development of a lightweight structures program. Lightweight structures are generally "characterized by timber stud walls, exterior aluminum siding, and interior veneer-plywood paneling" (Knox et al. 2000). Three explosive tests were performed on structures retrofitted with the polymer material. The first test consisted of two lightweight constructed wall panels. This test was used to study the performance of the retrofit material when subjected to high rates of strain caused by explosive loading. The following two tests were conducted using single-wide construction and house trailers. For the single-wide construction trailer, additional strengthening measures were tested along with the polymer retrofit material. Frames constructed from thin steel tubing were installed in an attempt to reduce the ceiling crushing seen in the proof-of-concept tests. It was predicted that the steel frames would have little impact on wall deflections. The steel frames were installed, and the spray-on polymer was applied to the interior wall surfaces and the steel frame to ensure a continuous layer of retrofit material. The house trailer was divided into three separate test sections. The right-end section and the middle

section of the house trailer had the same stud spacing for the steel frame and different thicknesses for the polymer retrofit. The left-end section had a much shorter stud spacing for the steel frame, with the same polymer retrofit thickness as the right-end section. The house trailer test was designed to "push the envelope of the retrofit technique" by using a higher explosive yield (Knox et al. 2000).

The results of the first two tests showed that the polymer retrofit technique was successful. Even though the lightweight wall panels and structures sustained severe damage, the polymer retrofit kept significant amounts of debris out of the interior of the test structures. The higher explosive yield of the third test resulted in numerous tears in the retrofit material, "significant enough to permit some debris fragments to enter the rooms" (Knox et al. 2000). The test structures equipped with the tubular steel frames experienced significant reductions in ceiling deflections compared to the proof-of-concept tests. The AFRL research team found that unsecured items inside the test structures, such as furniture and light fixtures, were a major source of potentially deadly flying debris. Based on the results of the tests, the research team concluded that the polymer retrofit technique would be an effective addition to a comprehensive security program.

The AFRL research team continued the development and testing of the polymer retrofit technique by shifting their focus to the retrofit of CMU walls. An overview and discussion of the CMU wall tests carried out by the AFRL, at Tyndall AFB, is presented by Connell (2002). Connell reported that three masonry wall tests were conducted by AFRL during the early part of 2001 with the spray-on polymer retrofit Polyurea. Two tests used a retrofit spray-on wall versus an unreinforced CMU wall without retrofit. The

first test, with a lower blast charge at a stand-off distance of 50 feet, showed that the unreinforced CMU wall collapsed unlike the retrofit sprayed-on wall, which stayed in place with some damage (Fig. 2.3-2).

Before After

Fig. 2.3-2. Test set-up and results

The second test, with a higher blast charge at a stand-off distance of 43 feet, showed that both the unreinforced masonry wall and the retrofit sprayed-on wall collapsed completely. The third test used the same charge as the second test but at a stand-off distance of 65 feet, with two retrofit sprayed-on walls. The first wall was sprayed only on the inside face and the other wall was sprayed on both the outside and inside faces. Both walls survived the blast load. These tests showed the effectiveness of the sprayed-on polymer in strengthening the unreinforced CMU walls. The application procedure for the polymer was not overly burdensome, and the test results indicated that peak pressures greater than 60 psi were easily achieved for one-way action walls, compared to a capacity of less than 10 psi for unreinforced walls.

Connell reported that challenges remained, however. The failure mechanism was highly dependent upon the peak load and duration and was not thoroughly understood. The failure of the walls was also very sensitive to the support conditions.

2.4 Arching

The earliest in-depth investigation of the arching action theory of unreinforced masonry walls was carried out by McDowell et al. (1956). It represented a rather radical departure from the resistance of lateral forces usually assumed for this type of construction. The theory was used to obtain the static load-deflection curves for masonry beams of solid cross section. The results showed significant improvement in the resistance of these beams to lateral uniform loads.

McDowell et al. (1956) noted that, under certain conditions, masonry walls withstood much larger loads than those predicted on the basis of conventional bending analysis. The additional strength was developed when the walls were butted up against supports that were essentially rigid. This type of wall exhibited three to six times the load-carrying capacity of simply supported walls. McDowell et al. (1956) ran a series of static tests on different sizes of solid, unreinforced masonry beams exposed to lateral uniform loads and compared the results to those derived from their proposed theory.

Gabrielsen et al. (1973 and 1975) performed extensive blast tests on arched unreinforced masonry walls. Shock-tunnel pressure waves were used to simulate the blast load required for each test. The tests showed that arched walls are considerably stronger, by as much as four to five times, than nonarched walls. Gabrielsen et al. (1975)

also shock-tunnel tested gapped arched walls and concluded that they were significantly weaker than the arched walls without gap.

Drysdale et al. (1994) used the same approach as that employed by McDowell et al. (1956) to develop a simpler equation for the arching resistance of unreinforced masonry walls under lateral loads. The approach considered arching for one-way action walls confined between rigid boundaries at their top and bottom interfaces.

Dinan et al. (2003) examined the arching resistance of polymer retrofit concrete masonry walls using the method outlined by Drysdale et al. and the WAC to arrive at resistance functions that matched well with full-scale test data.

2.5 Membrane Catcher System

Blast pressure causes fragmentation in unreinforced concrete masonry walls. The fragments can travel into the occupied space at high speed and cause injury and even death. The membrane catcher system is designed to catch the fragments and save lives. A typical unreinforced concrete masonry wall catcher system may consist of the CMU wall and the membrane catcher material on the inside face of the wall. The membrane catcher material is attached to the floor and the ceiling and not to the wall. The membrane catcher system may be made of metal such as thin steel or aluminum sheets. The membrane catcher system is attached to the floor and to roof of the room associated with the wall using sound structural interfaces.

Slawson et al. (1999) described the use of a typical membrane catcher system in a paper presented at the *9th International Symposium on Interactions of the Effects of Munitions with Structures*. Anchored fabrics were used to retrofit concrete masonry unit

walls exposed to blast pressure. SDOF and finite element models were used in an attempt to validate test results conducted in Israel during May 1998.

The anchored fabric retrofit technique was not intended to strengthen the masonry walls. Its purpose was to catch hazardous debris caused by the disintegration of the wall (Slawson et al. 1999). Anchored to the roof and floor slabs of a structure, on the inside face of a wall, the fabric acts like a net that catches broken pieces of the wall and reduces the threat to occupants. Two commercially available geofabrics were used during the Israeli explosive tests. The geofabrics were successful in preventing debris from entering the interior of the test structure.

A total of six wall panel models were generated using the WAC SDOF software and the DYNA-3D finite element software (Slawson et al. 1999). Each wall panel model was given a width of 120 inches and a height of 104 inches. For both the WAC and DYNA-3D models, there was one control wall and two walls that were retrofitted with the anchored fabric. The membrane resistance of the anchored fabric was added to the resistance function of the WAC-generated wall panels to account for the retrofit. The finite element models contained over 80,000 solid elements. The finite element retrofit models also contained a 40 x 40 mesh of linear-elastic membrane elements that represented the anchored geofabric and was placed 0.1 inch behind the wall.

Results from the WAC and DYNA-3D models were compared to the data collected from the explosive tests. The results from the models did not coincide well with the results from the explosive tests. The model results indicated that the maximum displacements for the retrofitted walls were being overestimated. It was suggested that

additional experimental data would be required to fully validate the computation procedures (Slawson et al. 1999).

Thornburg (2004) reports a test at Tyndall AFB in which two CMU walls were exposed to blast loads. One wall incorporated the membrane polymer catcher system, while polymer was sprayed directly on the other unreinforced concrete masonry wall. Both walls were constructed in exactly the same manner, except for the application of the polymer. The wall with the membrane polymer catcher system collapsed during the test, but its intended purpose remains viable for lighter blast loads.

2.6 Computer Modeling of Masonry Walls and Retrofit Measures

General out-of-plane behavior of unreinforced masonry walls can be better understood by considering static loading. Martini (1996a) reported a study in which a finite element model was constructed for the one-way, out-of-plane failure of unreinforced masonry walls subjected to static loading. This study was conducted as an investigative approach for two-way action walls. A discrete cracking material model involving 8-node elastic continuum elements were used to model masonry units, and 8-node surface contact elements was used to model joints. Uniform pressure was applied until the equilibrium of the analysis became unstable. The system was solved using ABAQUS. Load-displacement plots were then compared with the literature to verify the suitability of the model.

In another study, Martini (1996b) developed a two-way unreinforced masonry wall panel supported at the sides and bottom. Modified yield-line theory was used for unreinforced masonry walls by considering post-cracking mechanisms of moment

transfer for the horizontal and vertical directions. ABAQUS models of the wall were analyzed. The modified theory predicted lower failure loads than finite element results but closely matched failure patterns.

In 1996, Karagozian and Case developed several candidate retrofit designs for increasing the blast resistance of concrete masonry walls. The retrofit designs were direct adaptations of existing seismic retrofit designs for increasing the out-of-plane load capacity of under-reinforced walls (Wesevich and Crawford 1996). Several of the retrofit designs were chosen for use as articles in explosive tests to be conducted in Israel during October 1996. The choice of retrofit designs was based upon the availability of materials in third world countries, ease of construction, and the feasibility of applying the designs to existing structures. Three retrofit designs were chosen: a single steel pilaster retrofit, a steel knee-brace retrofit, and an interior shotcrete retrofit. Finite element models were developed for the chosen retrofit designs so that wall response predictions could be made prior to the explosive tests.

The finite element models for the retrofit designs were generated using DYNA-3D. Each model used 3-D continuum elements and material models that were formulated to account for the extensive nonlinear behaviors of material subjected to blast loads (Wesevich and Crawford 1996). The particular concrete material model used was developed for predicting the response of concrete to explosive loads. The material model was also validated for the prediction of light and severe damage to reinforced concrete and masonry walls subjected to blast loading.

The results of the DYNA-3D analysis indicated that the knee-brace and shotcrete options were the “best retrofit candidates in that the least amount of damage occurred to

the wall panels for the two designs" (Wesevich and Crawford 1996). The structural integrity of the wall panels retrofit with these designs remained sound. The success of the shotcrete retrofit seems to indicate that the use of other materials, such as composites that can be bonded to the wall surfaces, may also provide positive results.

In April 1997, a paper was presented at the *8th International Symposium on Interaction of the Effects of Munitions with Structures* that discussed the development of a finite element model for the study of masonry walls subject to air blast loads. Crawford et al. (1997a) evaluated the effects of explosive loads on masonry walls using a DYNA3D analytical model. The aim was to estimate the responses of lightly reinforced or unreinforced structures subjected to blast loads. An analytical wall model having the width of a single cell unit that includes two half-cells and a web was studied. The analytical model was validated for pressure versus impulse diagrams by comparing it with results obtained from field tests conducted in Sweden. Load was applied using blast curves generated by BLASTX (Britt and Lumsden 1994). The analytical model was used further to validate and update the P-I curves typically associated with simplified assessment codes, such as FACEDAP. Various retrofit techniques were assessed for increasing the strength of unreinforced or lightly reinforced masonry walls. It was found that "retrofit designs that uniformly reinforce a masonry wall, such as composite wrap and shotcrete, were shown to provide a better enhancement to blast protection than those that discretely reinforce a wall, such as pilasters.

Crawford et al. (1997b) published a study on retrofitting reinforced concrete structures to resist blast loads. Buildings designed for gravity loads and blast loads were analyzed, and the structural behavior was predicted using DYNA3D. Blast loads were

developed using BLASTX. A specially developed constitutive model was used to capture the nonlinear behavior of concrete subjected to blast loading. The material model considered the variation of Poisson's ratio as a function of load. Continuum elements were used for column perimeter, beam elements were used for steel reinforcement, and shell elements were used for floor joists and slabs. Two explosive charges were simulated at 10 feet, 20 feet, and 40 feet standoffs for bare columns, steel-jacketed columns, and fiber-reinforced polymer-jacketed columns for both cases. 5000 psi concrete and American Society for Testing and Materials A615 grade steel was used with a carbon wrap of 54 ksi strength and 7600 ksi stiffness. The failure of the bare columns due to shear at the supports was observed. The analyses clearly illustrated that jacketing prevented the failure of the columns, and that increasing the number of wraps increased column stiffness.

Krauthammer and Otani (1997) reported a study of meshing, gravity, and load effects on finite element simulations of blast-loaded reinforced concrete structures using DYNA3D. The near-cubical reinforced concrete structure was considered, and symmetry was used to reduce the structure to 1/8th of true size. The model consisted of a back wall, sidewall, and roof. Ten cases were analyzed with increasing reinforcement, load, and gravity effects. All of the cases were analyzed for coarse and fine mesh containing 4995 and 73211 elements, respectively. Reinforcement was modeled according to design drawings. The lumped mass approach was used for reinforcement in the coarse mesh model. A "soil and foam" material model with 8-node solid elements was used for the concrete material, whereas thin shell and beam elements were used to simulate steel reinforcement bars. Roof and sidewalls were subjected to peak pressures of 1115 psi, and

the back wall was subjected to 2470 psi. Maximum displacements were calculated for various cases. Deformations and stress distributions were analyzed for steel and concrete. Gravity loading affected the time of maximum displacement of the wall and roof and also increased the peak displacement.

Krauthammer and Otani (1997) concluded that the fine mesh resulted in more displacement than the coarse mesh, but, as the reinforcement was increased, the difference decreased due to the enhanced strength provided by the steel. In addition, transverse stress showed significant disagreements in shear and radial reinforcements due to the lumped mass approach used in the coarse meshing. Gravity load initialization was found to be necessary before load application.

Shope and Frank performed finite element analysis of blast-loaded concrete masonry unit walls in 1998. One-way action strip models and two-way action wall panel models subjected to blast loads were developed using the DYNA-3D software package.

For the one-way action models, two approaches were taken with regard to modeling the bond between the concrete masonry units and mortar layers. The first was the use of contact/sliding surfaces to represent the mortar joints, and the second was the use of continuum elements (Shope and Frank 1998). The contact/sliding surface approach yielded results that were “very sensitive” to a penalty stiffness factor that had “no physical basis” for selection. It was determined that the contact surface approach was not an appropriate method for this type of analysis; however, the use of continuum elements showed close agreement between DYNA-3D and theoretical single-degree-of-freedom results for one-way bending.

Significant differences in the results for two-way action wall panel models did arise between the finite element and SDOF analyses. The greatest difference was seen between the fixed support condition and arching results for two-way bending (Shope and Frank 1998). It was noted that resistance functions generated by the SDOF models could be modified to give results that were closer to those from the finite element analysis. Recommendations resulting from this research included refining material models, performing failure mode comparisons, and updating the finite element models as actual physical test data becomes available.

In June 1999, a study of finite element modeling techniques for a CMU wall subjected to airblast loading was performed using the DYNA-3D software (Dennis 1999). A simplified approach was used for this study because of modeling difficulties that arise when complex algorithms are implemented without the fundamental characteristics being known.

The finite element models were based upon nominal 8-inch x 8-inch x 16-inch hollow concrete masonry units that contained 3/8-inch mortar layers. Each masonry unit was comprised of 8-node solid elements. All masonry units were constructed as individual parts of a wall panel that were connected with slide surfaces that represented the mortar layers (Dennis 1999). The material properties for the concrete masonry units and the mortar were based upon the ACI 530-95 and ASTM C 270-89 standards. These properties were used in conjunction with material models that incorporated failure and strain-rate strengthening criterion.

Dennis (1999) reported the modeling of masonry walls subjected to blast loads using DYNA3D. Various uncertainties and complications, such as the strengthening of

concrete due to high strain rates and boundary conditions, were taken into consideration. A FORTRAN code accepting wall dimensions and expected block meshing was developed to generate the DYNA3D input file. Fidelity was limited to a maximum of five elements through the thickness of the face shell. Mortar joints were modeled using sliding surfaces defined in DYNA3D. Tied surfaces with and without failure criteria were used. Heuristic models were studied to verify the sliding-surface characteristics and material behavior. The "Drucker-Prager" material model was used for CMU blocks. Mortar was modeled with two constitutive conditions. The "Mohr-Coulomb" approach allowed mortar to fail in compression without restricting tension.

Another approach allowed the mortar to fail only in tension. A compressive strength of 2000 psi was assumed for the concrete blocks, and 1800 psi was assumed for mortar. To incorporate strain-rate strengthening, a step function was defined, that could double the material strength at a prescribed strain rate. To simulate one-way action, the wall was supported only at the ends. The wall was gradually loaded with uniform pressure to study static response. Convergence was tested for various combinations of mesh fidelity for web and faces when the wall was subjected to lateral static pressure.

However, these tests were carried out with "assumed" values of CMU mechanical properties. Midpoint velocity indicated the onset of instability and determined the static capacity of the wall. The results were then compared with "weak" (1800 psi) and "strong" (2800 psi) CMU. The strong wall failed due to mortar failure; the weak wall failed due to mortar failure and CMU tensile failure at the supports. Dennis (1999) concluded that, "If the fundamental material properties aren't more precisely known than that given in the published standards, the response is predictable only within a similarly

wide uncertainty bound". It was concluded that the convergence of the static numerical solution requires at least three elemental divisions in the CMU face shells and webs due to the local bending of the face shells near the supports. DYNA3D slide surface 9 used in the analyses exhibited anomalous behavior of the mortar by failing only in tension without showing any compression failure. The tensile bond strength model for mortar that permits failure of the mortar only in tension by setting high shear-failure criteria results in a more flexible response than the Mohr-Coulomb model, which can allow mortar to fail in tension or shear.

The U.S. Army Engineering Research and Development Center (ERDC) conducted experiments involving blast-loaded masonry walls in 1999 with the goal of validating the finite element modeling method. A series of five ¼-scale CMU wall experiments was performed to study the response of non-grouted, non-reinforced, one-way CMU walls to the blast pressure from high explosives (Dennis et al. 2000). A single one-way, ¼-scale CMU wall was also statically tested. Pre-test analysis and predictions were made for the ¼-scale experiments using the previously developed DYNA-3D modeling method.

The pre-test analysis was used, in part, to determine a standoff distance for the explosive charge that would ensure wall failure without the complete destruction of the test specimen. The originally calculated standoff distance was used for the first test. For the second and third tests, the standoff distance was reduced by 25%. The fourth test used the original standoff distance and was a repeat of the first test. The standoff distance for the final test was increased by 25% (Dennis et al. 2000).

Accelerometers and pressure gages were used to collect data for the five tests. Velocities and displacements for the ¼-scale walls were obtained by the integration of the recorded accelerometer data. Likewise, the recorded pressure histories were integrated to obtain the impulse history of the explosive load (Dennis et al. 2000). The test data was used to update the finite element models in the dynamic analysis. The average pressure histories from each of the five experiments were used to load the same finite-element model used to model the static experiment and the pretest blast experiments.

The results showed that the analysis method slightly overpredicted the maximum static capacity of the CMU wall (Dennis et al. 2000). The overprediction was attributed to the use of average CMU properties, and it was found that the use of lower-bound properties provided a very good estimate of the load-deflection function. The use of average properties also led to the slight underprediction of the response of the walls in several of the blast-load tests. For three of the five tests, the finite element analysis did not predict wall failure, even though it did predict moderate damage to the walls. Small adjustments to the applied pressure yielded results that more closely matched the failure of the experimental walls. The effects of small adjustments to the model indicate that considerable variability is to be expected in the results, and the effects also demonstrate that the analysis for both of these experiments provided reasonable, conservative results.

Connell (2002) evaluated the benefits of reinforcing masonry walls with elastomeric polymers subjected to blast. The AFRL at Tyndall AFB had been conducting tests to evaluate the effectiveness of inexpensive, lightweight polymer retrofits for protection against blast loading. The tests focused on the use of low-stiffness polymer material with a spray-on application process to reduce wall deflection and fragmentation.

The results clearly demonstrated that the spray-on polymer material was effective in reducing both wall deflection and fragmentation. Peak pressures greater than 60 psi were easily achieved for one-way action walls, compared to a capacity of less than 10 psi for unreinforced walls, but the large expense associated with performing explosive tests necessitated a reliance on computational techniques to investigate the effectiveness of retrofit materials. Connell was reasonably convinced that WAC was not suitable for the addition of low-stiffness polymers to masonry walls. He argued that the behavior of such a wall during a blast event is highly dynamic and nonlinear in nature. His attempts to use the following three available options in WAC to incorporate the effectiveness of retrofit polymers remained unsatisfactory:

- User defined.
- Unreinforced masonry walls (URM).
- Cavity wall.

Connell then developed high-fidelity FE models using the DYNA3D code to investigate the effectiveness of low-stiffness polymers on masonry walls. He investigated single CMUs, one-way action strips of masonry walls, and full-scale masonry wall panels. Using eroding elements allowed him to show a reasonable correlation between failure patterns seen in the actual explosive tests and failure patterns resulting from his finite element models. However, numerical values for wall response were not accurate, due to difficulties in implementing the proper failure criterion for the material models. The one-way action strip model failed in shear near the supports, while

the actual walls failed in bending at midpoint. Connell concluded that the difference in the failure modes was due to problems associated with the constitutive models, otherwise known as material types, in LS-DYNA. Connell concluded that the selection of a suitable constitutive model was the key to better model correlation with test results.

The research in this area continued using LS-DYNA finite element software to simulate full-scale models of concrete masonry walls (Moradi 2003). In order to converge on the most suitable constitutive model, Moradi examined the effect of time-dependent blast pressure on a single CMU, using four of the available constitutive material models in LS-DYNA. The approach used for the research was two-fold. First, explosive tests were planned with AFRL engineers and conducted at Tyndall AFB. During some of these tests, painted CMUs were placed on a radius at various distances from the blast source. Each color designated the distance of the CMU from the source. After the test, photographs from each test specimen and provided for this research.

Second, a high-fidelity model was developed using the DYNA-3D finite element software. The model was used to gain insight into the mechanisms that govern the failure of a single CMU. This model was used for blast loads analysis. The simulated blast loads were checked for accuracy in application, and the model was analyzed using four different constitutive relationships, or material cards, as follows:

1. MAT_SOIL_AND_FOAM
2. MAT_BRITTLE_DAMAGE
3. MAT_PSEUDO_TENSOR
4. MAT_WINFRITH_CONCRETE

Moradi compared the finite element results to the test data provided by AFRL to examine the performance of each constitutive model. For the MAT_SOIL_AND_FOAM stress, fringe levels indicated that the exposed wall of the CMU reaches its ultimate strength within the first few msec. Stresses remained at this level as the elements of the exposed wall experienced large displacements in the following msec of the blast. The results closely matched those obtained from the actual blast test conducted at by AFRL at Tyndall AFB.

For the MAT_BRITTLE_DAMAGE stress, fringe levels indicated that most sections of the CMU reached their ultimate strength within the first few msec. However, examination of the displacement fringes and time histories showed that most points on the CMU moved at the same level and at the same time. Displacements seemed to be significantly less than the MAT_SOIL_AND_FOAM case for the same loading conditions. The results matched some of those obtained from the actual blast test conducted by AFRL at Tyndall AFB at most distances, but failed to match those for higher peak pressures.

For the MAT_PSEUDO_TENSOR stress, fringe levels indicated that the exposed front wall of the CMU reached its ultimate strength within the first few msec. Stress levels tended to remain at this level as the elements of the exposed wall experienced large displacements in the msec following the blast. Examination of the displacement fringes and time histories showed that the midpoint of the right front wall of the CMU moved at significantly greater levels than the rear corner or a point on the middle rib of the CMU.

In most cases, the stress levels may have reached the ultimate strength, but fracture did not seem to occur.

For the MAT_WINFRITH_CONCRETE stress, fringe levels indicated that the exposed front wall of the CMU reached its ultimate strength within the first few msec. Stresses tended to remain at this level as the elements of the exposed wall experienced large displacements in the msec following the blast. Examination of the displacement fringes and time histories showed that the midpoint of the right front wall of the CMU displaced more than the other two points of interest. In most cases, the stress level may have reached the ultimate strength, but fracture did not seem to occur. The conclusion drawn was that although the MAT_WINFRITH_CONCRETE constitutive model predicted stress fracture fairly accurately, it seemed to have difficulties predicting displacements.

Overall, the MAT_SOIL_AND_FOAM constitutive model made better prediction than the other three. This model was also the simplest of the four and was developed for cases of plane soils, foams, and concrete. This closely matched the make-up of a common CMU composed of plain concrete material exhibiting simple fracture modes. The other three constitutive models were developed for more complex concrete and reinforced concrete structures. The MAT_PSEUDO_TENSOR model was used for buried, steel-reinforced concrete structures subjected to impulsive loads. Moradi therefore recommended the use of MAT_SOIL_AND_FOAM for analytical investigations of the effects of blast loads on CMU walls.

In the mean time, blast tests on retrofit masonry walls continued at AFRL at Tyndall AFB. Numerous explosive tests were conducted on one-way walls coated with

polyurea to study the composite behavior of wall and polymer. Flexural stiffness due to composite action is a "combination of increased flexural stiffness and the resistance provided by membrane action" (Dinan et al. 2003). For the completely bonded polymer, the bond in shear is much stronger than in tension; therefore, high strains are experienced by the polymer at mortar joints when the wall opens at the joints due to flexure. The front face of the wall fails due to the shear applied by the thrust line associated with the large displacement of the wall. This is one of the reasons that the wall failure point is difficult to determine. In addition, the polymer may not be uniformly sprayed over the entire surface of the wall. High strains in the polymer will develop due to mortar joint failure or due to polymer debonding. When the polymer is not bonded to the masonry, the strain will be more uniformly distributed over the membrane, and the problem becomes similar to the membrane subjected to uniform pressure.

The blast tests at Tyndall AFB demonstrated that low-stiffness polymers reduced the lateral deflection and fragmentation of unreinforced concrete masonry walls (Thornburg 2004). The results suggested that reinforcing masonry walls with elastomeric coatings could significantly increase survival and reduce injuries in blasts. The news prompted numerous manufacturers of polymeric and composite materials to submit candidate samples for use in upcoming blast tests; however, the enormous expense of explosive tests prohibited the evaluation of a broad survey of blast reinforcement candidate materials using a full-scale methodology. Instead, non-explosive methods, such as static flexure tests, the gas gun facility, and the drop tower facility were used to evaluate the potential of each candidate material for blast reinforcement of concrete masonry walls.

Thornburg conducted a host of tests on 53 candidate polymeric and composite materials to evaluate various behavior patterns and properties. The results would allow AFRL to design the follow-on phases of the concrete masonry reinforcement during blast events. The first series of tests were static flexure, from which bond failure mechanisms between the polymer and concrete substrate were identified. The concrete blocks were notched in the center to introduce failure similar to that seen at the mortar joints in full-scale wall tests. Tensile strength, elongation, and bond strength of materials in conjunction with their bonding agents were determined in the static flexure test when the materials remained bonded. For materials that debonded, the test was useful in identifying bond failure mechanisms. Three out of four of the tested materials debonded before material failure was reached.

Thornburg's second series of tests used the high-speed drop tower equipment. These tests provided a method of ranking the effectiveness of dynamic energy absorption and the shear failure mechanisms of potential blast reinforcement materials. Impact energy, total energy, strain energy absorption capacity, and maximum load were determined from the mass and velocity of the impact. The drop tower test provided insight into the failure modes of materials in the dynamic punching shear environment.

Thornburg's third laboratory test explored the use of a gas gun with projectile velocities approaching 1,000 ft/sec. Samples of the elastomeric polymer were placed in the gas gun and impacted with projectiles. The ballistic limit of several candidate materials was achieved for numerous specimens, and the total energy absorbed was calculated for each of these specimens. The gas gun facility was also used to test polymer-coated concrete blocks. The energy capacity of each was calculated from data

provided by the testing apparatus. The polymer coating did not experience local punching and did not fail during testing. Thornburg also discussed the uniaxial tension tests performed at the AFRL. The tests quantified the stress-strain properties of each of the 53 candidate materials through rupture and determined their other material properties. These materials exhibited a wide range of properties during the uniaxial tests, as documented by Thornburg.

In 2004, Sudame examined the impact of the work performed by Connell, Moradi, and Thornburg by developing computational models and performing input-sensitive studies of polymer retrofit concrete masonry walls (Sudame, 2004). Sudame developed a baseline model of a one-way flexure, single-CMU-width masonry wall for his investigation. The overall dimensions and support conditions reflected tests conducted at AFRL. After a number of frequency analyses, Sudame adopted a 5% global damping value for his investigation. He induced gravity loads using dynamic relaxation methods of LS-DYNA and noted they had little influence on the lateral displacements of the wall.

For the input-sensitive study, Sudame systematically altered the parameters of the baseline model in order to examine their effect on the global response of the wall. He varied such parameters as initial modulus, yield strength, rupture strain, polymer thickness, bond strength between mortar joints, and bond strength between polymer and CMUs. Significant reduction was noted in the internal energy of the polymer when the rupture strain was reduced from 10% to 2%; however, no impact was noted for displacements and velocities. Sudame changed the thickness of the polymer from 1/16th of an inch to 4/16th of an inch in increments of 1/16. He noted no significant change in

displacement and velocity, but the strain energy and the kinetic energy in the polymer increased significantly. Changes in the initial modulus of the polymer by multiples of 10 had no significant effect on the displacement and velocities; however, Sudame noted that an increase in the elastic modulus of the polymer decreased the peak strains in the polymer and increased the internal energy it absorbed. Overall, Sudame was able to achieve a close correlation between some of the test data and his computational models.

3 DYNAMIC TESTS

3.1 Tests Performed at Tyndall AFB in 2001 and 2002

In 2001, AFRL began a testing program at Tyndall AFB to evaluate the effectiveness of reinforcing walls for blast using spray-on polymer coatings. Twelve explosive tests were conducted. Seven of these involved testing of masonry walls and were known as Wall test 1, 2, 3, 9, 10, 11, and 12. Unreinforced concrete masonry walls were constructed for each test. Some walls were coated with polymer, while others were used as controls. The control wall collapsed in the first three tests, but the polymer retrofit walls survived in tests 1 and 3. After the effectiveness of the polymer masonry walls was established, some tests did not involve control walls. Bonding techniques, doors, and windows were part of this series of tests.

A typical test set-up consisted of reaction structures; concrete masonry walls, some of which had polymer retrofits; and a blast source at a certain stand-off distance, as shown in Fig. 3.1-1. The reaction structures were equipped with gauges to measure pressures, deflections, and accelerations. Predictions were made for each gauge in each test and compared to recorded data. High-speed and digital still photography were used to aid in the analysis of test data. Fig. 3.1-2 shows the pre-test finished walls.

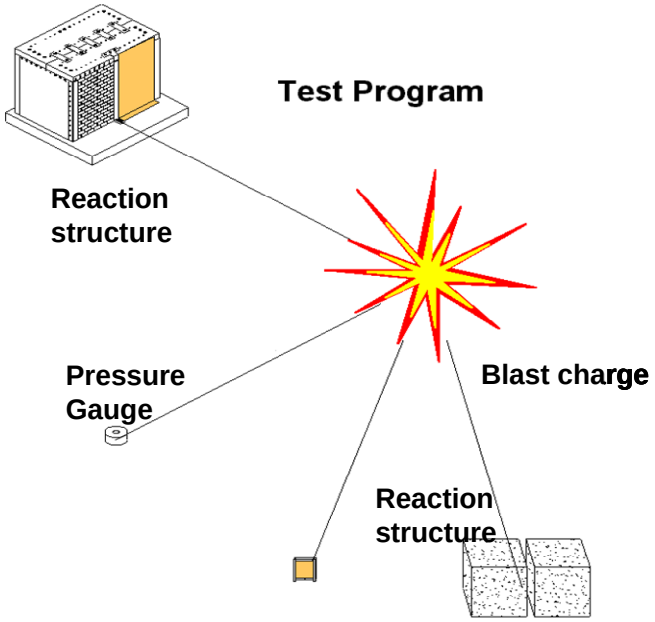

Fig. 3.1-1: Typical test set-up

Fig. 3.1-2: Typical finished test walls

The tests clearly indicated that the polymer reinforcement approach is effective in reducing the vulnerability of unreinforced, non-load-bearing CMU walls subjected to

blast loading. The application options are not overly burdensome, and the explosive tests indicated that a 10-fold increase in peak pressure is resisted by polymer-reinforced one-way flexure walls, compared to unreinforced concrete masonry walls. Although the reinforced walls are of little economic value after the blast event, they reduce the risk to building inhabitants and save lives.

However, predicting the lateral pressure that can be resisted by a polymer reinforced wall is complicated by the variability in mortar joint flexure bond and shear strength, inconsistencies in polymer thickness or continuity over surface irregularities, and the fracture of the front face of the masonry blocks. Overall, five factors characterize the behavior of the polymer-reinforced masonry wall subjected to blast:

1. A stress wave that may weaken parts of the system, such as the block/mortar bond.
2. High localized shear at the block/mortar interfaces closest to the supports, resulting in shearing of the polymer coating.
3. Fracture of the front face of some of the blocks due to high local stresses from peak pressure or due to flexural compression of the front face of the wall.
4. Tearing of the polymer reinforcement in tension as the wall flexes.
5. Tearing or loss of adhesion of the polymer at the connection to the host structure, resulting in the collapse of the system.

All control walls failed catastrophically without providing added failure mechanism data.

The spray-on polymer treatment demonstrated an excellent bond between the polymer and the masonry. The length of polymer being strained increases as the blocks separate. It is important to realize that the tensile bond between the mortar and the masonry is weak (50-150 psi). Once the polymer begins to strain, the length of polymer involved extends across the mortar joint for slightly more than half of the block height in each direction. The bond between block and polymer is stronger in shear than the tensile strength of the concrete. Consequently, the polymer cracks the concrete as strain progresses.

For the charge sizes and distances considered in this investigation, the forward pressure on the wall (positive phase) resulting from the test explosions lasts only about 10 msec. Although the peak pressure varied between tests, the shape and duration of the load curve did not vary substantially. Some damage may result from the initial stress wave that travels through the depth of the masonry; however, due to the mass involved, the flexural response of the system is spread over a broader timeframe (approximately 60 msec), and a velocity of approximately 300 in/sec is imparted to the wall.

Front face fracture of the masonry units has been consistently observed. The block is often broken into several pieces, but sometimes the front face shears from the webs and survives as one piece. The fracture tends to be concentrated near the supporting edges. It was also observed that the fracture point within the block is deepest nearest to the supports.

Wall test 12 was conducted to address some of the failure mechanism questions. The walls of test 12 were constructed without mortar, i.e., the blocks were simply stacked on top of each other in a typical running bond pattern. The thin gap at the top of the wall between block and structure was tuck pointed with mortar. A polymer coating was applied directly to the interior of the wall in the same way as the other tests for one wall, while the polymer coating was sprayed onto a plastic membrane liner on the inside of the other wall so that there was no bond between the masonry and the polymer reinforcement (catcher system).

The wall coated directly withstood the blast without collapse. Front face fracture occurred over the lower three courses of block and was sporadically distributed over several other blocks. Polymer tearing initiated for several inches from both sides at approximately the height-wise center of the wall. It also appears from careful post-test analysis of the reaction frames and high-speed videos that flexural rotation lifted the roof of the reaction frame. This indicates dramatic increases in the arching forces as compared to a standard mortared wall. The polymer of the second wall (polymer sprayed onto the membrane) tore at the top support attachment, and the wall collapsed. The lack of an integrated masonry-polymer system (no bond between the blocks and polymer) allowed the polymer coating to act as a “catcher” membrane and resulted in a higher concentration of force at the connection of the polymer to the reaction frame. Although collapse occurred, the rubble was contained to the forward part of the structure and, compared to a masonry wall without polymer reinforcement, a high level of occupant protection would have been provided.

Wall tests 9, 10, and 11 involved window and door openings. The overall objective of these tests was to examine the influence of typical window and door frame openings on polymer reinforcement effectiveness and failure mechanisms. These tests also involved a 1/8-inch coating with a 12-inch overlap onto the reaction structure. The walls in test 9 did not include an overlap of polymer coating onto the window or door frame. Walls in tests 10 and 11 involved a wider wall structure than the other walls (16 feet vs. 7.5 feet) to eliminate edge condition effects on walls with openings. Wall test 11 involved a heavily anchored window frame with polymer overlap onto the frame.

Overall, the polymer provided the same level of effectiveness for walls with the openings as walls without openings. Front face fracture occurred, with an evident tendency for fracture around the stiff window and door frames. There was evidence of increased tendency for mortar joint cracking compared to walls of the same test and construction parameters without door or window openings. A large lower portion of wall test 9 (containing a door frame) was breached. There was also evidence of a tendency for tear initiation of the polymer coating at the corners of the window frames.

Flexural wall response dissipates as cross-sectional structural integrity is lost. The two primary causes for the loss of structural integrity under blast loads are mortar joint separation due to bond, flexure, or shear, and the failure of the front face of individual blocks. In some of the tests, large areas maintained integrity, with mortar failure limited to three or fewer joints. Careful post-test analyses revealed that wall behavior involves several mechanisms at different stages of the wall response. The order of these failure mechanisms can vary. If the slope change at the critical stress area is severe, then shear may develop in the polymer coating at the rough block edges. The

polymer tears sooner in these situations than in those where the polymer is subjected predominantly to tension.

Wall Test 1

Fig. 3.1-3 shows the walls after the blast test. The wall without polymer retrofit (left wall) collapsed, whereas the wall with polymer retrofit (right wall) stayed in place.

Fig. 3.1-3: Wall damage after the test

Retrofitted Wall: The top courses of the block experienced front face failures. Some of the webs in these courses were fractured. There was defacing at the bottom of the CMU wall. Cracks in the mortar joints were visible at the bottom and midpoint. On the inside of the wall, there was a polymer tear at the midpoint mortar joint crack. The top and bottom courses were held in place by angles and were not damaged. The retrofit was successful in preventing debris from entering the structure. The stress strain curve for the polymer retrofit (Fig. 3.1-4) used in this test is a smoothed version of the curve shown in Sudame (2004).

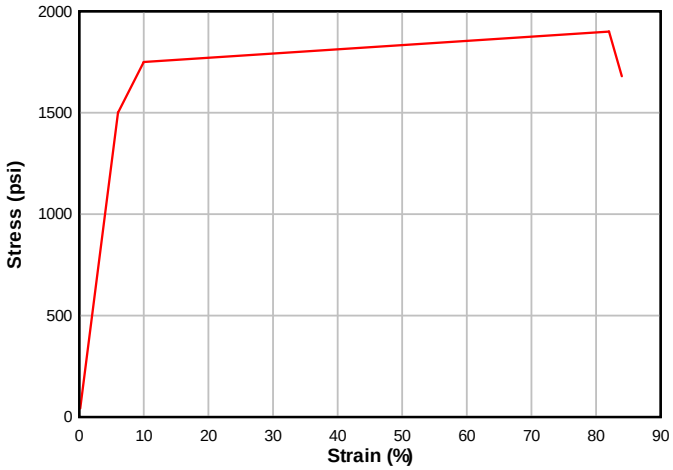

Fig. 3.1-4: Static stress-strain curve for the spray-on polymer

The maximum displacement for this test was measured at 7.2 inches by laser deflection gauge L1 (B) located at the center of the wall, and the displacement and velocity time histories are shown in Fig. 3.1-5.

Unretrofitted Wall: This wall collapsed.

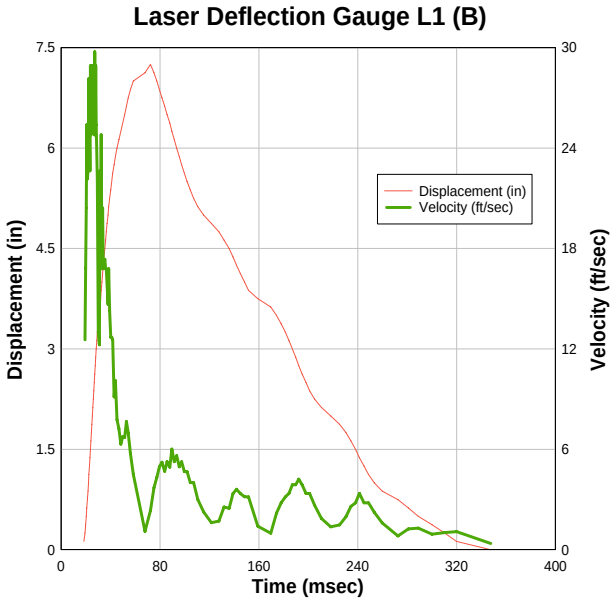

Fig. 3.1-5: Centerline deflection for the retrofit CMU wall

Wall Test 2

The higher charge in this wall test greatly exceeded the lateral load capacity of the walls, as both the retrofitted and unretrofitted walls collapsed. A tear occurred at the midpoint of the polymer and extended across the entire width of the right wall. The stress-strain curve for the polymer retrofit used in this test is shown in Fig. 3.1-4. Collapse prevented a measurement of the maximum displacement.

Wall Test 3

1/4-inch Thick Interior Retrofitted Wall: The top courses in this wall experienced front face failures and web shear. Mortar joints at the midpoint experienced visible cracks across the entire width of the wall. In the interior, there was significant tearing of the polymer near the top of the wall. The poor bond that was observed between the polymer and the floor had minimal effects on the performance of the polymer. Displacement was highest at the top of the wall. There was minimal deflection at the bottom of the wall. Overall, the polymer was successful in preventing fragments from entering the reaction structure. The stress-strain curve for the polymer retrofit used in this test is shown in Fig. 3.1-4.

1/8-inch Thick Interior/Exterior Retrofitted Wall: The post-test polymer membrane shape did not match the interior residual shape. Front face failure and polymer separation were the primary explanations. It appeared that the polymer coating pulled apart and took the bonded block fragments with it. The polymer remained bonded to the majority of the wall. There was a 4-inch tear in the polymer near the top exterior.

On the interior of the wall, there was an 18-inch tear and protruding block faces. Deflection in this wall was highest at courses 16 and 17. Deflections above this line were curved; those below the line were linear. Joints 16 and 17 appeared to be the weakest joints in the wall.

Left Retrofitted Cubicle (6 inches Overlap): Several of the top and bottom courses suffered complete defacing. The polymer on the inside of the structure was undamaged. The shorter wall had less deflection, preserving the integrity of the polymer. Nearly 70% of the wall experienced front face failure; however, the polymer was successful in keeping debris out of the reaction structure.

Right Retrofitted Cubicle (12-inch Overlap): The bottom three and top two courses experienced complete exterior defacing. Nearly 60% of the wall experienced full or partial front face failure. Interior mortar joints were unaffected. The deflection of the wall was greatest at courses 10 and 11. On the interior, there was a 4-inch of tear in the polymer near the top of the wall, and there was 2 feet of tear at the bottom. Nonetheless, the polymer was successful in preventing wall fragments from entering the reaction structure.

Wall Test 9

Wall with Door: Bottom courses on both sides of the doors and blocks near the top experienced front face failure (Fig 3.1-6). There were wide cracks in mortar joints at the midpoint. Tearing of the polymer occurred along the entire width of the wall at courses 2 and 3. There was also a small tear at the upper left corner of the top of the door. The polymer failed late in the wall response at the bottom left of the door. This

allowed some block fragments to barely enter the structure. The door hinges failed, and the door entered the structure. The stress-strain curve for the polymer retrofit used in this test is shown in Fig. 3.1-4.

Wall with Window: The top courses experienced complete front face failure. Many other blocks in this wall experienced partial front face failure. There were significant and sporadic mortar joint cracks throughout the wall. There was a 2-inch tear at the lower left corner of the window and a ½-inch tear near the upper right corner. The polymer was successful in preventing fragments from entering the structure; however, the window glazing and the wooden perimeter around the window frame, which were not protected by the polymer, entered the structure.

Fig. 3.1-6: Pre- and post-test pictures of walls in test 9

Wall Test 10

Wall with Door: Front face failure occurred on the right side of the wall near the bottom of the door. There was also defacing across the top of the structure. There were some cracks, indicative of shear failure, near the top of the door. There was a significant polymer tear on the interior of the wall at joints 11 and 12. There were smaller midpoint

tears. The stress-strain curve for the polymer retrofit used in this test is shown in Fig. 3.1-4.

A single block at the back of the wall protruded into the structure; however, it remained bonded to the polymer and did not break away from the wall. The door was torn from its hinges but did not enter the structure. The polymer was successful in preventing the entrance of flying debris. The strength of the center wall strip containing the door frame appears to have prevented the wall from collapsing.

Cubicle: The wall in the cubicle for test 10 collapsed. The cubicle was not wired.

Wall Test 11

There was significant damage in many courses of the wall on the front face. There were mortar failures in a step-like fashion from the window to the top of the wall. Several small tears occurred in the interior polymer near the bottom. The polymer used on the wall was successful in preventing secondary fragmentation. The stress-strain curve for the polymer retrofit used in this test is shown in Fig. 3.1-4.

Wall Test 12

Bonded Retrofit Mortarless Wall: Front face failure occurred mostly at the bottom of the wall, although there was sporadic defacing throughout. Blocks near the top of the wall dislodged outwardly. There were problems with the polymer due to temperature conditions when it was applied. The cure time of the polymer was approximately twice as long as on a warmer day, which caused air pockets between the layers of the polymer. There were some tears in the polymer, both through the air

pockets and otherwise. The retrofit was still successful in preventing flying debris. The stress-strain curve for the polymer retrofit used in this test is shown in Fig. 3.1-4.

Unbonded Retrofit, Mortarless Wall: The wall with the polymer separated by a plastic membrane sheared at the top attachment and collapsed. This confirms that the bonding of the polymer is an important parameter in its effectiveness. The tears in the polymer were thought to be caused by the collapse of the wall.

3.2 Tests Performed at Tyndall AFB Since 2003

BREW Test 1

In this test, an unreinforced lightweight CMU wall 8 feet wide by 10 feet high is used in the modified opening of a coupled culvert structure. The interior surface of the wall was painted and allowed to dry thoroughly before trowel-on polymer 0.20 - 0.40 inch thick is applied. A one-step smooth trowel process is used on the west half of wall, whereas on the east half a notched trowel application was used to set the coating thickness (ridges), the coating was cured overnight, and polymer was applied to fill the grooves and establish a smooth finish. The stress-strain curve for this test was provided by AFRL, and a smoothed version is shown in Fig. 3.2-1.

The trowel-on polymer retrofit on the CMU wall preformed well during the blast test. Though the exterior wall sustained considerable damage, no tears, thinning, or loss of adhesion was visible on the polymer retrofit, and secondary fragments were prevented from entering.

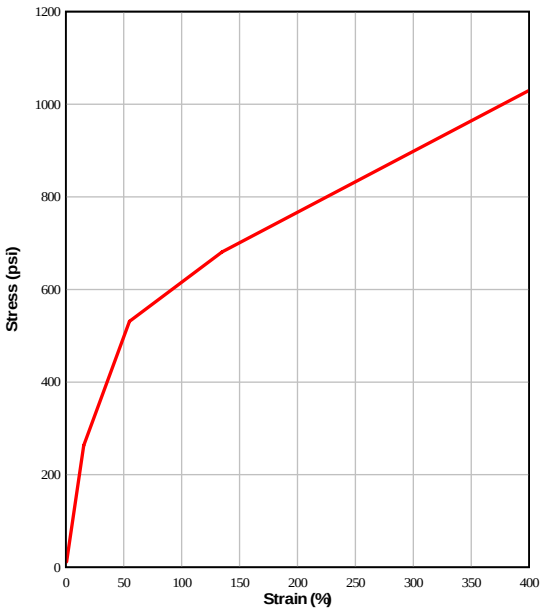

Fig. 3.2-1: Stress strain curve for BREW test 1

Fig. 3.2-2 shows the displacement time history measured by displacement gauge D3 at the center of the wall.

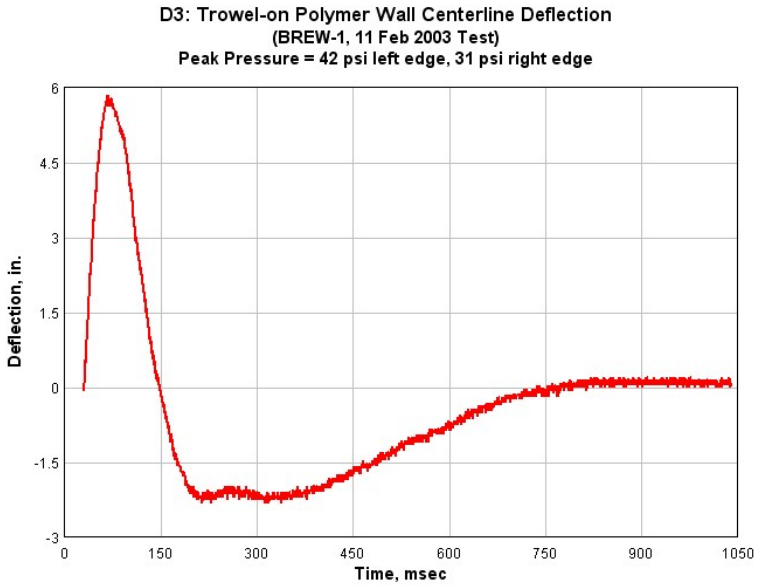

Fig. 3.2-2: Centerline deflection for trowel-on polymer CMU wall

Some of the lessons learned are as follows:

1. The thickness, trapped air, adhesion, and performance differences between application methods (1-step smooth trowel and 2-step notched trowel) appear negligible.
2. The resulting thickness with existing trowel-on methods is 2 to 3 times the standard spray application, yielding similar performance results.
3. Thickness control and finish aesthetics for the trowel-on application method need improvement.

BREW Test 2

An unreinforced CMU wall 7.5 feet wide by 12 feet high with trowel-on polymer retrofit (stress-strain curve shown in Fig. 3.2-1) and a PAL 4 window were used in the test. The test objectives were as follows:

1. Evaluate performance of trowel-on polymer on non-reinforced CMU wall with a window 4 feet wide by 6 feet high centered in the wall.
2. Determine if CMU blocks restrained against movement will experience front face failures in this threat.

The one-step trowel-on polymer has a thickness of 0.20-0.40 inch. The trowel-on polymer retrofit came very close to preventing the wall from collapsing. A sub-standard

overlap on the ceiling initiated the collapse after a maximum deflection estimated at 12-14 inches was reached. The lessons learned from this test are as follows:

1. A consistent adhesion and thickness of the trowel-on polymer overlap on the ceiling is critical to the success of a trowel-on polymer retrofit and more crucial than with spray-on polymer when the overlap area is irregular.
2. There is a need to devise trowel-on polymer application methods to deal with ceiling overlap irregularities that can be reasonably expected in existing facilities.
3. The front faces of CMU blocks restrained against movement did not fail for this threat. Consequently, it is unlikely that the local response/behavior of CMU front faces is a major factor in the front-face failures observed in successful polymer-reinforced CMU walls.

BREW Test 3

These walls were not constructed with CMUs.

BREW Test 4

One CMU wall was tested, but the wall dimensions are unknown.

BREW Test 5

Two unreinforced CMU walls were tested. The two walls had different polymer retrofits sprayed on their inside face. The stress-strain curves for these retrofit polymers were not available. Both walls survived the test.

BREW Test 6

A standard CMU wall with a 120-mil polymer retrofit on the inside face anchored to floor and ceiling and a polymer retrofit on the exterior face was tested. The post-test exterior view showed the remains of the CMU wall partly standing due to the polymer's ability to return to its original shape. Results also showed that supports kept the polymer intact, enabling it to provide sufficient protection from fragmentation. Any damaged elements were retained outside of the structure, and much of the CMU wall remained. There was minimal debris entering the structure, and the wall exhibited very little deflection. The stress-strain curves for this retrofit polymer were not available.

BREW Test 7

Two 12 feet by 8 feet CMU walls were tested. One wall incorporated 1/4-inch thick polymer retrofit. The stress-strain curve for this polymer was provided by AFRL, and a smoothed version is shown in Fig. 3.2-3. The other wall used a different 1/4-inch thick polymer retrofit (stress-strain curve not available). Both walls survived the blast test.

BREW Test 8

Two 12 feet by 8 feet CMU walls were tested. One wall incorporated 1/8-inch thick polymer retrofit, and the other wall used a different 1/8-inch thick polymer retrofit. The left wall survived with some damage to the outside face, and the right wall

experienced partial collapse. The stress-strain curve was provided by AFRL and a smoothed version is shown in Fig. 3.2-4.

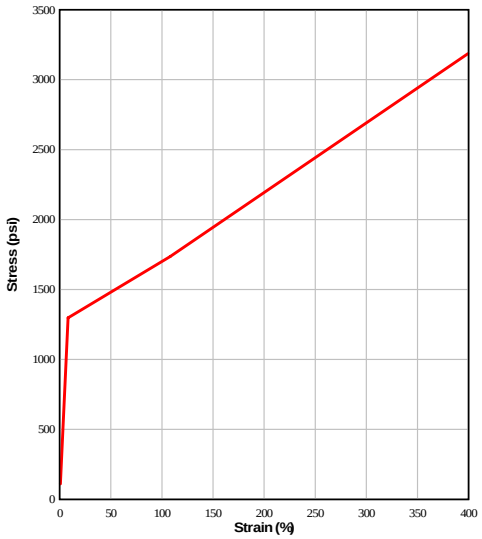

Fig. 3.2-3: Stress strain curve for BREW test 7a

BREW PSEAG Test

A standard CMU wall was retrofitted with a catcher-type polymer sheet. The stress-strain curve was provided by AFRL, and a smoothed version is shown in Fig. 3.2-5. Several parameters in this test were different than those in any of the other tests discussed. A simulated vehicle search area was set up that included two walls, one of which had a retrofit over a common CMU wall construction. The test included multiple barriers used around the vehicle to replicate the damage incurred by the structures and barriers due to the pressure and fragmentation from explosives concealed in a vehicle. The wall deflected excessively but survived the test.

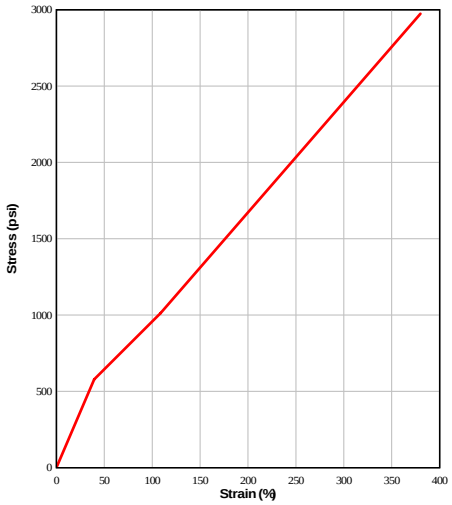

Fig. 3.2-4: Stress strain curve for BREW test 8

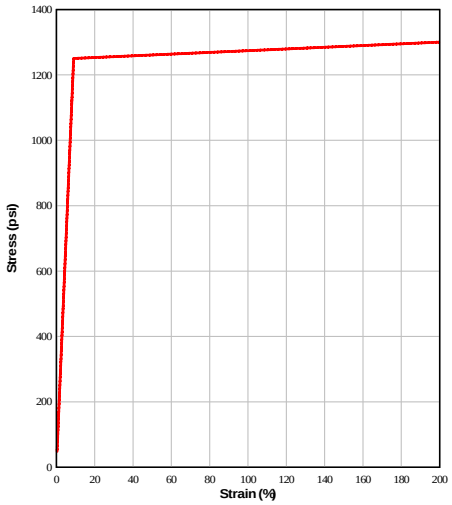

Fig. 3.2-5: Stress strain curve for BREW test PSEAG

3.3 Test results

The results of the tests discussed in this section are shown in Table 3.3-1. The table shows the tests numbered consecutively, the thickness and type of retrofit used in each test, the height and width of each wall, the size of the door or window if present, the

maximum reflected pressure measured at the center of the wall, the impulse associated with that pressure, and the maximum lateral wall deflection at its mid-point.

The wall tests conducted by AFRL indicate that a polymer retrofit approach is effective in reducing the vulnerability of unreinforced concrete masonry walls (Thornburg 2004). Although most of the walls did not collapse, they were of little structural value after the blast event. Their value, however, resided in the fact that they reduced the risk to building occupants and saved lives.

The response of polymer retrofit walls to blast is very complex and highly sensitive to loading (peak pressure and impulse) and support conditions (Thornburg 2004). It is crucial to develop an engineering description of their resistance to lateral pressure up to their ultimate load-carrying capacity.

Table 3.3-1: Test results

Wall Test	Retrofit (in)	h (ft)	Width (ft)	Door (ft x ft)	Window (ft x ft)	Max. Reflected Pressure (psi)	Impulse (psi-msec)	Test Max. Defl. (inch)
1	1/8 Line-X XS-350	12	7.5	None	None	57	212	7.2
2	1/8 Line-X XS-350	12	7.5	None	None	238	398	Failed
3	1/4 Line-X XS-350	12	7.5	None	None	59.4	227	9.38
3a Cubicle	1/8 Line-X XS-350 6 inches of overlap	8	8	None	None	64.2	Not available	4.94
3b Cubicle	1/8 Line-X XS-350 12 inches of overlap	8	8	None	None	69.1	Not available	5.94
9a	1/8 Line-X XS-350	10	7.5	None	2.5 x 2.5	61.1	230	7.71
9b	1/8 Line-X XS-350	10	7.5	7 x 3.5	None	61.1	230	5.63
10	1/8 Line-X XS-350	12	16	7 x 3.5	None	43.3	188	7.4
11	1/8 Line-X XS-350	12	16	None	4 x 3	38.3	Not available	9.5

Table 3.3-1: Test results – Continued

Wall Test	Retrofit (in)	h (ft)	Width (ft)	Door (ft x ft)	Window (ft x ft)	Max. Reflected Pressure (psi)	Impulse (psi-msec)	Test Max. Defl. (inch)
12a	1/8 Catcher Retrofit Line-X XS-350 Mortarless	12	8	None	None	41.8	Not available	Failed
12b	1/8 Line-X XS-350 Mortarless	12	8	None	None	41.8	Not available	8.1
BREW 1	0.2 - 0.4 B1	10	8	None	None	42.1	213.72	5.8
BREW 2	0.2 – 0.4 Trowel-on B1	12	7.5	None	4 x 6	41.2	234.63	Failed
BREW 4	1/8 Line-X XS-350 12 Assumed	12 Assumed	8 Assumed	None	None	40.4	192.89	8.5
BREW 5	0.12 Polypropylene	12	7.5	None	None	22.2	147.41	3.69
BREW 6	0.12 Catcher Retrofit B&H Clear	12	8	None	None	54.7	Not available	Not available Survived
BREW 7	1/4 3572-37-1	12	8	None	None	43.8	247.94	7.7
BREW 8	1/8 3572-74-2	12	8	None	None	50	242.62	11.6
BREW PSEAG	1/8 Catcher Retrofit B&H	12	8	None	None	53.89	192.87	12.9

4 FINITE ELEMENT MODELING

As mentioned in Chapter 2, a number of available constitutive (material) models in LS-DYNA were examined to arrive at the one most suitable for the behavior of concrete masonry walls during blast (Moradi 2003). The focuse was on a single CMU, and four of the most promising constitutive models in LS-DYNA were used in the finite element analysis.

1. MAT_SOIL_AND_FOAM – Material type 5 in LS-DYNA
2. MAT_BRITTLE_DAMAGE – Material type 96 in LS-DYNA
3. MAT_PSEUDO_TENSOR – Material type 16 in LS-DYNA
4. MAT_WINFRITH_CONCRETE – Material type 84 in LS-DYNA

The LOAD_BLAST option of LS-DYNA was used to simulate the blast. Analyses were performed for a maximum of 25 msec using the CONWEP (LS-DYNA 1999) blast loads for different charges and stand-off distances. Moradi calculated the blast pressure using CONWEP for each distance and applied it to the front face of the CMU. Stress, displacement, and energy results were studied for each load level to examine the failure modes of the CMU. The results of the analyses for the four selected constitutive models were compared to those of the blast tests provided by AFRL.

4.1 Wall Models

Connell (2002) constructed a finite element model of a full-scale wall with the polymer retrofit material alone as shown in Fig. 4.1-1 (the colors have no significance).

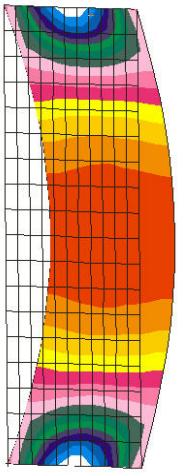

Fig. 4.1-1: Finite element model of a full-scale wall with retrofit only

The model was analyzed using the MSC-NASTRAN finite element code. A wall 12 feet in height by 7 feet 4 inches in width was meshed into 18 elements vertically by 11 elements horizontally. Only the top and bottom of the wall were restrained in translation to simulate one-way bending action. The elements were 0.125-inch thick and were loaded with uniform lateral pressure. They were assigned a nonlinear stress-strain relationship based upon material properties obtained from tests performed by the AFRL. The results of the analysis are shown in Fig. 4.1-2, which is known as the static resistance function of the retrofit material. The curved part of the resistance function pertains to the elastic membrane action of the material, and the linear straight part of the curve represents the plastic membrane action of the material. This figure indicates that the retrofit material provides little resistance until large displacements have occurred. It

further shows that the retrofit stays in its elastic membrane phase for displacements of up to 25 inches.

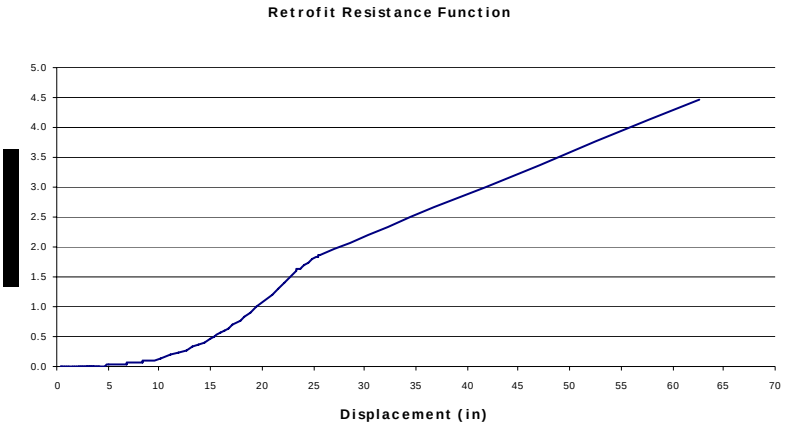

Fig. 4.1-2: Polymer retrofit material resistance function

Sudame (2004) constructed a baseline model for a series of input-sensitive studies. The model contained 48760 solid elements and 8070 shell elements and was subjected to the following AFRL load I and load III conditions. While load I was used in field tests conducted by AFRL, load III was not used in the field. The time histories, peak pressures, and impulses of the two loads are given below:

(1) Load I: peak pressure = 66.3 psi, impulse = 214.8 psi-msec, load time history is shown in Fig. 4.1-3.

(3) Load III: peak pressure = 129.9 psi, impulse = 356.8 psi-msec, load time history is shown in Fig. 4.1-4.

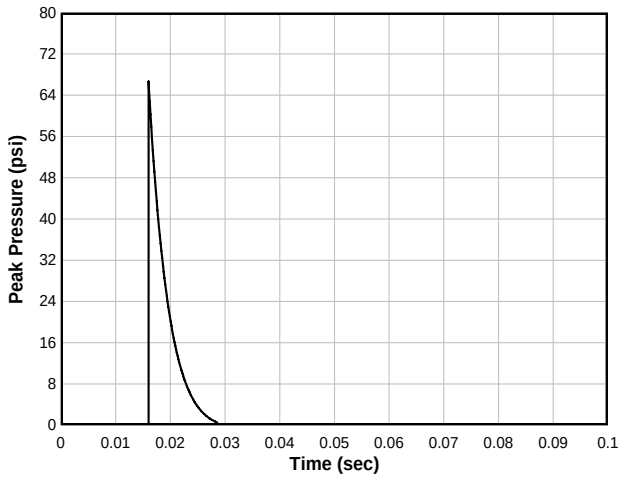

Fig. 4.1-3: Load time history for load I

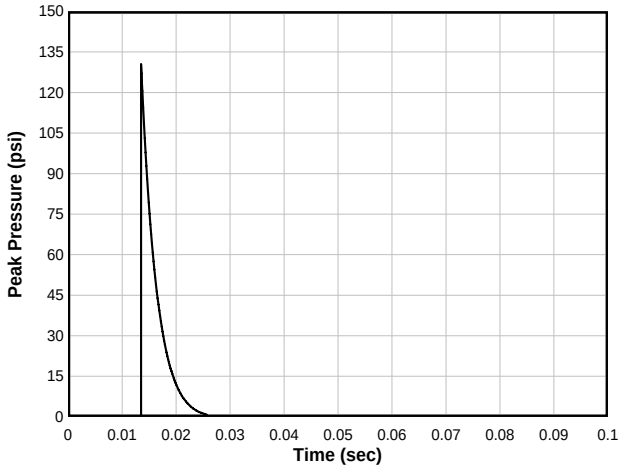

Fig. 4.1-4: Load time history for load III

The masonry wall structures involved in the explosive tests conducted by AFRL had six key components that had to be accurately included in the model development: the CMU, mortar joint interfaces, polymer retrofit (material behavior and interface with masonry), and roof and floor boundaries. A picture of a typical test wall was provided by AFRL and is shown in Fig. 4.1-5.

Fig. 4.1-5: Test wall setup

Each test wall is 12 feet tall by 8 feet wide and made of 8-inch CMU block. The system was subjected to the blast loads described herein. There is a rapid variation of stresses and strains in the wall components. To effectively capture this phenomena, the selection of appropriate material models is critical.

The setup used unreinforced masonry walls measuring 7 feet 4 inches in width and 12 feet in height, as shown in Fig. 4.1-6. The density of masonry concrete is approximately 0.07 pound/inch^3, which results in a weight of each block of approximately 32 pounds. The walls were constructed in reusable reaction structures. 3-inch x 4-inch x 0.25-inch steel angles were placed at top and bottom of the test wall to restrain lateral movement (Thornburg 2004).

The typical CMUs used in the tests were standard hollow concrete blocks weighing 32 pounds. The dimensions of the blocks were 7.625-inch x 7.625-inch x 15.625-inch. The outer edges of the block were 1.25-inch thick, and the center web was 1-inch thick. The blocks have a nominal compressive strength of 2000 psi. Mortar joints

of approximately 3/8-inch thickness with type-N mortar separated the blocks (Connell 2002).

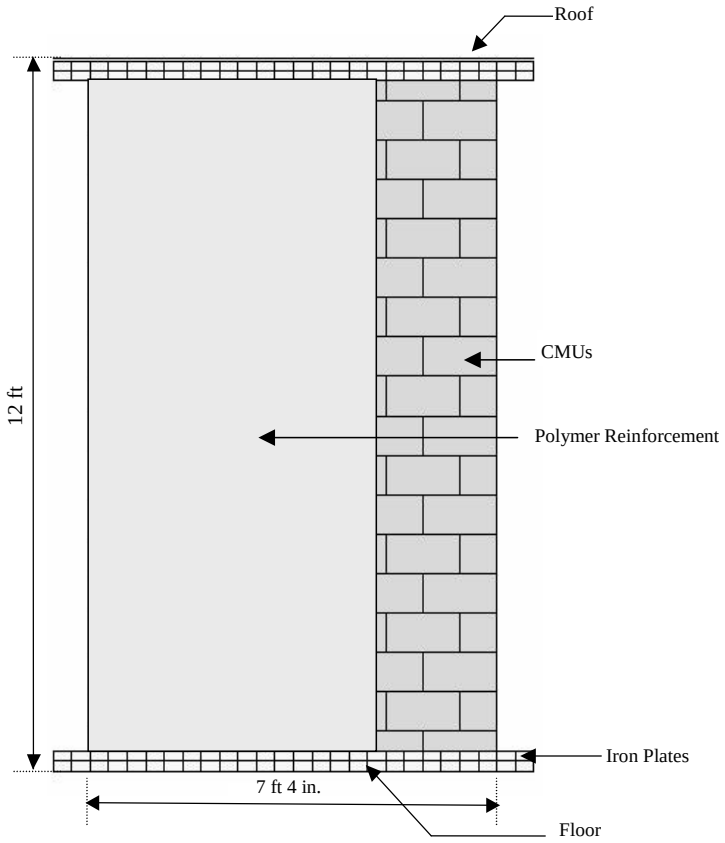

Fig. 4.1-6: Schematic of wall setup

The spray-on polymer used for reinforcing was primarily comprised of polyurea. Table 4.1-1 provides the key mechanical characteristics of the material considered (Davidson et al. 2004). The stress-strain curve obtained from static uniaxial tension tests conducted by AFRL is shown in Fig. 3.1-4, where it is noted that the material exhibited a discernible yield point and an elongation capacity of approximately 80% (Knox et al. 2000).

Sudame's baseline model consisted of 18 hollow concrete blocks connected by a mortar interface. Mortar was simulated only over the flanges of the concrete blocks.

Table 4.1-1: Properties of Polyurea

Property	Value
Modulus of Elasticity	34000 psi
Tangent Modulus	3400 psi
Elongation at Rupture	89%
Stress at Rupture	2011 psi
Maximum Tensile Strength	2039 psi
Density	90 pound/ft^3
Poisson's Ratio	0.4
Shear Modulus	11620 psi

The CMUs were supported by the rigid floor boundaries. A gap was placed between the top most block and the roof boundary with the thickness of one mortar layer. This provided room for the rotation of the top block.

A boundary 1-inch wide extending through the width of one block on the backside at the top and bottom provided a restraint against any lateral movement of the wall. The side subjected to the blast load is referred to as the "front". A 0.125-inch polymer coating was simulated only on the rear of the block. The distance between the boundaries and the block was equal to the thickness of the polymer. Fig. 4.1-8 illustrates the overall model setup. The colors shown in Fig. 4.1-8 are a visual aid and have no significance. Various contact definitions and parameters were selected as follows:

(1) The MPP version of LS-DYNA does not support the CONTACT_ TIEBREAK_SURFACE_TO_SURFACE contact type. Interfaces between blocks and mortar layers were modeled using the TIEBREAK_NODE_ TO_SURFACE contact type. Node sets were made slaves, and the segment sets were made master in each block-

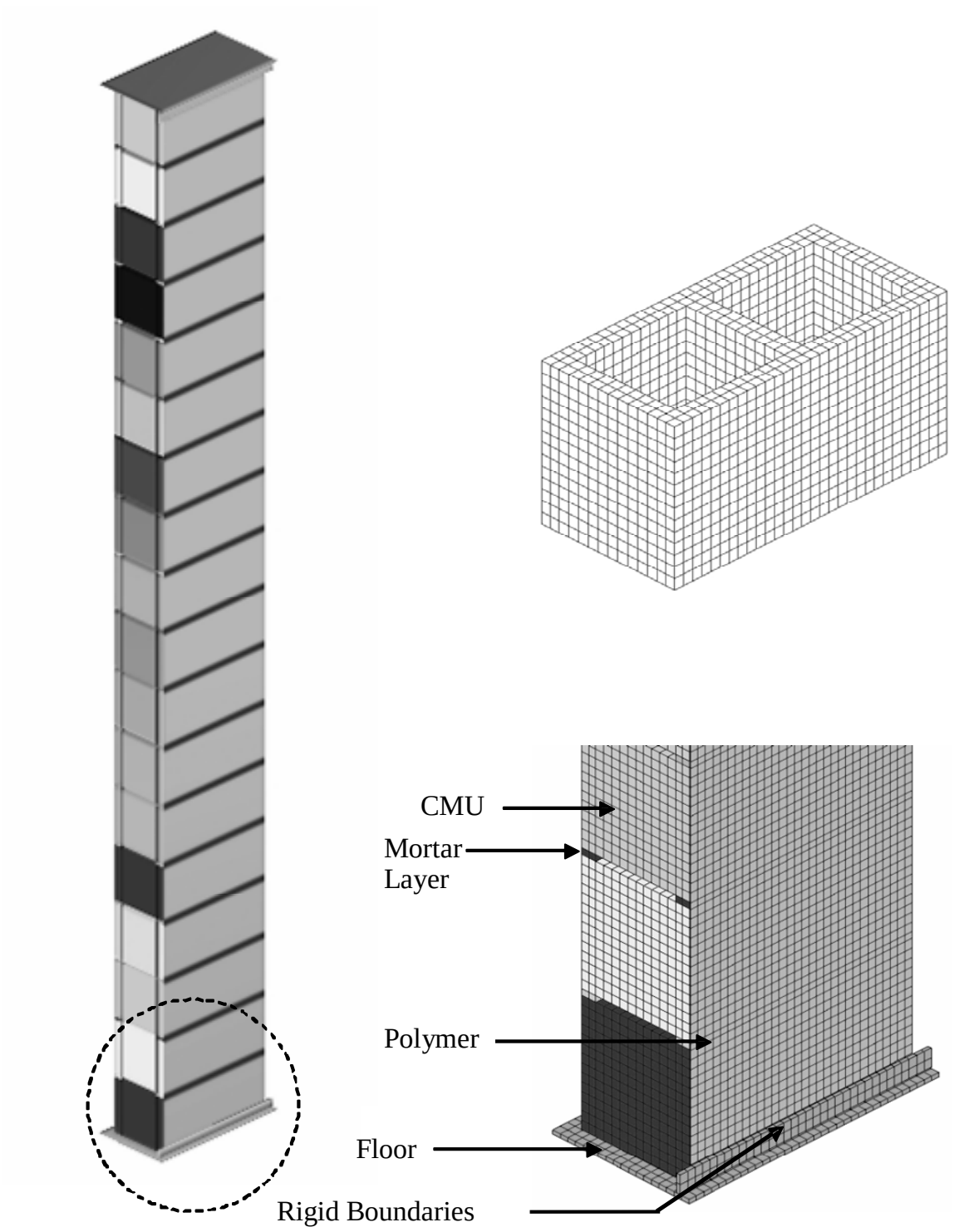

Fig. 4.1-8: Baseline model setup

mortar interface contact. Failure criteria was dictated by NFLS equal to 100 psi and shear SFLS equaling 250 psi (Drysdale et al. 1994).

(2) The TIEBREAK_NODE_TO_SURFACE contact definition was used for contact between the polymer and the blocks. Polymer nodes were made to act as slaves and the block segment sets as master.

The spray-on polymer approach results in a very strong bond between the concrete and the polymer (Thornburg 2004), so a value of 1 was used for the static coefficient of friction. The value of dynamic friction chosen was 0.8, which is the friction between concrete and rubber (Avallone and Baumeister 1987). Pull tests on polymer-reinforced concrete block resulted in concrete spalling without separation of polymer from concrete (Dinan et al. 2003); therefore, a 150-psi tensile limit was used as the normal failure force for the bond between polymer and concrete, and a shear failure force of 1000 psi was used for contact definition.

The rigid top and bottom boundaries resist the lateral translation of the wall, which results in high shear forces at the top-most and bottom-most mortar joint interfaces. Relative motion occurs between the lowermost block and the block above it due to less freedom for rotation. A similar phenomenon is observed near the upper block (Fig. 4.1-9 b); however, the space between the top block and roof boundary allows the upper block to rotate. Less shear is observed at the top mortar joint as compared to the shear at the bottom mortar joint. The amount of rotation that occurs depends on the presence of rigid boundaries on the front side and their width. Absence of the boundaries results in more rotation and less shear.

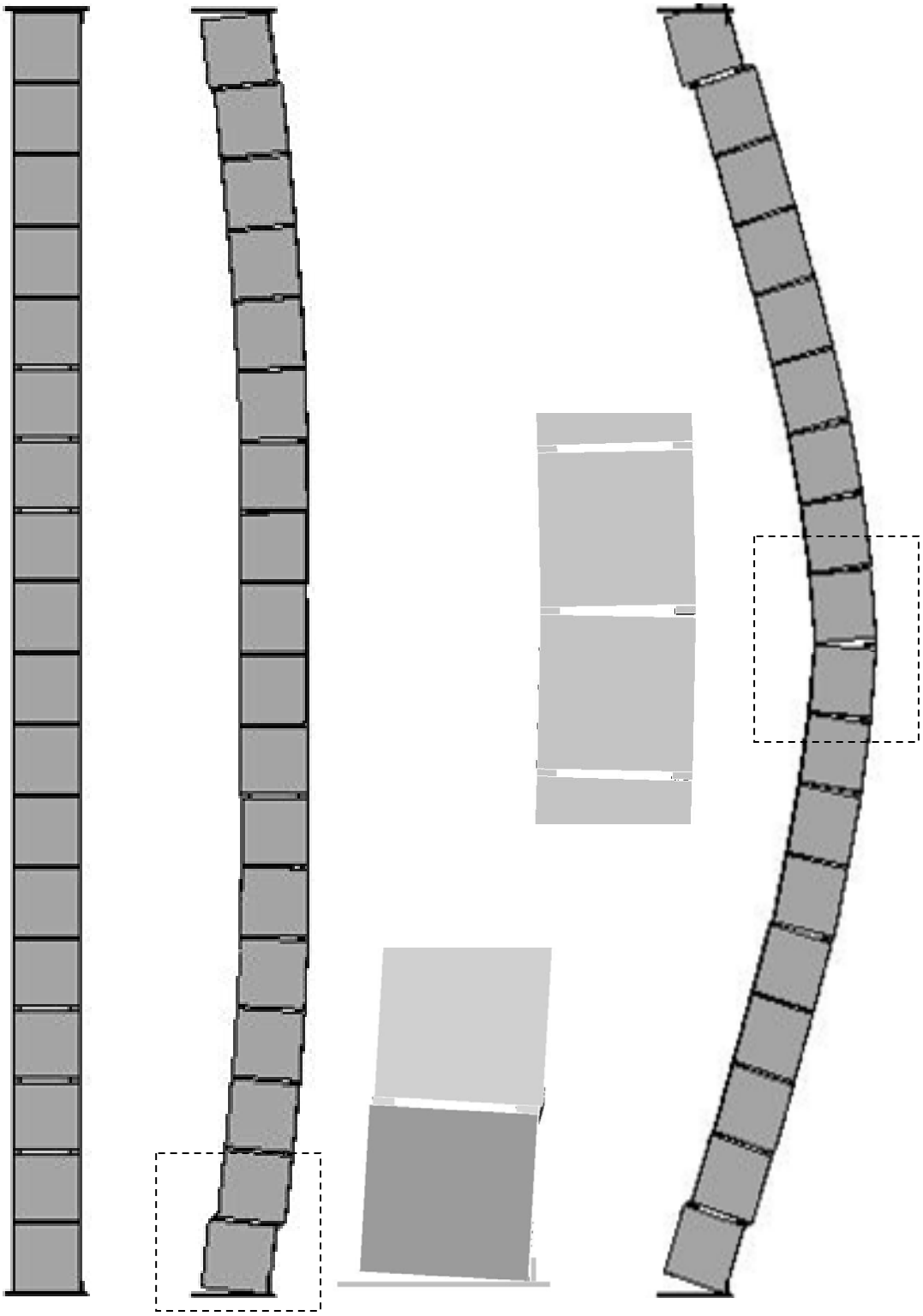

(a) Initial Stage (b) Shear at Supports (c) Bending at Center

Fig. 4.1-9: General Wall Behavior

A noticeable flexural response then occurs. The blocks near the midpoint separate in tension, and the wall continues to deflect until its movement is resisted by the polymer reinforcement (Fig. 4.1-9c). At this point, the polymer is subjected to tension. If the polymer has low rupture strain, it fails in tension, allowing further movement of the wall. If the polymer does not undergo failure, it rebounds slightly.

Fig. 4.1-10 shows the maximum displacement attained by the wall at the midpoint for the two loading cases. The maximum displacements is 7.5-inch and 12.7-inch for loads I and III, respectively. In the early phases of the response to load I , the polymer experienced a maximum tensile stress of 1400 psi and an effective stress of 1600 psi near the top and bottom mortar joints.

The stresses then advanced toward the center of the wall but concentrated at the mortar interfaces, with a tensile stress magnitude in the range of 1000 psi to 1200 psi and an effective stress magnitude in the range of 1000 psi to 1500 psi. The maximum polymer strain was 2.4%. The stress distribution under load III is different from that caused by load I, due to the higher magnitude of the loading. The stresses did not propagate gradually from the supports to the central portion.

Instead, the entire wall displayed high stress at the same time, indicating the crushing of the front face of the wall. The blocks at the midpoint were partially crushed. The maximum first principal stress was 330.4 psi. The maximum stresses were concentrated at the mortar joint elements, indicating high compression. The highest strain rates were observed on the front faces of the blocks. The maximum strain rate in the blocks varied between 100 sec^{-1} and 200 sec^{-1}. As in the previous load case, a maximum shear stress of 115 psi was noted and occurred at mortar joints.

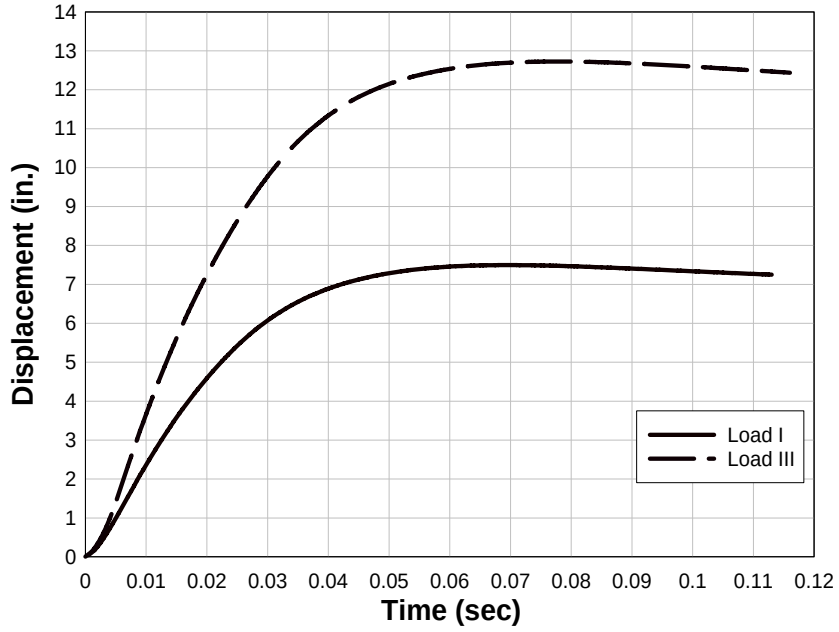

Fig. 4.1-10: Maximum displacements for baseline model for load I and load III

Under load III, the polymer experienced a maximum tensile stress of 2100 psi and an effective stress of 2150 psi near the top and bottom mortar joints in the early phases of the response. The stresses then advanced toward the center of the wall but concentrated at the mortar interfaces, with tensile and effective stress magnitudes in the range of 1500 psi to 2000 psi. The maximum polymer strain was 3.4%.

The finite element model developed by Sudame (2004) was used to predict wall behavior for the tests shown in Chapter 3. The model was modified for each test condition accordingly to incorporate various polymer retrofit membranes and blast loads. This effort in discussed in Chapter 7.

5 RESISTANCE FUNCTION DEVELOPMENT

5.1 Approach

Unreinforced masonry walls laterally supported along their top and bottom edges resist lateral forces by spanning vertically between these supports (Drysdale et al. 1994). Flexural stresses normal to the bed joints eventually result in tensile failure when a crack occurs along a course of the bed joint. The failure mechanism can be very complex and depends upon the type of supports provided at the top and bottom edges, and the magnitude of axial forces from self-weight and any superimposed loads.

In general, the weight of the wall produces a uniform compressive stress throughout the wall. Initially, any tensile stresses developing from the bending of the wall due to lateral loads will be suppressed by the compressive stresses due to the weight of the wall. As the lateral forces increase, the impact of compressive stresses decrease on the tension face of the wall, and eventually tensile stresses begin to develop. Because the flexural strength of the mortar joints is quite variable and depends on construction techniques and weather, it is possible that cracks will initiate at the early stages of tensile stresses. Therefore, it is conservatively assumed in the development of the static resistance function that the wall cannot resist tensile stresses.

Once tensile stresses develop on the tension side of the wall, cracks will initiate (Baker 1977 and 1980) along two or three units in the course and then immediately propagate for the full length of the wall (Fig. 5.1-1).

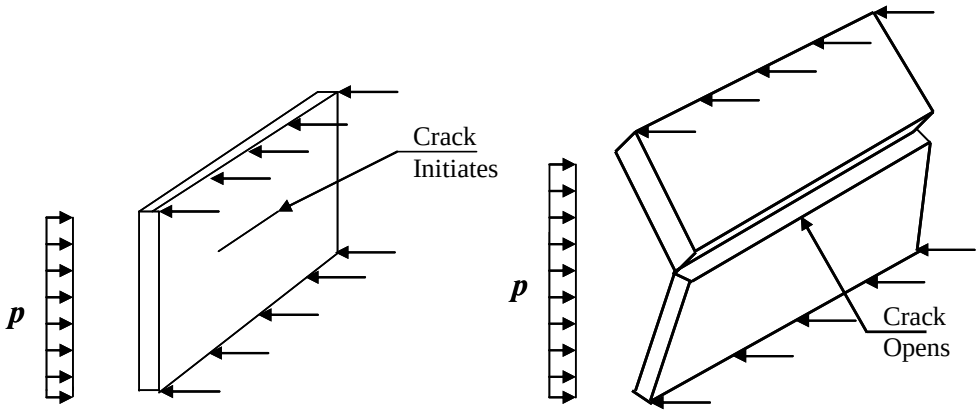

Fig. 5.1-1: Unreinforced masonry wall spanning vertically and subjected to lateral load

The formation of cracks does not constitute wall failure, even in an unreinforced masonry wall (Paulay and Priestley 1992). The resultant compressive force *R* in the compression zone of the central crack counteracts the vertical loads due to wall weight and surcharge, and creates a balancing moment against lateral loads (Fig. 5.1-2). As lateral loads increase so do compressive stresses that cause *R*, and subsequently the wall resistance. The increase in compressive stresses and the triangular distribution of these stresses cause *R* to move more and more toward the compression face of the wall (Fig. 5.1-3). A maximum compressive stress block will develop in the compression side of the wall that equals the masonry compressive strength. The wall collapses when *R* moves outside of the line of action of the vertical loads, namely wall weight and surcharge. The triangular distribution of stresses across the area of the unreinforced concrete masonry is used for general application to a variety of concrete masonry units and is at best an approximation for hollow blocks.

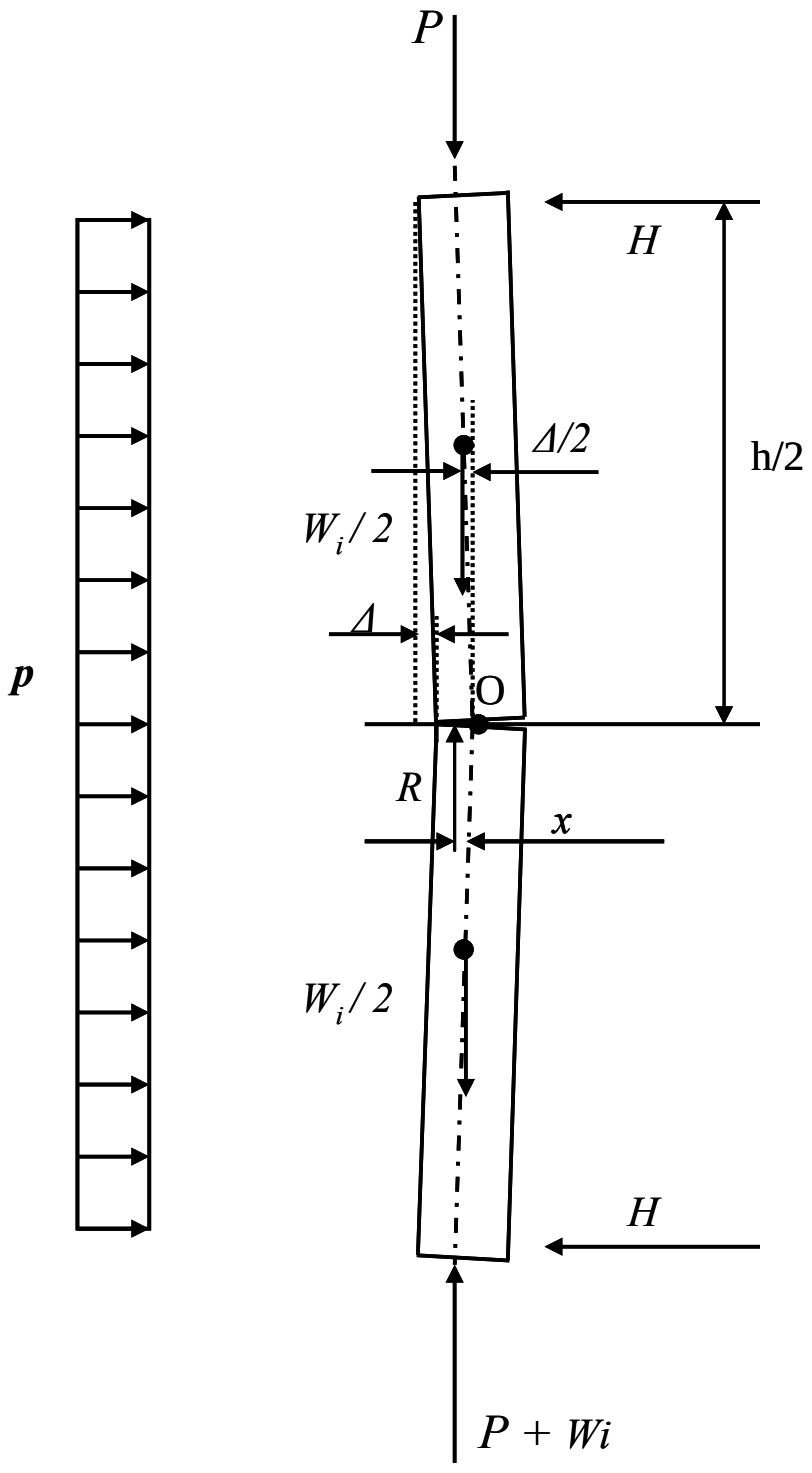

Fig. 5.1-2: Moment equilibrium for face-loaded wall

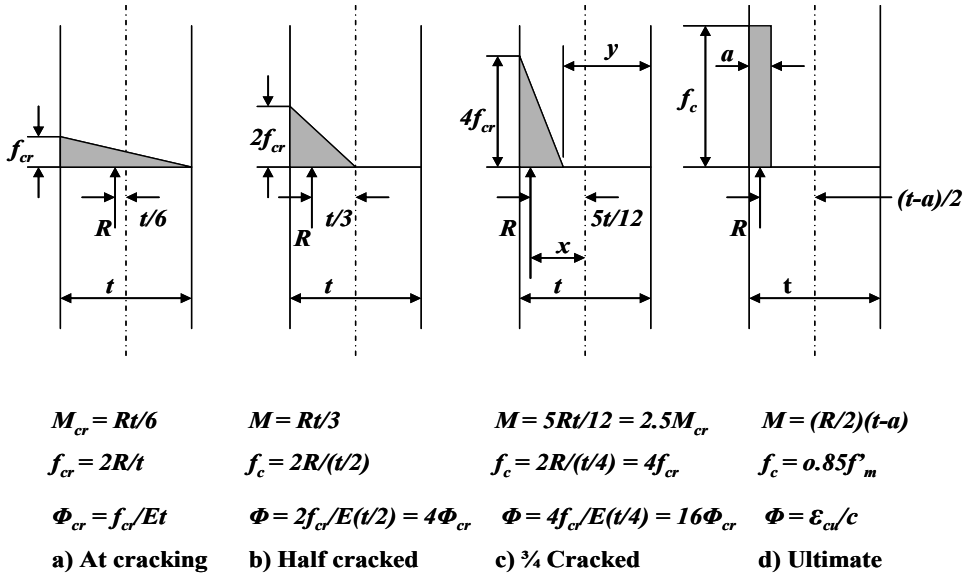

Fig. 5.1-3: Stress distribution
Reference: Priestley and Paulay 1992

Walls constructed using hollow concrete masonry block often have mortar along the front and back faces of the block. This approximation still applies, since the majority of the wall's resistance develops when R is located in the vicinity of the compression face of the block, as shown in Fig. 5.1-3d.

5.2 Unreinforced Concrete Masonry Wall - Analytical Model

In beginning to develop the equations to predict conditions for wall failure, some simplifying assumptions are necessary:

1. The wall is load-bearing and experiences one-way bending action.
3. If the wall is built from hollow concrete masonry, the cells are ungrouted.
4. The wall is not reinforced with steel bars.

5. The tensile strength of concrete masonry and mortar joints is ignored.
6. The lateral load on the wall is constant over the wall height (h).
7. The wall is partially fixed at the top and bottom interfaces.

The last assumption is made to help develop the necessary equations for wall failure with varying degrees of end fixity. Although most unreinforced concrete masonry walls are simply supported at the top and bottom supports, the ability to specify end fixity makes it convenient when a specific wall design develops moment capacity at the top and bottom supports. The design engineer can determine the degree at which the top and bottom supports develop moment in the wall and determine the percent end fixity for the analysis. The designer can also be conservative and assume simply supported conditions at the top and bottom supports. It will be shown that, as long as the end fixity is below 75%, the maximum moment occurs at the midpoint of the wall, and the derivations will stand. The equations will include options to vary the degree of end fixity (α) from 75% to 0% (simply supported). Consider the wall in Fig. 5.2-1, with fixed-end conditions at top and bottom, and lateral pressure p. Summing moments about the base of the wall results in:

$$\circlearrowleft^{+} \sum M_{base} = 0 = Hh - \frac{ph^2}{2} - \frac{w_i \Delta}{2}$$

$$H = \frac{ph}{2} + \frac{w_i \Delta}{2h} \qquad (5.2\text{-}1)$$

$$\circlearrowleft + \sum Mo = 0 = -\frac{ph^2}{8} + \frac{w_i \Delta}{4} + \left(\frac{ph}{2} + \frac{w_i \Delta}{2h} \right) \frac{h}{2} - \frac{\alpha p h^2}{12} + P\Delta - Rx$$

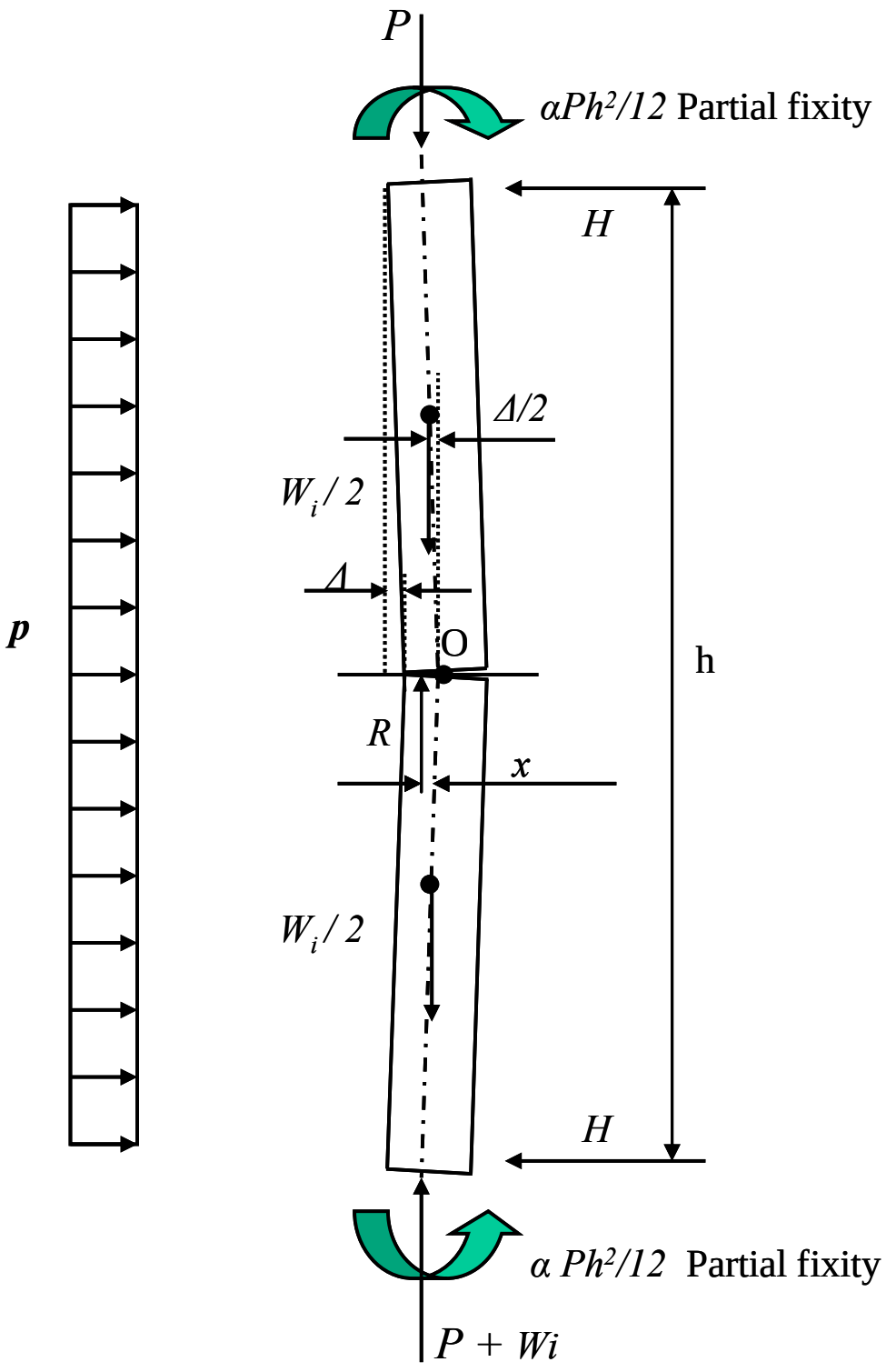

Fig. 5.2-1: Free-body diagram of wall

$$\Delta = \frac{Rx}{\frac{w_i}{2} + P} - \frac{(3 - 2\alpha)ph^2}{12w_i + 24P} \tag{5.2-2}$$

$$R = \frac{w_i}{2} + P \tag{5.2-3}$$

To address the percentage of end fixity, take the current case, where the end moments are equal to $\alpha ph^2/12$. The total combined moment within a uniformly loaded beam is:

$M_{Total} = M_{end} + M_{middle} = ph^2/8$

100% fixed end beams: $M_{end} = ph^2/12$ *and* $M_{middle} = ph^2/24$ ⇒ $M_{total} = ph^2/8$

0% fixed end (S.S.) beams: $M_{end} = 0$ *and* $M_{middle} = ph^2/8$ ⇒ $M_{total} = ph^2/8$

Partially fixed end beams: $M_{end} = \alpha ph^2/12$ and $M_{middle} = (3\text{-}2\alpha)\ ph^2/24$ ⇒

$M_{total} = ph^2/8$

For the moment at the midpoint to be greater than the moment at the two ends, α must be less than 75%.

Since it is assumed that masonry cannot develop tensile stresses, once the compressive stresses caused by gravity and surcharge are overcome, stresses in the masonry are distributed in a triangular form (Fig. 5.1-3). R is the resultant force on this triangular stress distribution. As the lateral load increases and the crack in the masonry grows, the triangular stress distribution increases in intensity but decreases in length, and R moves towards the compression face of the wall. This process continues until a compression block is developed very near the compression face of the wall with a stress

intensity equal to the strength of the masonry. Failure occurs when *R* moves outside of the line of action of self-weight and surcharge.

It can be shown from Fig. 5.1-3c that if:

y = length of crack x = distance from R to wall center line

$$x = \frac{t}{2} - \frac{t - y}{3}$$

$$x = \frac{t + 2y}{6} \qquad (5.2\text{-}4)$$

Substituting equations 5.2-3 and 5.2-4 into equation 5.2-2 results in a final equation for wall displacement versus lateral load, as shown in equation 5.2-5.

$$\Delta = \frac{t}{6} + \frac{y}{3} - \frac{(3 - 2\alpha)ph^2}{12w_i + 24P} \qquad (5.2\text{-}5)$$

Which yields:

$$\Delta = \frac{t}{6} + \frac{y}{3} - \frac{ph^2}{4w_i + 8P} \qquad \text{for } \alpha = 0\% \quad \text{(Simply supported ends)}$$

$$\Delta = \frac{t}{6} + \frac{y}{3} - \frac{ph^2}{6w_i + 12P} \qquad \text{for } \alpha = 50\% \quad \text{(Partially (50%) fixed ends)}$$

Elastic deflection of the wall prior to crack is calculated using equation 5.2-6. This equation accounts for variations in the end fixity of the wall and is derived using an equation provided by Manual of Steel Construction, 1980 for a beam with uniformly distributed load and equal end moments (M_e):

$$\Delta_{\max.elastic} = \frac{ph}{48EI}\left(\frac{5h^3}{8} - \frac{6M_e h}{p}\right)$$

If the moment at each end of the beam, $M_e = \frac{\alpha p h^2}{12}$

Where α is the % fixity at ends of the beam, then:

$$\Delta_{\max.elastic} = \frac{(5-4\alpha)ph^4}{384E_c I} \qquad (5.2\text{-}6)$$

It is easily shown that equation 5.2-6 yields:

$\Delta_{\max.elastic} = \frac{5ph^4}{384E_c I}$ For simply supported beams (α = 0%) Checks ✓

$\Delta_{\max.elastic} = \frac{ph^4}{384E_c I}$ For fixed end beams (α = 100%) Checks ✓

Resistance Function

Equations 5.2-5 and 5.2-6 present a two-equation, three-unknowns (Δ, y, and p) situation. Furthermore, equation 5.2-6 can only be used for the elastic deflection of the wall. The solution may be found by examining the curvature of the wall as it goes through bending (Paulay and Priestly 1992). At the onset of crack, the curvature at the central section of the wall (Fig. 5.1-3) is:

$$\Phi_{cr} = \frac{\sigma_{cr}}{E_c t} \qquad \text{and} \qquad \Delta_{cr} = \frac{(5-4\alpha)ph^4}{384E_c I}$$

It may be assumed conservatively that the displacement Δ increases in proportion with the central curvature, thus the following equation is derived for the wall curvature as crack grows:

$$\Phi_{cr} = \frac{\sigma_{crG}}{E_c(t-y)}$$

Also: $$\sigma_{cr} = \frac{2R_{cr}}{t} \quad \text{and} \quad \sigma_{cr\,G} = \frac{2R_{crG}}{(t-y)}$$

Setting: $$\beta = \frac{\Phi_{crG}}{\Phi_{cr}} = \frac{R_{crG}t^2}{R_{cr}(t-y)^2}$$

Then: $$\Delta_{crG} = \beta\,\Delta_{cr} \qquad (5.2\text{-}7)$$

The wall resistance function in terms of displacement versus lateral load can now be derived in an iterative fashion. At the onset of crack ($y = 0$), the problem is reduced to two equations (5.2-5 and 5.2-6) and two unknowns (Δ and p). As crack grows ($y > 0$), Δ is calculated using equation 5.2-7, and p is subsequently calculated using equation 5.2-5. When this process is programmed for small increments of y, the result is the full resistance function of the wall through failure, as shown in Fig. 5.2-2.

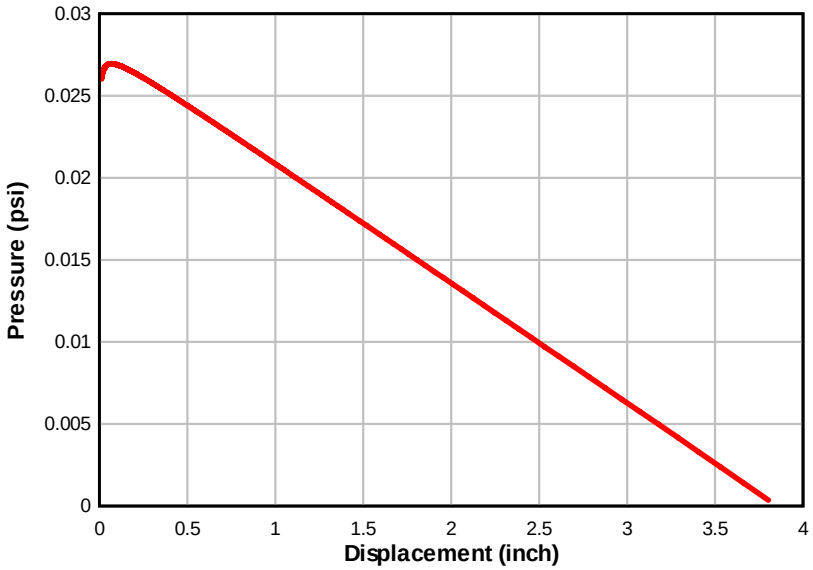

Fig. 5.2-2: Resistance function – unreinforced CMU wall

5.3 Membrane Retrofit Concrete Masonry Wall – Analytical Model

The assumptions made for the unreinforced case apply for this case as well. Consider the wall in Fig. 5.3-1, with partially fixed-end conditions at top and bottom, and lateral pressure p. The added parameter is the membrane retrofit at the crack opening. Although the membrane retrofit covers the entire inside surface of the wall, the tributary length (l) of the membrane affected by the crack opening is far less than the height of the wall. The tributary length depends on how the membrane retrofit is attached to the concrete masonry and how far the membrane strain extends past the crack opening. The shorter the tributary length, the higher the membrane strain due to the crack opening. During blast tests conducted by Dinan et al. (2003), it was observed that the length of polyurea membrane retrofits strained on each side of the crack opening was generally equal to one half of the concrete masonry block height. The approximate tributary length

of the polymer membrane retrofit is therefore assumed to be between 8 to 12 inches in this research.

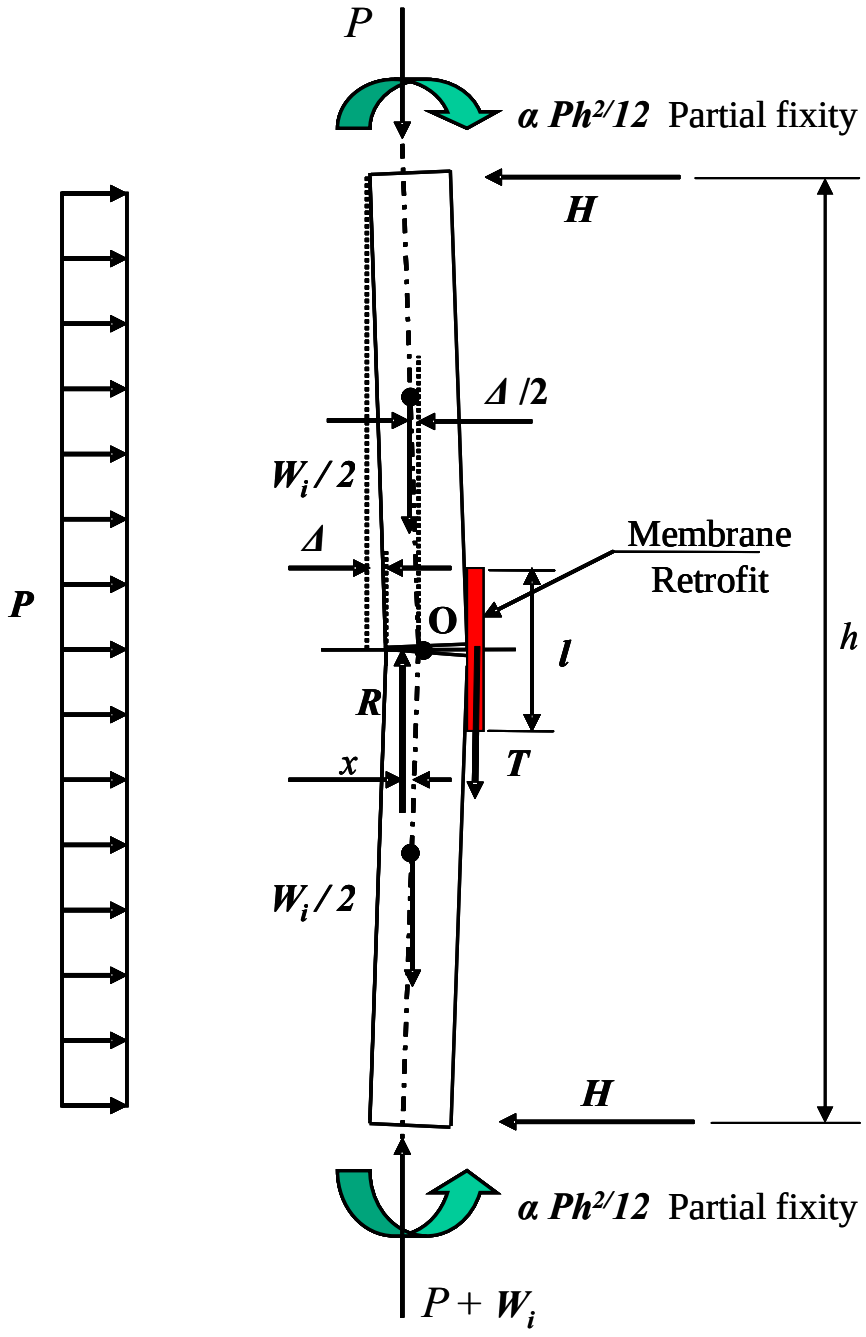

Fig. 5.3-1: Free-body diagram of polymer retrofit concrete masonry wall

More accurate estimates of the tributary length of specific polymers may be obtained by test or analysis and used in the analytical model. For membrane retrofits discretely fastened to the masonry wall, the tributary length is the vertical distance between fasteners (Fig. 5.3-2).

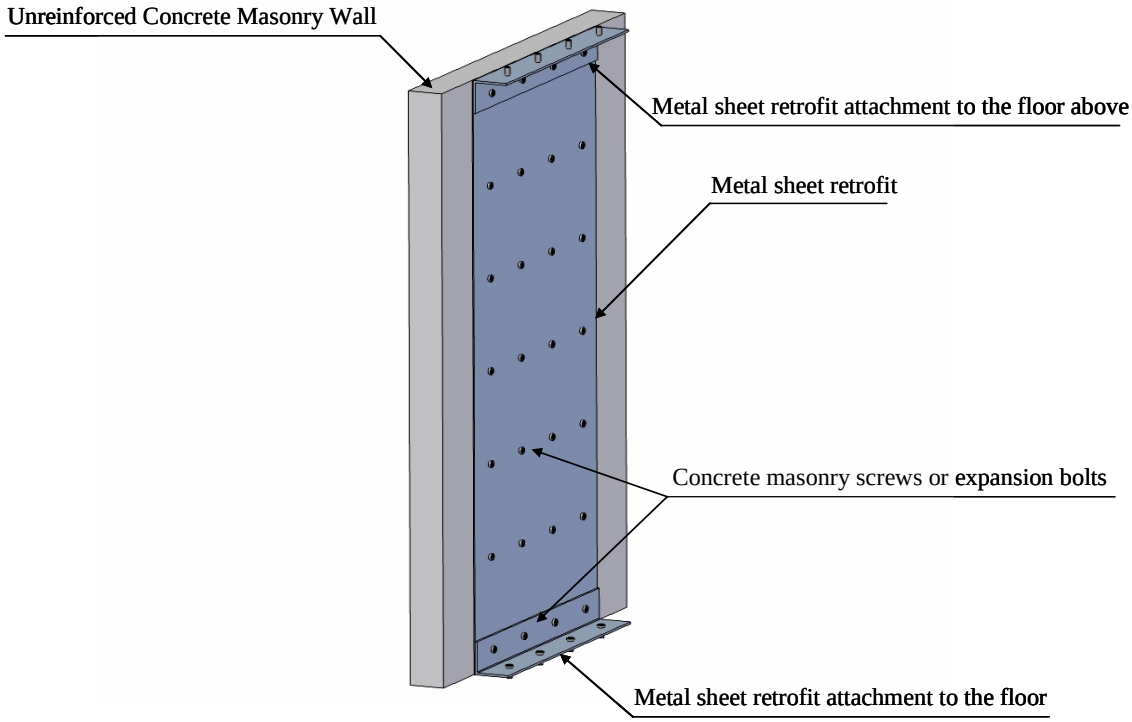

Fig. 5.3-2: Sheet metal retrofit

Summing moments about the base of the wall result in:

$$+\circlearrowleft \sum M_{base} = 0 = Hh - \frac{ph^2}{2} - \frac{w_i \Delta}{2}$$

$$H = \frac{ph}{2} + \frac{w_i \Delta}{2h} \qquad (5.3\text{-}1)$$

$$+\circlearrowleft \sum Mo = 0 = -\frac{ph^2}{8} + \frac{w_i \Delta}{4} + \left(\frac{ph}{2} + \frac{w_i \Delta}{2h}\right)\frac{h}{2} - \frac{\alpha p h^2}{12} + P\Delta - Rx - \frac{Tt}{2}$$

$$\Delta = \frac{Rx}{\frac{w_i}{2} + P} - \frac{(3 - 2\alpha)ph^2}{12w_i + 24P} + \frac{Tt}{w_i + 2P} \tag{5.3-2}$$

$$R = \frac{w_i}{2} + P + T \tag{5.3-3}$$

It is necessary to find a relationship between wall deflection and crack opening. This is simplified by the assumption that the two portions of the wall on each side of the crack remain plane and without distortion. The relationship can be deducted from Fig. 5.3-3, as follows:

$$\frac{\Delta}{\frac{h}{2}} = \frac{\delta}{t}$$

$$\delta = \frac{2\Delta t}{h}$$

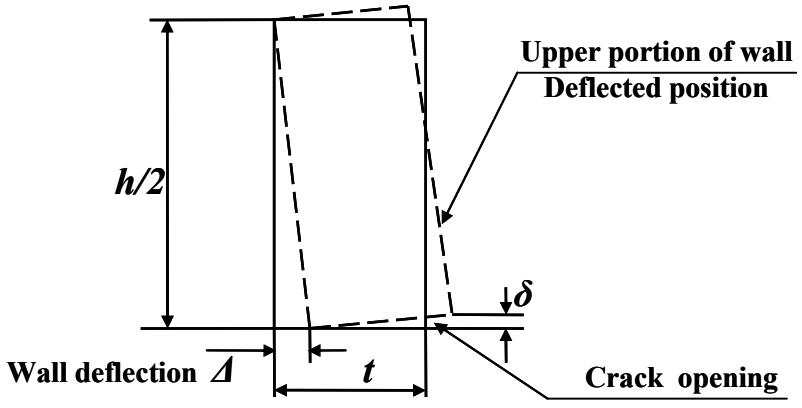

Fig. 5.3-3: Wall deflection versus crack opening

$$f_t = \frac{E_r \delta}{\frac{l}{2}}$$

$T = f_t A = f_t t_r$ (1) per unit width of membrane retrofit

$$T = \frac{4E_r t_r t\Delta}{lh} \tag{5.3-4}$$

The discussions for stress distribution across the concrete masonry cross-section are applicable to this case as well. As the crack grows and the membrane retrofit stretches past its yield point, the modulus of elasticity of the membrane retrofit used in equation 5.3-4 follows the values defined in its stress-strain curve. Fig. 3.1-4 shows an example of a stress-strain curve for a typical polymer.

Substituting equations 5.2-4, 5.3-3, and 5.3-4 into equation 5.3-2 results in a final equation for wall displacement in terms versus lateral load:

$$\Delta = \frac{\left(\frac{t}{6} + \frac{y}{3} - \frac{(3-2\alpha)ph^2}{12w_i + 24P}\right)}{1 - \left(\frac{4E_r t_r t}{lh}\right)\left(\frac{4t + 2y}{3w_i + 6P}\right)} \tag{5.3-5}$$

Prior to the crack, the thin membrane retrofit has little impact on the stiffness of the concrete masonry wall. Therefore, the elastic deflection of the wall prior to crack is calculated using equation 5.2-6. The wall resistance function in terms of displacement versus lateral load is derived in an iterative fashion. At the onset of crack (y = 0), the problem is reduced to two equations (5.3-5 and 5.2-6) and two unknowns (Δ and p). As crack grows (y > 0), Δ is calculated using equation 5.2-7, and p is subsequently calculated

using equation 5.3-5. When this process is programmed for small increments of y, the result is the full resistance function of the wall through failure. Fig's. 5.3-5, 5.3-6, and 5.3-7 show the resistance functions for two different thicknesses of polymer, steel, and aluminum retrofits, respectively. The resistance function is truncated when:

1. The maximum compressive stress in the CMU material exceeds $0.85f'_m$
2. The calculated pressure or resistance is a negative value.
3. The maximum tensile or shear stresses in the membrane retrofit exceed its ultimate strength.
4. The maximum shear in fasteners or adhesive bond for the membrane retrofit is exceeded.

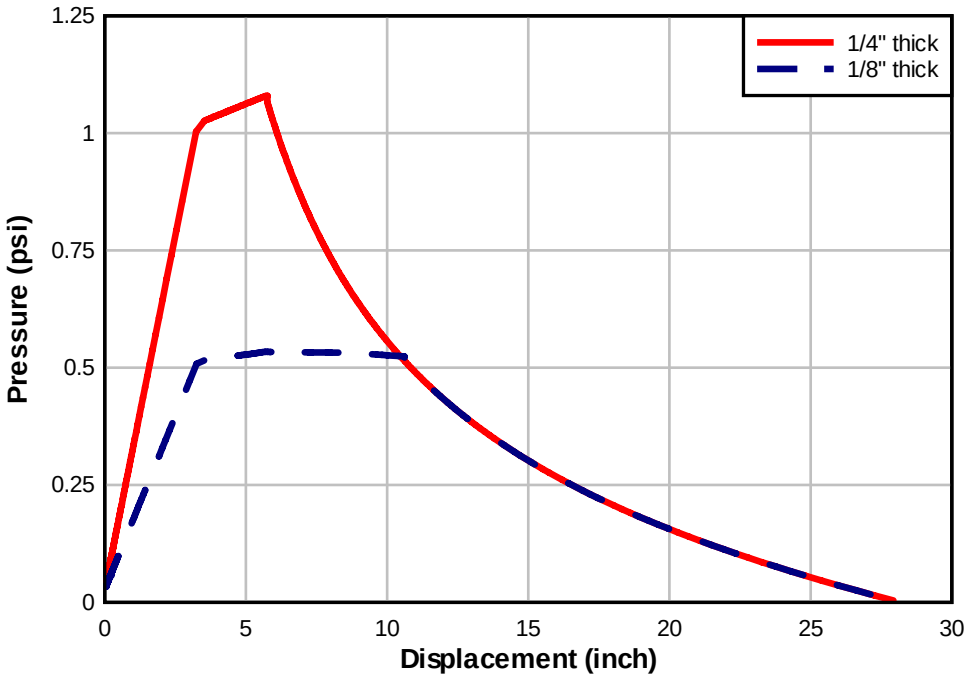

Fig. 5.3-5: Resistance function – polymer retrofit

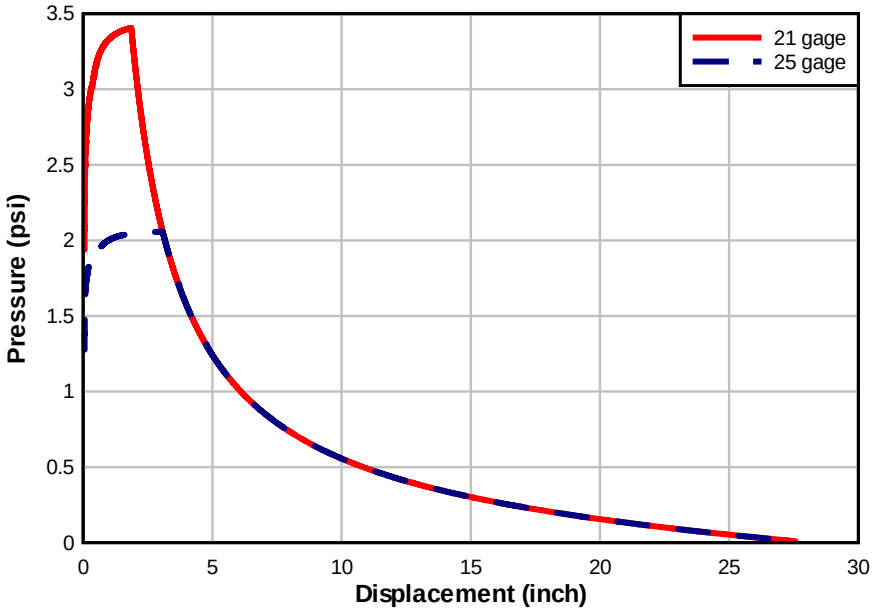

Fig. 5.3-6: Resistance function – steel sheet retrofit

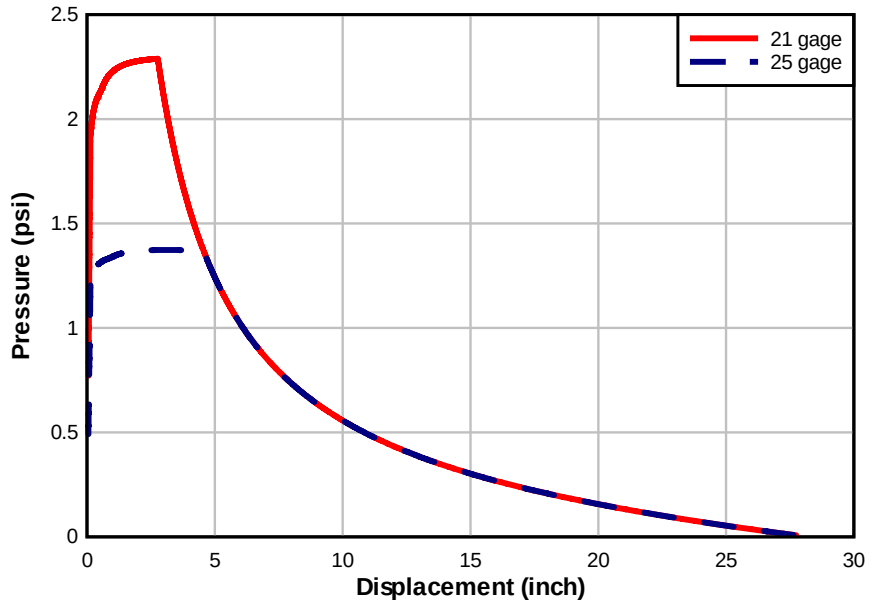

Fig. 5.3-7: Resistance function – aluminum sheet retrofit

5.4 Arching Action of Membrane Retrofit Concrete Masonry Wall – Analytical Model

When a wall is built between and in tight contact with supports that serve as restraints against outward movement, elongation of the tension face due to bending cannot occur without inducing a compressive force (Drysdale et al. 1994). Under lateral load, this induced in-plane compressive force results in arching, which increases the cracking load significantly. With increased loading, flexural cracking occurs at the supports and the midspan, as shown in Fig. 5.4-1.

As the load increases, the wall is pushed against the unyielding supports, creating thrust forces V_u at the ends. A three-hinged arch is formed where the external moment is resisted by the internal couple $V_u\, r_u$ where r_u is the height of the arch. The thrust force is a function of the material properties of the mortar joint and the contact area.

$$M_u = V_u\, r_u \tag{5.4-1}$$

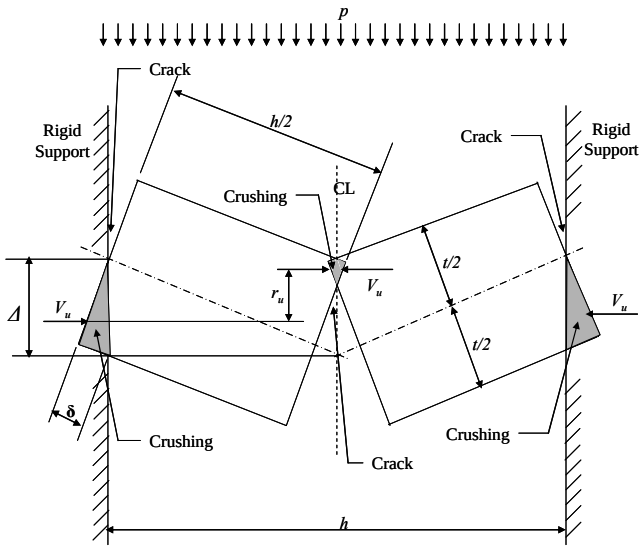

Fig. 5.4-1: Wall in a deflected position

Consider the wall in Fig. 5.4-2, with thrust forces at top and bottom due to arching, and membrane retrofit on the tension face. Although the membrane retrofit covers the entire inside surface of the wall, the tributary length of the membrane affected by crack opening is far less than the height of the wall. The tributary length (l) of the membrane retrofit is treated in the same manner as in Section 5.3.

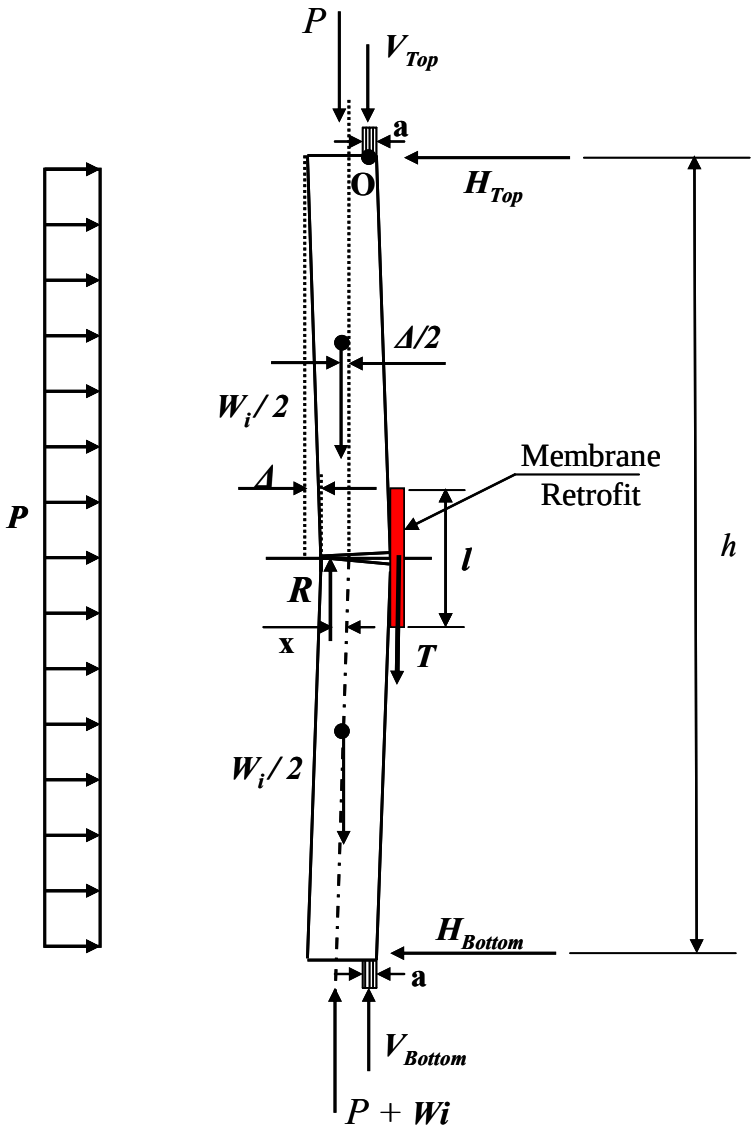

Fig. 5.4-2: Free-body diagram of wall

Summing moments about the base of the wall result in:

$$\circlearrowleft^{+} \sum M_B = 0 = H_{Top} h - \frac{ph^2}{2} + P\left(\frac{t-a}{2}\right) + w_i\left(\frac{t-a}{2} - \frac{\Delta}{2}\right)$$

$$H_{Top} = \frac{ph}{2} - \left(P + w_i\right)\left(\frac{t-a}{2h}\right) + \frac{w_i \Delta}{2h} \tag{5.4-3}$$

$$H_{Bottom} = \frac{ph}{2} + \left(P + w_i\right)\left(\frac{t-a}{2h}\right) - \frac{w_i \Delta}{2h} \tag{5.4-4}$$

Summing moments about point "O" results in:

$$\circlearrowleft^{+} \sum Mo = 0 = P\left(\frac{t-a}{2}\right) + \left(\frac{w_i}{2}\right)\left(\frac{t-a}{2} - \frac{\Delta}{2}\right) - R\left(x + \frac{t-a}{2} - \Delta\right) - T\left(\frac{a}{2} + \Delta\right)$$

$$+ \left(\frac{ph}{2}\right)\left(\frac{h}{4}\right) \tag{5.4-5}$$

$$\Uparrow + \sum Fy = 0 = R - P - T - V_{top} - \frac{w_i}{2}$$

$$R = T + P + V_{top} + \frac{w_i}{2} \tag{5.4-6}$$

Stresses in the masonry are distributed in a triangular form, as shown in Fig. 5.1-3, and the relationship between *x* and *y* distances are shown by Equation 5.2-4. As the crack opens, tension in the membrane retrofit is calculated using 5.3-4.

$$T = \frac{4E_r t_r t}{lh} \Delta = \Omega \Delta$$

Where: $\Omega = \frac{4E_r t_r t}{lh}$ (5.4-7)

As the crack grows and the membrane retrofit stretches past its yield point, the modulus of elasticity of the membrane retrofit used in equation 5.4-7 follows the values defined in its stress-strain curve.

McDowell et al. (1956) proposed the strain equation in the arching section of the wall:

$$\varepsilon = \frac{2\delta}{\frac{h}{2}}$$

$$\sigma = \frac{4E\delta}{h} = \frac{4E\frac{2\Delta t}{h}}{h} = \frac{8E\Delta t}{h^2}$$

$$V_{Top} = \frac{8E\Delta ta}{h^2} = \eta\Delta \quad (5.4\text{-}8)$$

where: $\eta = \frac{8E_c ta}{h^2}$

The width of the arching area may be taken as the face shell thickness of the individual concrete masonry unit or, following a simplified equation proposed by Drysdale et al. (1994):

$$a = 0.1t \quad (5.4\text{-}9)$$

Substituting equations 5.2-4 and 5.4-6 through 5.4-8 into equation 5.4-5 and simplifying:

$$0 = \eta\Delta^2 - \left(\Omega\left(\frac{4t+2y}{6}\right) + \eta\left(\frac{4t+2y-3a}{6}\right) - P - \frac{w_i}{4}\right)\Delta - \left(P + \frac{w_i}{2}\right)\left(\frac{t+2y}{6}\right) + \frac{ph^2}{8} \tag{5.4-10}$$

And in terms of pressure:

$$p = -\frac{8}{h^2}\left(P\left(\frac{t-a}{2}\right) + \frac{w_i}{2}\left(\frac{t-a}{2} - \frac{\Delta}{2}\right) - \left(T + P + V_{Top} + \frac{w_i}{2}\right)\left(x + \frac{t-a}{2} - \Delta\right) - T\left(\frac{a}{2} + \Delta\right)\right) \tag{5.4-11}$$

Before initiation of crack at y = 0, it is safe to assume that the tension in the retrofit is zero and the arching forces are also zero. Equation 5.4-10 reduces to:

$$\left(P + \frac{w_i}{4}\right)\Delta - \left(P + \frac{w_i}{2}\right)\left(\frac{t}{6}\right) + \frac{ph^2}{8} = 0$$

Hence:

$$\Delta = \frac{\left(P + \frac{w_i}{2}\right)\left(\frac{t}{6}\right) - \frac{ph^2}{8}}{P + \frac{w_i}{4}} \tag{5.4-12}$$

It is safe to assume that when y = 0, the wall exhibits elastic bending, and its deflection equation is shown below for a fixed-end beam:

$$\Delta = \frac{ph^4}{384E_cI} \tag{5.4-13}$$

Equating equations 5.4-12 and 5.4-13 results in equation 5.4-14, from which pressure at $y = 0$ is calculated and later deflection Δ:

$$p = \frac{\left(P + \frac{w_i}{2}\right)\left(\frac{t}{6}\right)}{\left(\frac{h^4}{384E_cI}\right)\left(P + \frac{w_i}{4}\right) + \frac{h^2}{8}} \tag{5.4-14}$$

It may be assumed conservatively that the displacement Δ increases in proportion with the central curvature. Therefore, equation 5.2-7 holds for this case as well. The wall resistance function in terms of displacement versus lateral load can now be derived in an iterative fashion. At the onset of crack ($y = 0$), the problem is reduced to two equations 5.4-13 and 5.4-14 and two unknowns (Δ and p). As crack grows ($y > 0$), Δ is calculated using equation 5.2-7, and p is subsequently calculated using equation 5.4-11. When this process is programmed for small increments of y, the result is the full resistance function of the wall through failure. Fig. 5.4-3 is the arching resistance function of an unreinforced CMU wall. Figs. 5.4-4, 5.4-5, and 5.4-6 are the arching resistance functions of the unreinforced CMU wall with polymer, steel, and aluminum retrofits respectively. The resistance function is truncated for four conditions stated in the previous case.

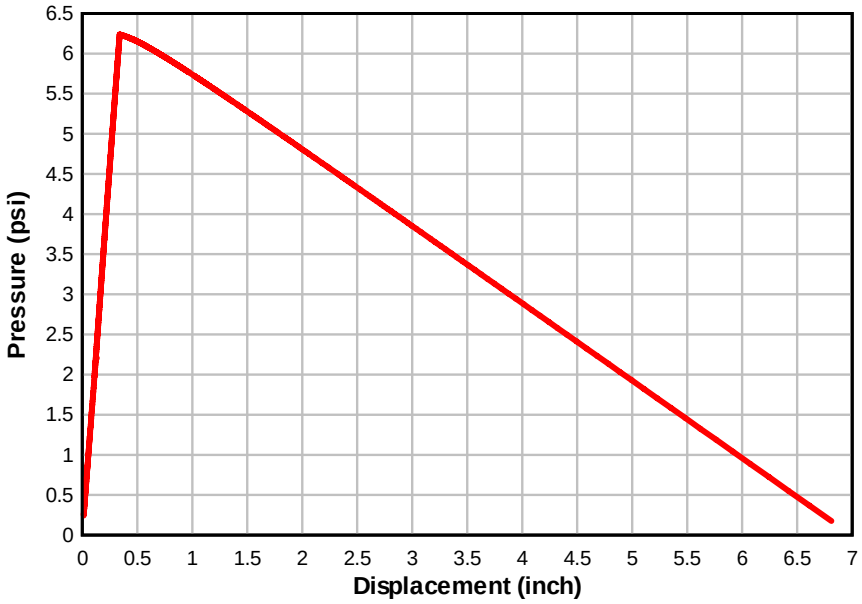

Fig. 5.4-3: Arching resistance – unreinforced CMU wall

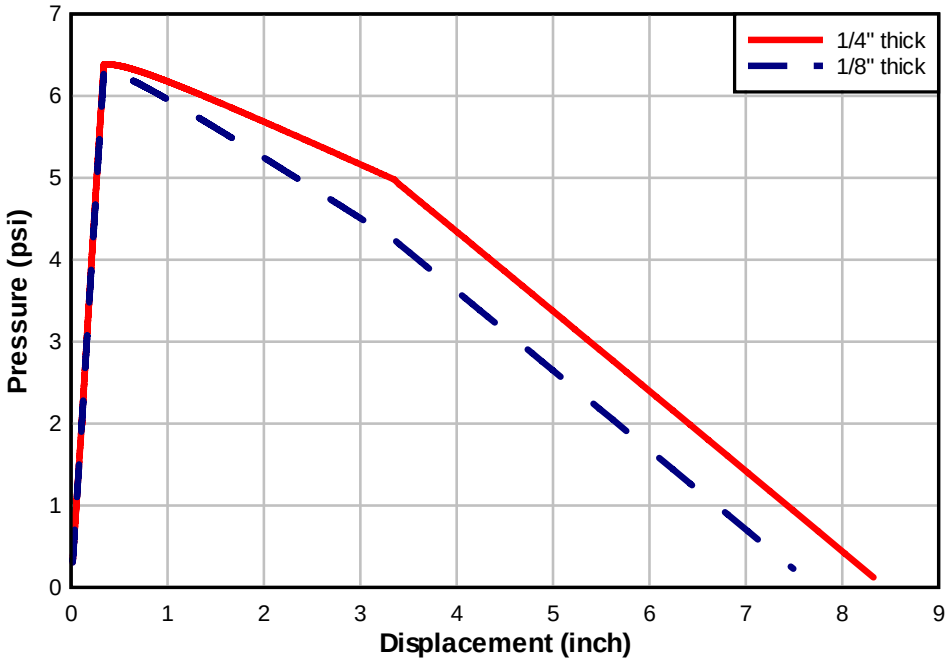

Fig. 5.4-4: Arching resistance – polymer retrofit

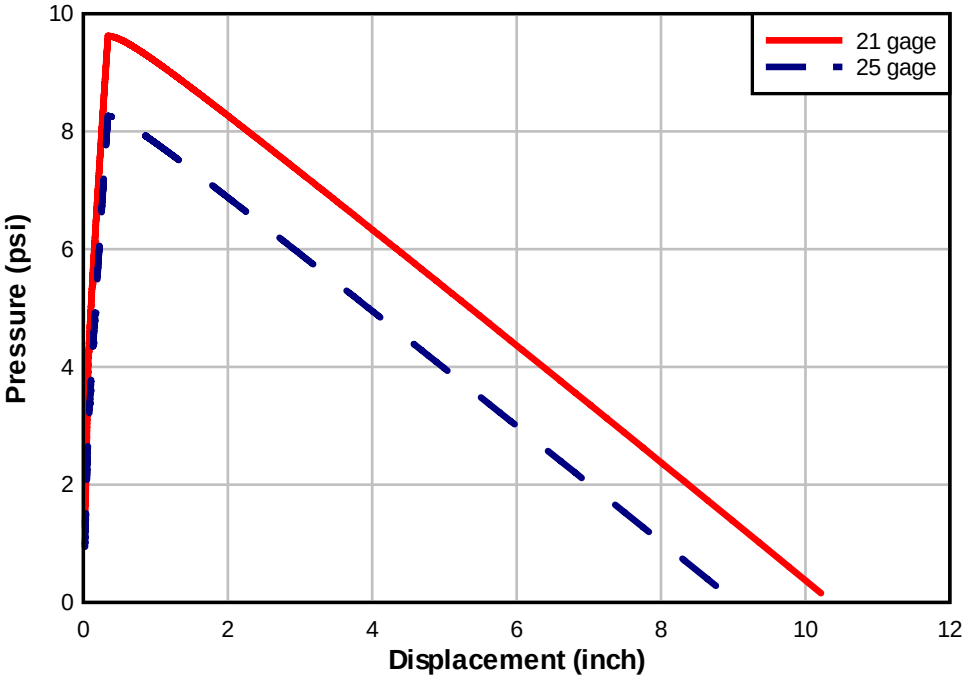

Fig. 5.4-5: Arching resistance – steel sheet retrofit

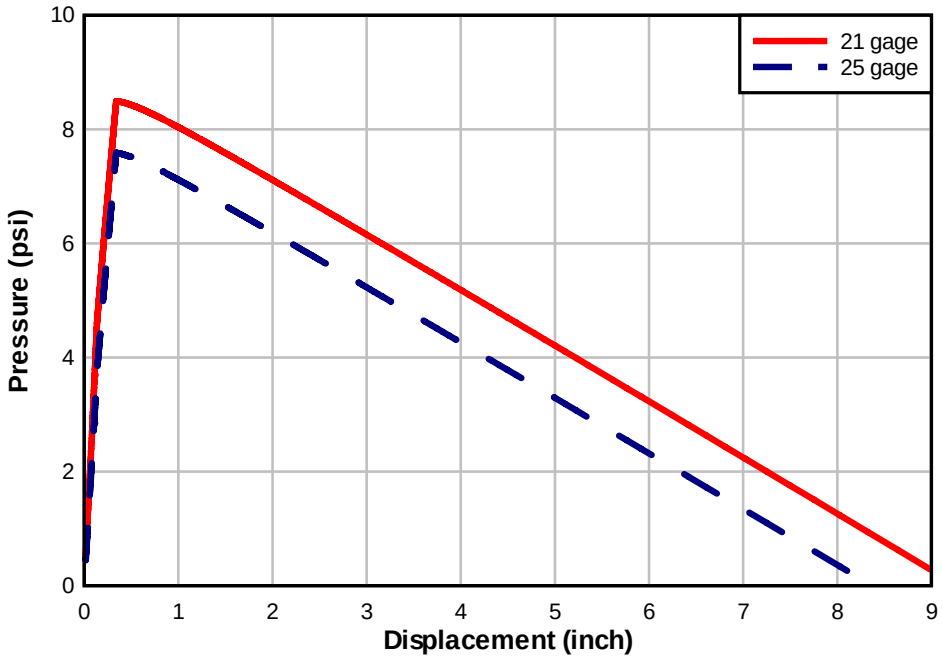

Fig. 5.4-6: Arching resistance – aluminum sheet retrofit

5.5 Catcher System Resistance Function Development

In the cases studied in this research thus far, the membrane retrofit was firmly attached to the unreinforced concrete masonry wall. Another system of interest is when the membrane retrofit is not firmly attached to the wall (Fig. 5.5-1, left wall). This system will be referred to as the catcher system and resists blast pressure in three distinct phases. In the first phase, the unreinforced concrete masonry wall goes through the initial elastic response, the subsequent initiation of cracks, the nonlinear rocking response, and eventual failure and collapse. In the second phase, the membrane retrofit responds as an elastic membrane. In the third phase, the membrane retrofit reaches yield and responds as a plastic membrane. Each phase is examined separately, and deflection versus pressure equations are developed for each phase. The final resistance function of the system is the summation of the resistance functions for the three phases.

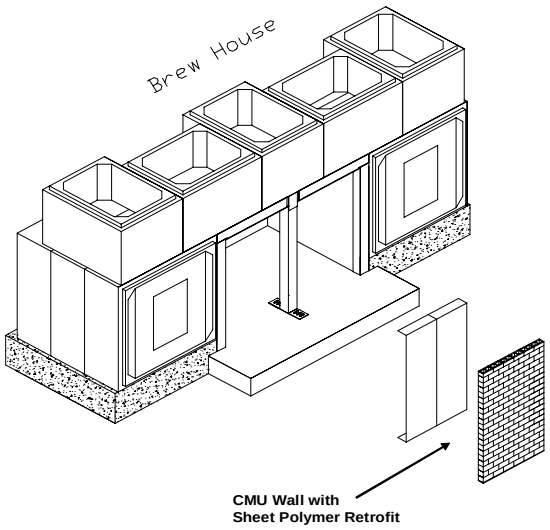

Fig. 5.5-1: Unreinforced CMU wall with membrane catcher system on the left

Phase 1 - Unreinforced Concrete Masonry Wall

The equations for the resistance function of unreinforced concrete masonry walls were developed in Section 5.2.

Phase 2 - Elastic Membrane Behavior of the Retrofit

The retrofit is assumed to behave like a thin, flexible membrane supported on both ends and loaded uniformly along its length. The membrane deflects elastically until yield. The deflection-pressure relation is found in Roark and Young (1975):

$$y = \sqrt[3]{\frac{3ph^4}{64E_r A_r}} \tag{5.5-1}$$

Or in terms of pressure versus deflection:

$$p = \frac{64E_r A_r y^3}{3h^4} \qquad \text{Cubic equation} \tag{5.5-2}$$

Phase 3 - Plastic Membrane Behavior of the Retrofit

After yield, the retrofit system continues to behave like a thin, flexible membrane until failure. An equation originally developed by Lane (2003) is used:

$$y = \frac{ph^2}{8A_r F_{yr}} \tag{5.5-3}$$

Or in terms of pressure versus deflection:

$$p = \frac{8 A_r F_{yr} y}{h^2} \qquad \text{linear equation} \qquad (5.5\text{-}4)$$

These phases are used in the resistance function calculations in order to arrive at the complete resistance function plot of the unreinforced concrete masonry wall with a membrane catcher system (Fig. 5.5-2).

The resistance function is truncated for these conditions:

1. The maximum tensile or shear stresses in the membrane catcher system exceed its ultimate strength.
2. The maximum tension or shear at the interfaces for the membrane catcher system is exceeded.

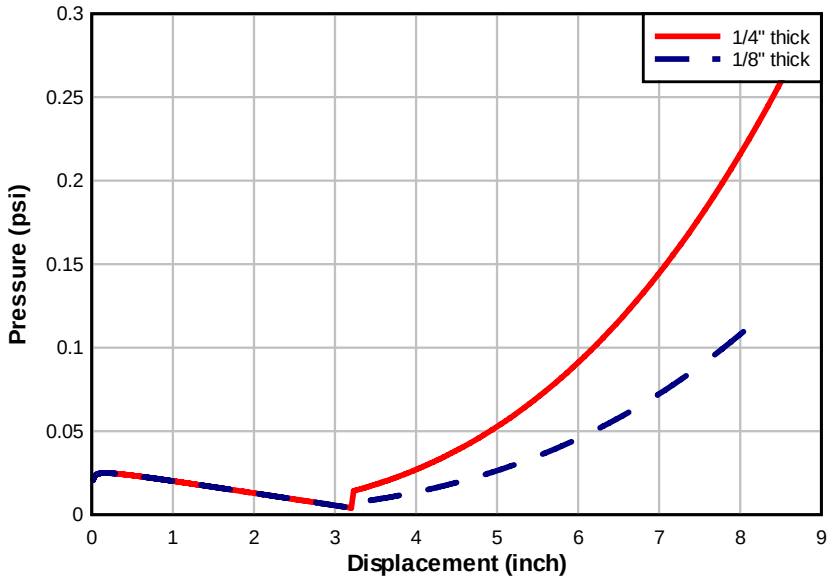

Fig. 5.5-2: Resistance function – polymer catcher system retrofit

5.6 Effect of Windows and Doors

In common building construction, concrete masonry walls often incorporate windows and/or doors. The impact of window or door openings on the wall resistance and response to lateral pressure depends on several factors:

1. Windows and doors are designed to resist the lateral pressure experienced by the wall and stay intact: The lateral pressure on the wall remains the same, but the resistance of the wall is reduced and so is the weight of the wall. The reduction in the resistance function of the wall was examined by Mays et al. (1998) for reinforced concrete walls and by Flanagan and Bennett (1999) in the context of masonry. The factor designated by B_w is computed for the wall and used to reduce the resistance function of the same wall with no openings.

$$B_w = \frac{A_{OP}}{A_{Surface}} \tag{5.6-1}$$

Where:

A_{OP} = Solid surface area of wall with openings

$A_{Surface}$ = Solid surface of wall with no openings

2. Windows and doors are not designed to resist the lateral pressure experienced by the wall and are blown out of place or destroyed, leaving an opening: The lateral pressure on the wall, the mass of the wall, and the resistance function of the wall are reduced. The reduction in the resistance function of the wall is calculated

using Equation 5.6-1. The reduction in lateral pressure, as well as the reduction in the weight of the wall, may be approximated using the same equation.

5.7 Wind Capacity

In general, a 70-mph wind is associated with 12.6 psf of pressure on the surface of a building (Laursen 1978). Wind pressure is proportional to the square root of wind speed; therefore, a simple relationship, as shown in equation 5.7-1, will allow for the computation of wall wind capacity in terms of mph when the wall pressure capacity is calculated using the methodology set forth herein.

$$\text{Wall wind capacity} = 70\sqrt{\frac{144p}{12.6}} = 236.6\sqrt{p} \quad \text{mph} \qquad (5.7\text{-}1)$$

Where: p = Maximum pressure capacity of the wall (psi)

5.8 CMU Material Properties

Weight = 32 lb Volume = 367 in^3

Mass density = 0.0002247 lb s^2/in^4

Ultimate compressive strength (f'_m) = 2000 psi

E_c = 2,000,000 psi *Poisson's ratio* = 0.15 to 0.2 G = 833,333 psi

Ultimate tensile strength = $\frac{1}{10} f'_m$ = 200-250 psi

Ultimate shear strength = 100 psi Mortar f'_c = 1800-2500 Psi

Mortar tensile strength = 225 psi

Mortar tensile bond strength = 50 – 150 psi

The modulus of elasticity is calculated based on the following equation:

E_c = (750 to 1000) x f'_m = 1,500,000 to 2,000,000 psi

5.9 Polymer Retrofit Material Properties

Connell (2002) reported that the spray-on polyurea-based liners were selected for evaluation as a retrofit material during the blast tests at Tyndall AFB. The selected polymer was the pure polyurea, due to its strength, flammability, and cost. This polymer has many commercial applications, ranging from marine use to linings for feed and storage tanks. The particular material used during the tests was Line-X XS-350. Material tests were performed using three samples of XS-350 in order to determine important engineering properties. Table 5.9-1 shows the results of the material tests for these three samples, and Fig. 3.1-4 shows its strain-stress curve used in this research.

Table 5.9-1: XS-350 Material Properties

Sample	Maximum tensile strength (psi)	Elongation at max. tensile strength (%)	Maximum elongation (%)	Secant modulus (psi)	Toughness (psi*in/in)
XS-350A	1,839	46.37	53.62	26,133	846
XS-350B	2,039	73.74	83.48	24,218	1,459
XS-350C	1,920	88.62	94.40	22,028	1,522
Mean	1,933	69.58	77.17	24,126	1,276

6 RESPONSE MODEL DEVELOPMENT

6.1 Single-Degree-Of-Freedom System

An approximate design method first suggested by Biggs (1964) is adopted in this study for idealization of the one-way masonry wall as a SDOF system. To remain consistent, the nomenclature used by Biggs will also be used. A mass, spring, and damper system is depicted in Fig. 6.1-1 to simulate the wall system, and the general equation of motion for forced vibration is:

$$M_e \ddot{z}(t) + C_e \dot{z}(t) + K_e z(t) = F_e(t) \tag{6.1-1}$$

Where:

M_e = The equivalent mass of the SDOF

C_e = The equivalent damping coefficient of the SDOF

K_e = The equivalent stiffness of the SDOF

$F_e\ (t)$ = The equivalent load-time history applied to the SDOF

t = Time (in this chapter)

The equivalent system parameters are used to better match the deflection of the concentrated mass in the SDOF with some point on the structure, generally the midspan deflection. Damping was considered by both Moradi (2003) and Sudame (2004) in their

analysis of a single CMU as well as CMU walls. The impact of damping on the wall displacements and stresses proved to be insignificant in all cases.

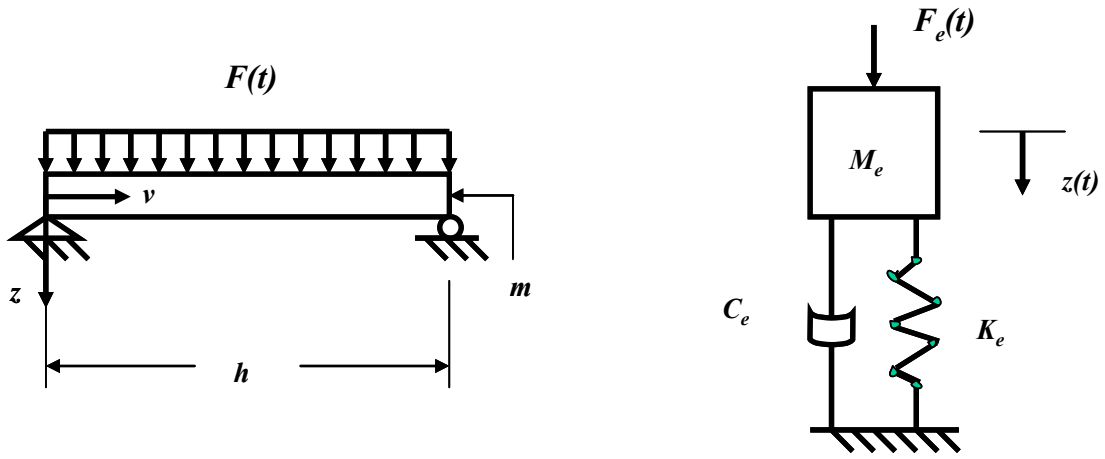

Fig. 6.1-1: Beam idealized as mass-spring-damper system

In addition, structural damping during plastic response cannot be clearly defined or verified experimentally and has no physical significance during the plastic deformation of the structural element (Kiger and Salim 1999). Therefore, the effects of structural damping will not be considered in the plastic region of response. For the purposes of this study, the damping coefficient is assumed to be zero, and equation 6.1-1 reduces to:

$$M_e \ddot{z}(t) + K_e z(t) = F_e(t) \tag{6.1-2}$$

To arrive at the equivalent mass and stiffness of the system, the first mode of the beam is required; however, to simplify the work of the design engineer, an approximate

deflected shape in the form of a fourth-order polynomial will be assumed to represent the first elastic mode of the system:

$$\varphi(v) = \frac{16}{5h^4}\left(h^3 v - 2hv^3 + v^4\right) \tag{6.1-3}$$

The equivalent mass, M_e, of the SDOF system representing a system with continuous mass distribution, m, is given by Biggs:

$$M_e = \int^h m\, \varphi^2(v)\, dv \tag{6.1-4}$$

The mass factor K_m is defined as the ratio of the equivalent mass to the actual total mass of the structure.

$$K_m = \frac{M_e}{M_t} \tag{6.1-5}$$

In the case of a beam with a constant mass along its length, $M_t = mh$, and M_e is given by equation 6.1-4, hence the mass factor is given by:

$$K_m = \frac{m\int m\varphi^2(v)dv}{mh} = \frac{1}{h}\int m\varphi^2(v)dv \tag{6.1-6}$$

The equivalent force is given by:

$$F_e = \int^h w(v)\,\varphi(v)\,dv \tag{6.1-7}$$

The load factor, K_L, is then defined as the ratio of the equivalent force to the actual force of $F_t = w(v)h$, which for a uniform load becomes $F_t = wh$

$$K_L = \frac{F_e}{F_t} = \frac{\int^h w(v)\varphi(v)dv}{wh} = \frac{1}{h}\int^h \varphi(v)dv \tag{6.1-8}$$

Biggs (1964) defines the resistance of an element, R, as the internal force restoring the element to its unloaded static position, and defines it in terms of the load distribution for which the analysis is being made. The stiffness of the element is simply the ratio of the rate of resistance to the incremental change in deflection:

$$K = \frac{\Delta_R}{\Delta_z} \qquad \text{and} \qquad K_e = \frac{\Delta_{Re}}{\Delta_z} \tag{6.1-9}$$

For the beam to be in equilibrium, resistance must always be equal to the force:

$$\frac{F_e}{F_t} = \frac{R_e}{R_t}$$

$$K_L = \frac{K_e z}{Kz} = \frac{K_e}{K} \tag{6.1-10}$$

Biggs introduces one final factor, K_{LM}, the load-mass factor, in order to simplify the equation of motion in terms of that factor alone. K_{LM} is defined as the ratio of the mass factor to the load factor. Equation 6.1-2 may now be written in terms of the real system with transformation factors, equations. 6.1-5, 6.1-8, and 6.1-10:

$$K_m M_t \ddot{z}(t) + K_L K z(t) = K_L F(t) \tag{6.1-11}$$

Dividing this equation by K_L we arrive at:

$$\frac{K_m M_t}{K_L} \ddot{z}(t) + K z(t) = F(t) \qquad M_t = \text{Total mass of system} = mh \tag{6.1-12}$$

By calling K_{LM} (load-mass factor) = $\frac{K_M}{K_L}$ we arrive at our final equation of motion:

$$K_{LM} M_t \ddot{z}(t) + K z(t) = F(t) \tag{6.1-13}$$

The natural period, T, of the system is given by (Biggs, 1964):

$$T = 2\pi \left(\frac{K_{LM} M_t}{K} \right)^{\frac{1}{2}} \tag{6.1-14}$$

Since the resistance of the wall $R(z) = Kz$, the equation of motion in terms of the resistance of the system is shown:

$K_{LM} M_t \ddot{z}(t) + R[z(t)] = F(t)$ or $\ddot{z}(t) = \frac{F(t)}{K_{LM} M_t} - \frac{R[z(t)]}{K_{LM} Mt}$ (6.1-15)

Where K_{LM} is a constant that depends on the shape function of the applicable behavior region. This equation of motion can now be solved numerically for $z(t)$, which gives the total motion-time history of the mass in the idealized system, and is the same as the transverse midspan deflection-time history of the wall. The appropriate transformation factors and element stiffness values must be applied during the various stages of analysis. The equation of motion can be solved by direct numerical integration.

Several numerical integration schemes are described by Biggs, including the constant velocity procedure, the linear acceleration method, the Newmark "beta" method, and several finite difference methods. The Newmark "beta" method is a very versatile method for solving differential equations incrementally. The central difference method corresponds to a Newmark time scheme with parameter values beta = 0 and γ = ½. The central difference formula relates the acceleration, $\ddot{z}(t)$ at time t to the displacement $z(t - \Delta)$, $z(t)$, and $z(t + \Delta t)$ corresponding to displacement at times $t - \Delta t$, t, and $t + \Delta t$, respectively, according to:

$$\ddot{z}(t) = \frac{\left(z(t - \Delta t) - 2z(t) + z(t + \Delta t)\right)}{\Delta t^2} \quad (6.1\text{-}16)$$

Substituting equation 6.1-16 into equation 6.1-15 and rearranging to solve for $z_{t+\Delta t}$ in terms of $z_{t-\Delta t}$ and z_t yields:

$$z(t+\Delta t) = \frac{F_t \Delta t^2}{K_{LM} M_t} + \left(2 - \frac{R_z \Delta t^2}{K_{LM} M_t}\right) z(t) - z(t-\Delta t) \qquad (6.1\text{-}17)$$

The central difference method is an explicit time scheme, because the unknown $\ddot{z}(t)$ is only a function of known values. Equation 6.1-17 allows for the displacement at the next time increment $z(t + \Delta t)$ to be calculated in terms of system constants and the current and previous displacement values $z(t)$ and $z(t - \Delta t)$. Note that F_t is non-zero only when a load is being applied to the structure and that R_z is a function of the displacement.

6.2 Blast Loads

For the SDOF analysis, the time histories of the blast loads were arrived at using charge size and standoff distance in the SBEDS (2006) program. Both positive and negative phases of the time histories were used to calculate the response.

6.3 Strain Rate Effects of Polymer Materials

Many polymers that may be appropriate for structural retrofitting purposes stiffen significantly and become brittle under high strain rates. Since the polymer coating is strongly bonded to the concrete block substrate, significant strains in the polymer occur when cracks occur. The polymers used in the AFRL blast tests have as much as 90% elongation ability under static loading, but resistance function calculations show that the polymer retrofit is strained (10% - 30%). Parametric FE studies by Sudame (2004) illustrated that the polymer strength parameters, such as initial modulus and yield point, have less effect on the maximum wall displacement than parameters that largely

influence strain energy absorption potential, such as polymer coating thickness and elongation capacity.

For the polyurea material used in the AFRL blast tests referenced in this paper, the strain rate characteristics were taken from the strain rate-dependent tensile tests conducted by the University of Dayton Research Institute (Hill 2003). In the best case, the tests showed a 75% increase in the initial modulus of elasticity of one of the polyurea specimens; however, the impact on the flexural behavior of the wall proved to be insignificant. Analysis shows that increases of one order of magnitude (10 times) or more in E tend to have a significant effect on the flexural behavior of the wall. The challenge remains in finding polymer retrofits with such high modulus of elasticity.

The tensile tests (Hill 2003) showed significant increases in the yield strength and ultimate strength of polyurea at high strain rates. The maximum strength reported was at 2,984 psi, for a strain rate of 450/s, which is 50% higher than the maximum strength reported for the average to low strain rates. This also has little impact on the response of the wall as the no-arching scenario shows a 16% improvement in response, and the wall with arching shows little to no improvement in its response.

6.4 Analysis Results of the SDOF System

The resistance functions developed in Chapter 5 and equation 6.1-17 were programmed into Microsoft Excel and solved for different wall heights and material property conditions. To check the validity of the technique, analysis results are expected to match closely with the actual test results in the field. The wall height is the actual unsupported length of the tested wall from the top support to the bottom support. The

test wall acts as a one-way beam and resists the incoming blast pressure with simple bending and shear.

In Chapter 5, it was demonstrated that the resistance of membrane retrofit concrete masonry walls with arching action can be several times greater than the same walls without arching. For wall test 1, the response from the SDOF analysis without arching is shown in Fig. 6.4-1 to be 14.5 inches, which is 97% more than the response of 7.3 inches from the arching action SDOF analysis. The maximum mid-span test deflection for wall test 1 is shown at 7.2 inches, which is only 1% less than the value calculated for the arching action case. For wall test 3, the SDOF analysis shows failure for the case without arching (Fig. 6.4-2). The maximum mid-span test deflection for wall test 3 is shown at 9.38 inches, which is 36.4% less than the value calculated for the arching action case. The results for all of the other wall tests show a similar pattern, where the SDOF without arching deflections are twice the values shown by the tests, and the arching SDOF deflections remain closer to those shown by the tests.

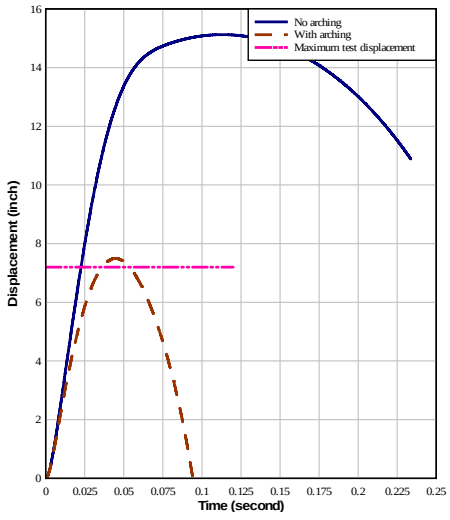

Fig. 6.4-1: SDOF analysis results for test 1

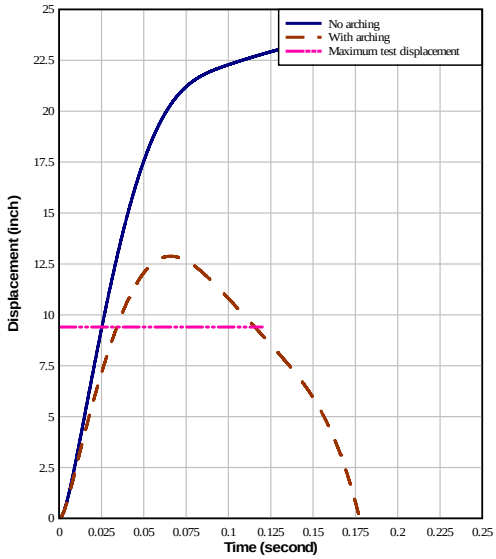

Fig. 6.4-2: SDOF analysis results for test 3

Overall, analyses were performed for wall tests 1, 2, 3, 9, 10, 11, 12, BREW 1, BREW 2, BREW 3, BREW 4, BREW 5, BREW 6, BREW 7, BREW 8, and BREW PSEAG. The results are also tabulated in Table 7.1-1 of Chapter 7 in order to compare them to the finite element analysis results described in that chapter. The table shows wall dimensions, membrane retrofit type and thickness, and test, SDOF and finite element analysis results.

6.5 Wall Reaction Forces

The horizontal reactions of the wall at the top and bottom supports are calculated using an approximate method suggested by Biggs (1964) for a simply supported beam with uniform pressure. To be conservative, a worst case combination of the elastic and plastic scenarios is used in equation 6.5-1. This equation is programmed into Excel used for the SDOF analysis, and horizontal reactions are calculated for each time step.

$$Horizontal\ Reaction = 0.39R + 0.11F \quad (6.5\text{-}1)$$

Where:

R = Wall resistance

F = Blast force

The vertical reactions of the wall are calculated using arching forces (for the arched case), the dead weight of the wall, and any surcharge that may be present (equations 6.5-2 and 6.5-3). For the cases without arching, V_{Top} and V_{Bottom} are set at zero in these two equations.

$$Vertical\ Reaction\ at\ Top = P + V_{Top} \quad (6.5\text{-}2)$$

$$Vertical\ Reaction\ at\ Bottom = W_i + P + V_{Bottom} \quad (6.5\text{-}3)$$

Where:

V_{Top} = Arching force at the top support

V_{Bottom} = Arching force at the bottom support

W_i = Weight of wall

P = Surcharge

7 FINITE ELEMENT ANALYSIS

7.1 Wall Analysis

The model discussed in Chapter 4 was analyzed for some of the wall tests tabulated in Chapter 3. The model could only be used for wall tests 1, 2, 3, BREW 6, BREW 7a, BREW 8, and BREW PSEAG because of its height of 144 inches, lack of any openings to account for windows and doors, and lack of information related to wall size or membrane retrofit properties for the remaining wall tests.

As noted in Chapter 4, Moradi (2003) examined four promising constitutive models in LS-DYNA for the analysis of a single block of concrete masonry (CMU). The results were verified by actual blast tests, and the MAT_SOIL_AND_FOAM constitutive model was deemed to be the best choice for the analysis of concrete masonry walls. This constitutive model is generally used for geomaterials and simulates crushing through the volumetric deformations.

Subsequently, Sudame (2004) used the MAT_SOIL_AND_FOAM in his analysis of the full-scale membrane retrofit concrete masonry walls. The results were in close agreement for the single-wall test (load I) used in the analysis; however, Sudame was unable to distinguish between the arching case and the case without arching. The corresponding changes in boundary conditions regarding the lack of a gap (arching) and the presence of one (no arching) did not result in significant differences in the final displacement response of the wall. The left picture in Fig. 7.1-1 shows no gaps between

the base of the wall and support, and the right picture in the same figure shows a gap between the base of wall and the support. At the top interface of the wall, the same conditions are repeated.

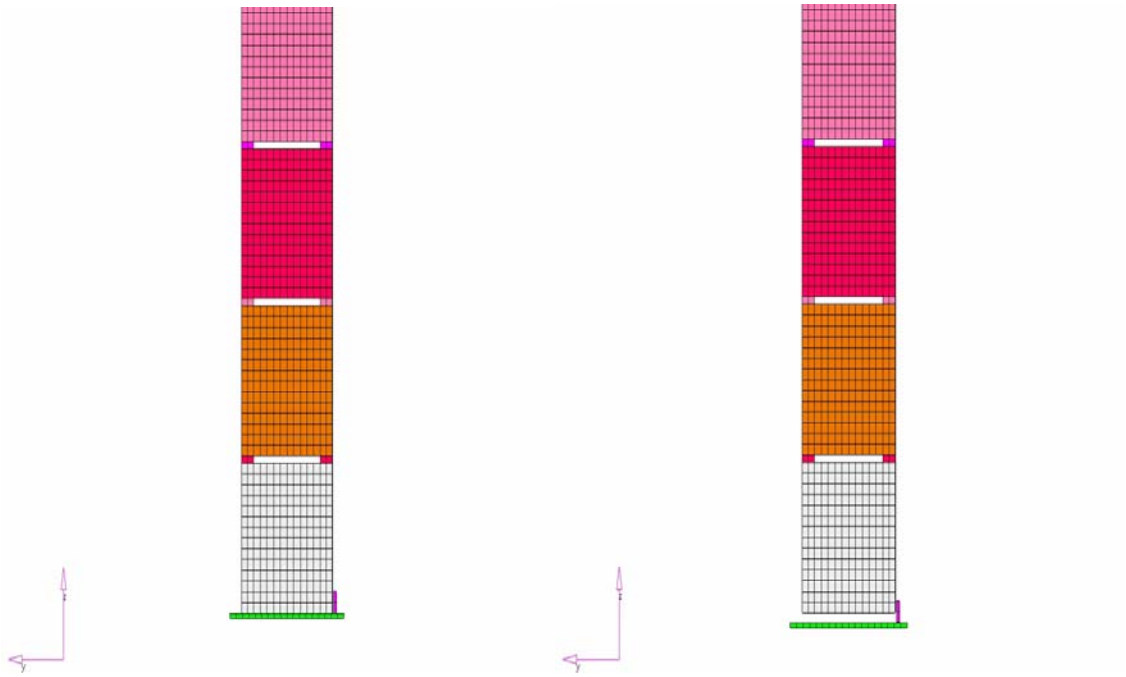

No-gap model Gap model

Fig. 7.1-1: F.E. model with and without gap

To further investigate the impact of arching forces on the behavior of membrane retrofit concrete masonry walls, another promising constitutive model was selected for analysis. The MAT_BRITTLE_DAMAGE model is anisotropic and designed primarily for concrete and steel reinforced concrete, though it can be applied to a wide variety of brittle materials (LS-DYNA 1999). It admits progressive degradation of tensile and shear strengths across smeared cracks that are initiated under tensile loadings and compressive failure that can be disabled if not desired.

This constitutive model was incorporated in the finite element model of the wall, and analyses were performed using blast load pressure curves generated with SBEDS (2006) program. It is important to note that the pressure curve generated using SBEDS or other available methods (Fig. 7.1-2, right graph) is at best an approximation and does not completely match the measured pressure curve from the actual test (Fig. 7.1-2, left graph).

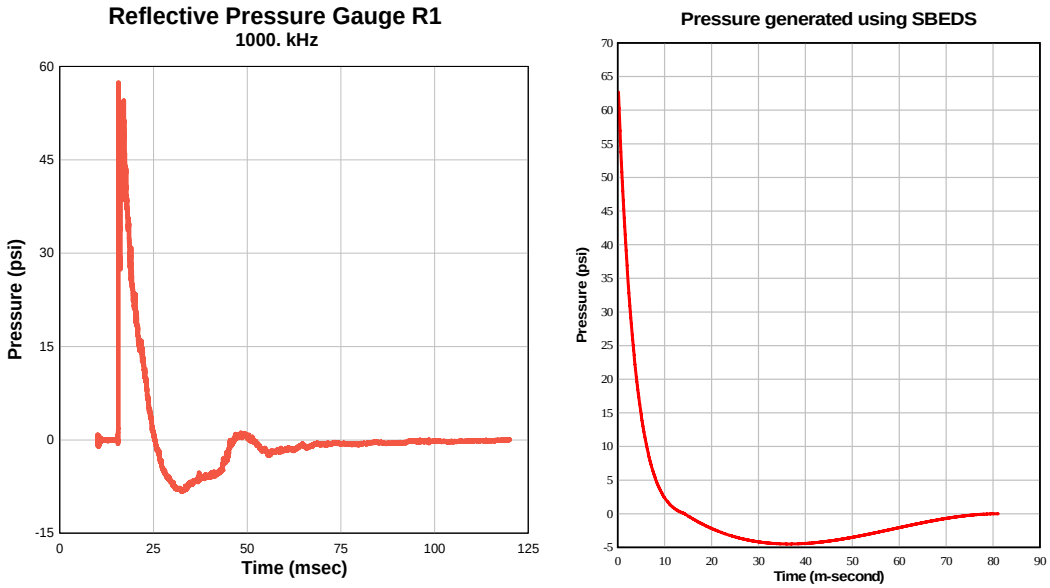

Test pressure vs time Analysis pressure vs time

Fig. 7.1-2: Blast load for test 1

The analysis results showed distinct differences between the arching cases and those without arching. For wall test 1, the results showed significant arching forces for the no-gap boundary conditions, as shown in Fig. 7.1-3, and zero arching forces for the boundary condition with a gap. For the overall response of the wall, the results showed significant differences between the arching case and the case without arching. A

maximum displacement of 6.9 inches was computed for the arching case as compared to wall failure for the no-arching case (Fig. 7.1-4). In the no-arching case, the finite element run terminated due to excessive displacements, as evident by the discontinuity at the peak of the blue curve in Fig. 7.1-4. The results show a crack developing at the midpoint of the wall on the tension face and opening wider as the wall deflects (Fig. 7.1-5). In the arching case, the crack continues to open but the masonry elements remain in contact at the mid-point of the wall on the compression face (Fig. 7.1-6). The membrane retrofit remains intact for the most part in the arching case, but completely fails for the no-arching case. The maximum displacement results of the finite element analysis are within 4.2% of the test results at 7.2 inches for wall 1.

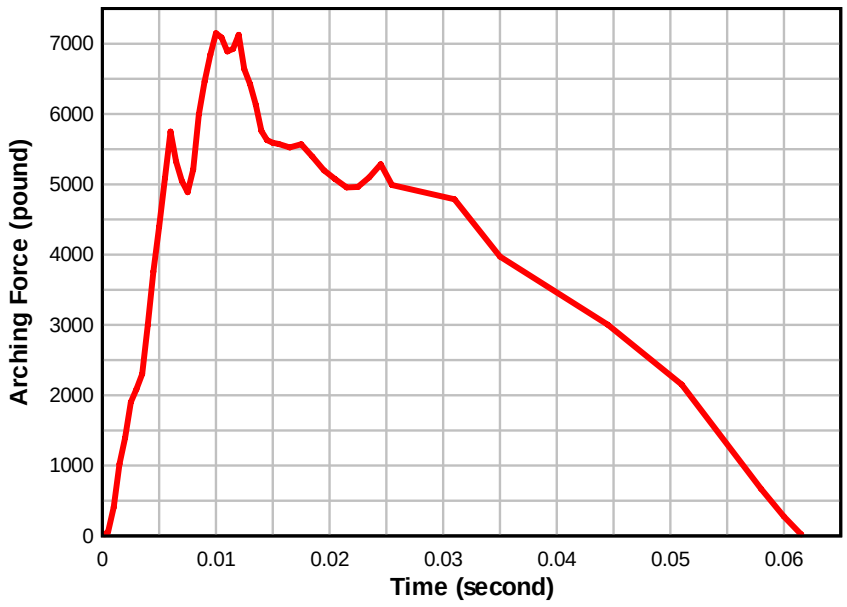

Fig. 7.1-3: Arching forces for test 1

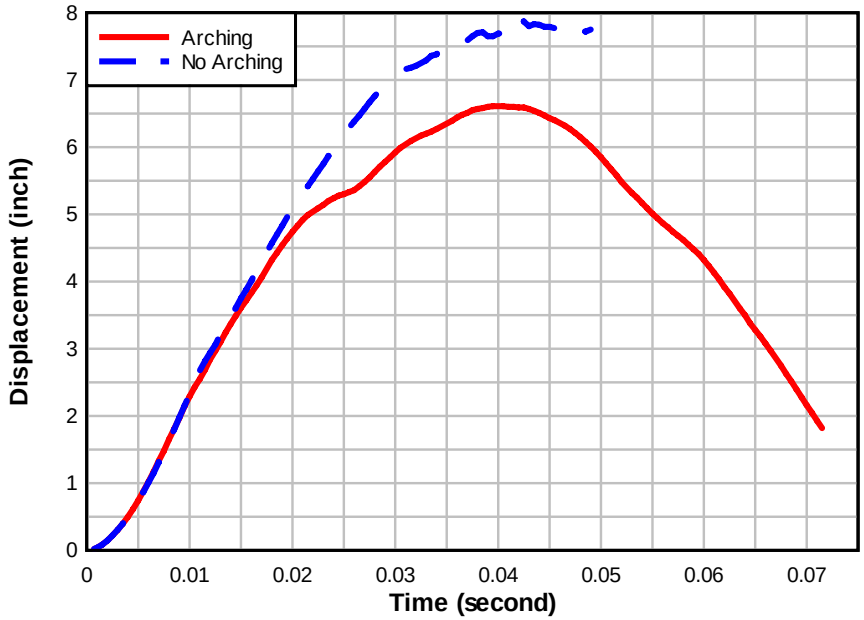

Fig. 7.1-4: Wall midpoint maximum displacements for test 1

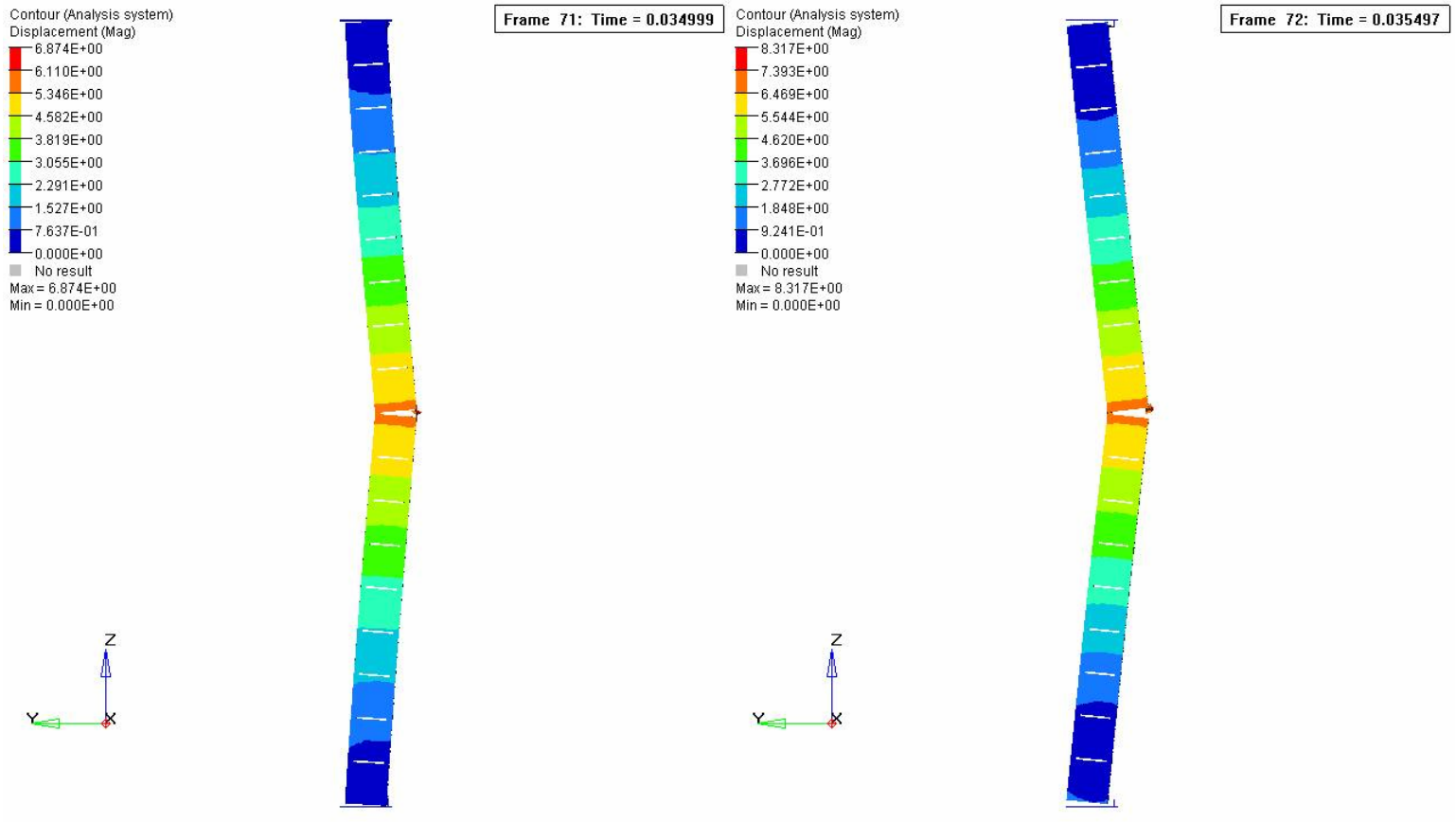

Arching Model

No Arching Model

Fig. 7.1-5: Wall deflected shape for test 1

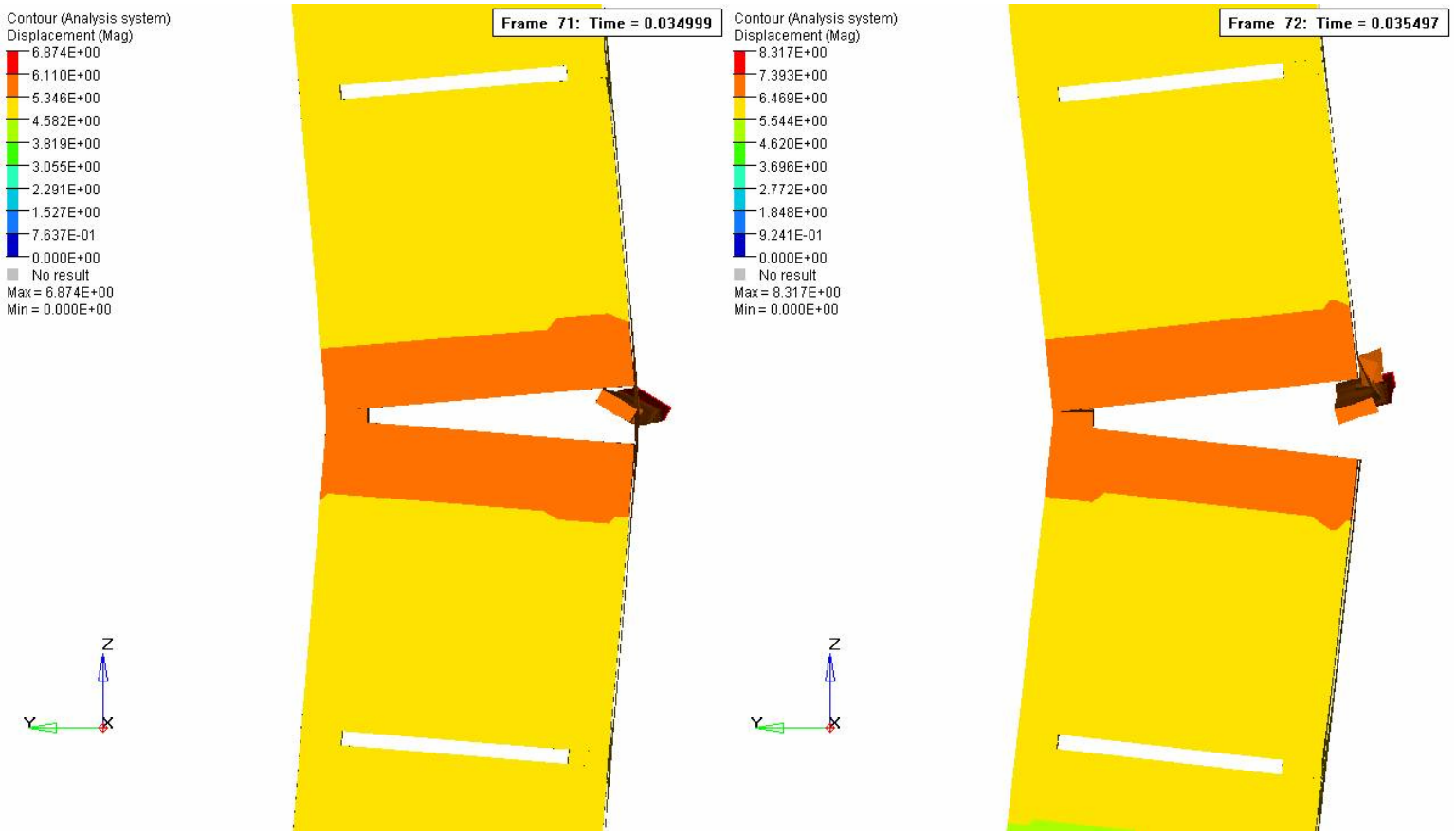

Arching Model No Arching Model

Fig. 7.1-6: Mid-point crack details for test 1

For wall test 2, the intentional selection of a large charge size caused the complete collapse of the membrane retrofit wall during the test. Finite element analysis of the arching and no-arching cases produced the same results for wall test 2.

For wall test 3, only the wall with membrane retrofit on the inside face of the wall was examined. The membrane retrofit thickness was increased to 0.25 inch accordingly, and analyses were performed for the no-gap boundary condition and the boundary condition with gap. Results showed significant arching forces for the no-gap model, as shown in Fig. 7.1-7, and zero arching forces for the model with gap.

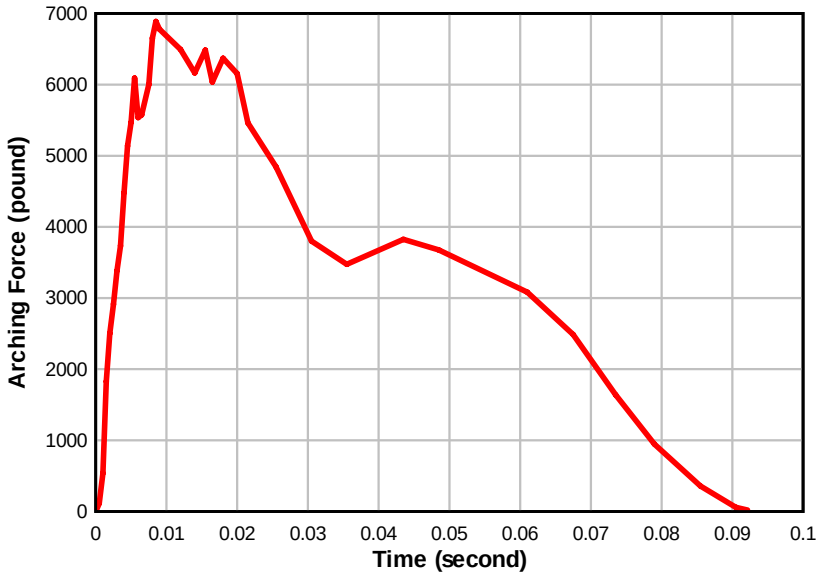

Fig. 7.1-7: Arching forces for test 3

The no-gap (arching) case showed a maximum displacement of 8.68 inches at the midpoint of the wall, versus the gap (no-arching) case that failed (Fig. 7.1-8). The deformed shape of the wall is shown in Fig. 7.1-9 for the model with no-gap and the model with gap. The failure in the model is distinct in the close-up view of the cracked

section of the wall midpoint as shown in Fig. 7.1-10. The gap model in the right section of Fig. 7.1-10 shows clear separation between the top and bottom halves of the wall. The maximum displacement results for wall test 3 are within 7.5% of the test results of 9.38 inches.

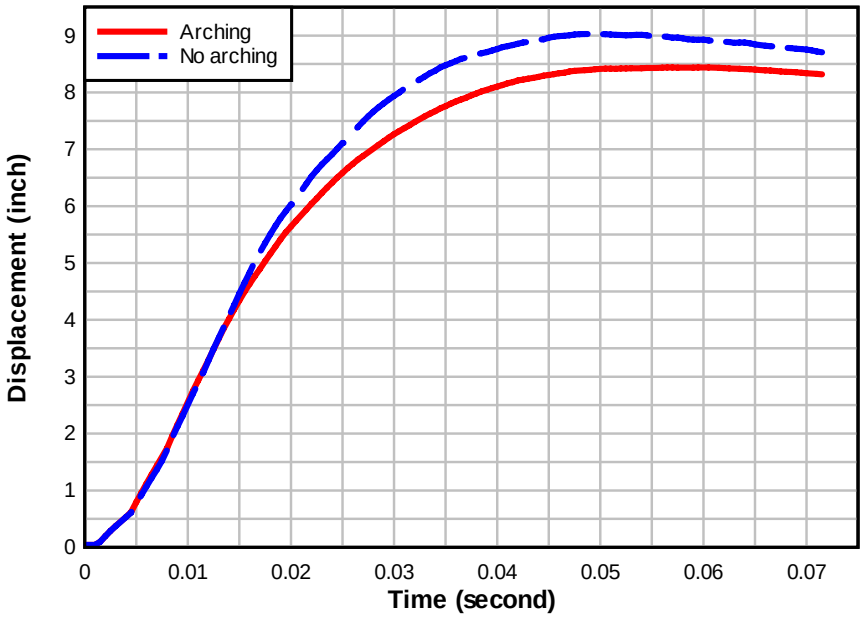

Fig. 7.1-8: Wall midpoint maximum displacements for test 3

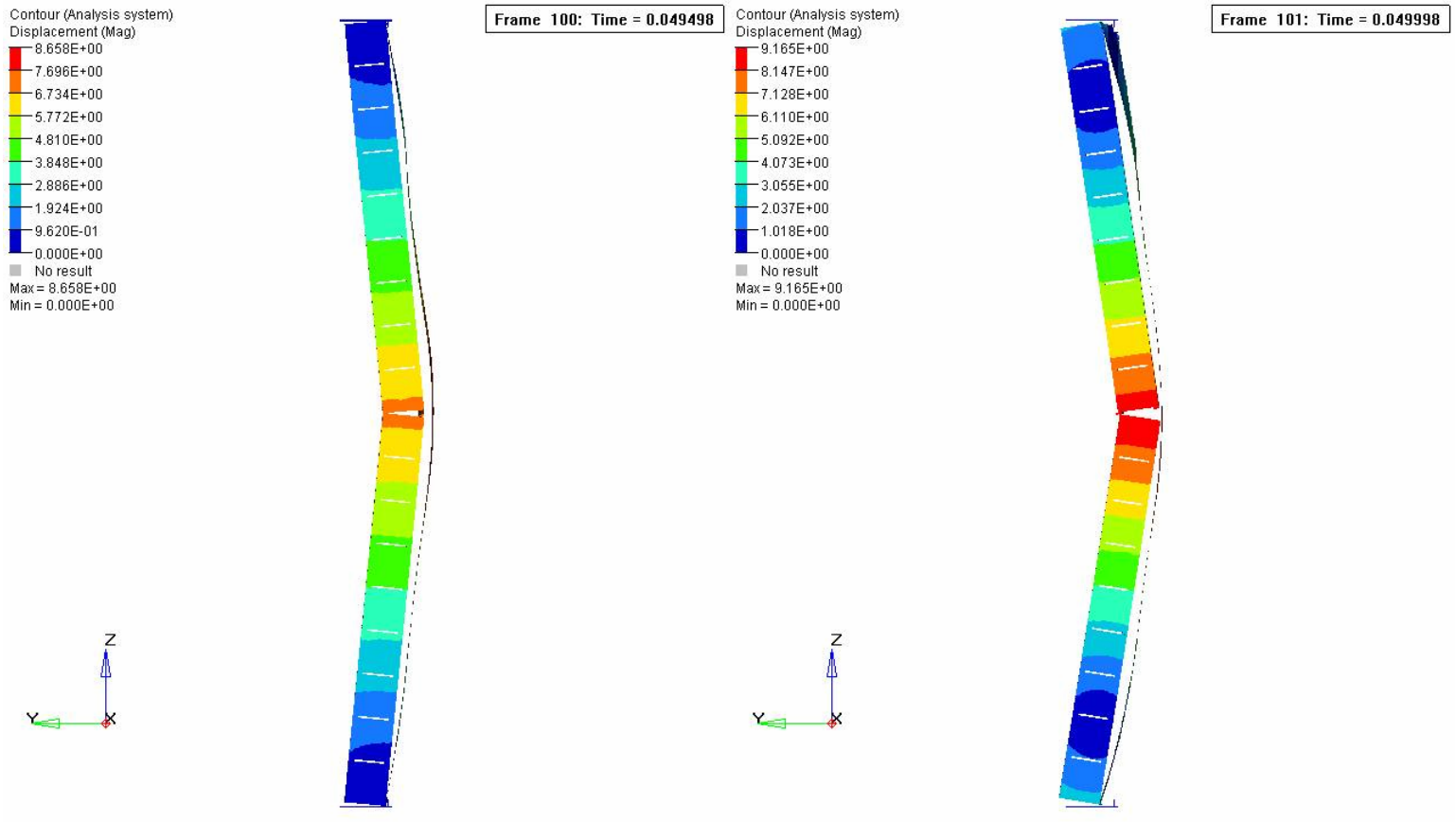

Arching Model

No Arching Model

Fig. 7.1-9: Wall deflected shape for test 3

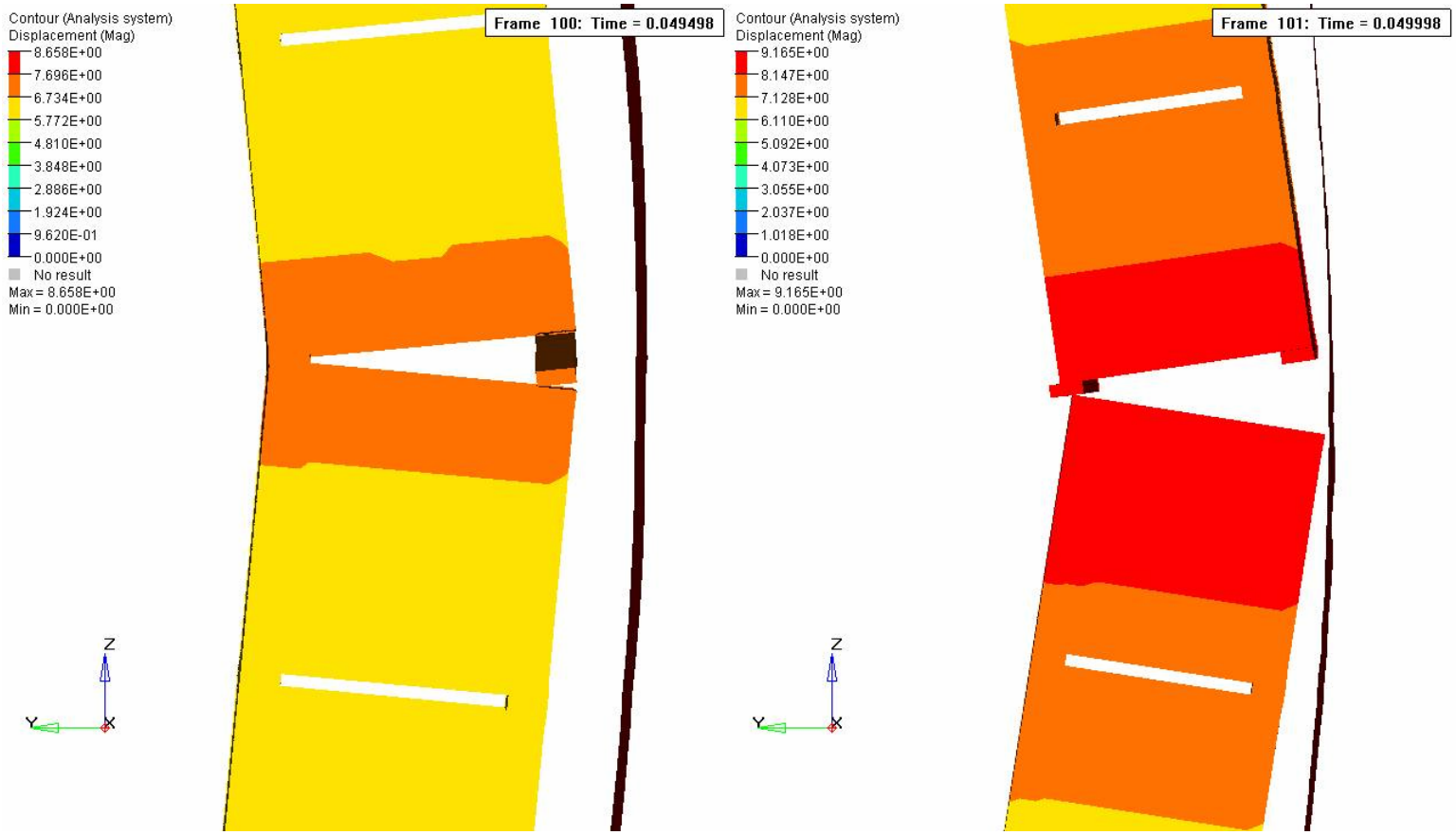

Arching Model No Arching Model

Fig. 7.1-10: Mid-point crack details for test 3

In wall test BREW 6, the membrane retrofit is not attached to the concrete masonry wall and acts as a catcher system. The thickness of the membrane retrofit was changed to 0.12 inch, its material properties were properly described, and the contact forces between it and the concrete masonry elements were removed to simulate the unbonded conditions. Results showed significant differences in which the no-gap (arching) case showed a maximum displacement of 7.65 inches at the midpoint of the wall, versus the gap (no-arching) case that failed. The maximum displacement results for wall test BREW 6 are within 21% of the test results of 9.71 inches.

In wall test BREW 7, only the wall with the 0.25-inch PPG membrane retrofit was analyzed, since the material properties of this retrofit were available. Results showed significant differences in which the no-gap (arching) case showed a maximum displacement of 6.21 inches at the midpoint of the wall, versus the gap (no-arching) case that failed. The maximum displacement results for wall test BREW 7 are within 26% of the test results of 8.36 inches.

In wall test BREW 8, two walls with identical construction and membrane retrofits were tested. One wall showed a maximum midpoint displacement of 9.7 inches during the test, while the second wall showed a maximum displacement of 11.5 inches. The results showed significant differences. The no-gap (arching) case showed a maximum displacement of 6.52 inches at the midpoint of the wall, versus the gap (no-arching) case that failed. The analyses maximum displacement results for wall test BREW 8 are within 33% of the test results for one wall and 43% for the other wall.

In wall test BREW PSEAG, the membrane retrofit is not attached to the concrete masonry wall and acts as a catcher system (similar to BREW 6). The contact forces

between the membrane retrofit and the concrete masonry elements were removed to simulated the unbonded conditions. Results showed significant differences in which the no-gap (arching) case showed a maximum displacement of 7.73 inches at the midpoint of the wall, versus the gap (no-arching) case that failed. The maximum displacement results for wall test BREW PSEAG are within 40% of the test results of 12.9 inches.

The results of the finite element analysis are also tabulated in Table 7.1-1 for ease of comparison with blast test results as well as the resistance function SDOF analysis results.

Table 7.1-1: Comparison of test, resistance function SDOF analysis, and the finite element analysis results

Wall Test	Retrofit (in)	h (ft)	Width (ft)	Test Max. Defl. (in)	SDOF Max. Defl. (in)	% Diff. with test	FE Analysis Max. Defl. (in)	% Diff. with test
1	1/8 Line-X XS-350	12	7.5	7.2	14.92 - No arching 7.3 - Arching	107.2 1.4	Failed – No arching 6.9 - Arching	4.2
2	1/8 Line-X XS-350	12	7.5	Failed	Failed	---	Failed	---
3	1/4 Line-X XS-350	12	7.5	9.38	Failed – No arching 12.8 - Arching	--- 36.4	Failed – No arching 8.68 - Arching	--- 7.5
3a Cubicle	1/8 Line-X XS-350 6 inches of overlap	8	8	4.94	18.29 – No arching 3.42 - Arching	270.0 30.76	----	---
3b Cubicle	1/8 Line-X XS-350 12 inches of overlap	8	8	5.94	18.29 - No arching 3.42 - Arching	207.9 42.4	---	---
9a	1/8 Line-X XS-350	10	7.5	7.71	12.35 - No arching 4.1- Arching	60.2 46.8	---	---
9b	1/8 Line-X XS-350	10	7.5	5.63	13.01 – No arching 2.85 - Arching	131.1 49.4	---	---
10	1/8 Line-X XS-350	12	16	7.4	7.0 - Arching	5.4	---	---
11	1/8 Line-X XS-350	12	16	9.5	10.0 - Arching	5.3	---	---

Table 7.1-1: Comparison of test, resistance function SDOF analysis, and the finite element analysis results – Continued

Wall Test	Retrofit (in)	h (ft)	Width (ft)	Test Max Defl. (in)	SDOF Max. Defl. (in)	% Diff. with test	FE Analysis Max. Defl. (in)	% Diff. with test
12a	1/8 Catcher Retrofit Line-X XS-350 Mortarless	12	8	Failed	27.3 – No arching 10.5 - Arching	---	---	---
12b	1/8 Line-X XS-350 Mortarless	12	8	8.1	19.4 - No arching 9.1 - Arching	139.5 12.3	---	---
BREW 1	0.2 - 0.4 B1	10	8	5.8	21.6 - No arching 4.73 - Arching	272.4 18.4	---	---
BREW 2	0.2 – 0.4 Trowel-on B1	12	7.5	Failed	25.0 - No arching 13.1 - Arching	---	---	---
BREW 4	1/8 Line-X XS-350 12 Assumed	12 Assumed	8 Assumed	8.5	19.4 - No arching 9.19 - Arching	128.2 8.1	---	---
BREW 5	0.12 Polypropylene	12	7.5	3.69	20.4 - No arching 3.24 - Arching	454.1 12.2	---	---
BREW 6	0.12 Catcher Retrofit B&H Clear	12	8	Not available Survived	27.4 - No arching 9.71 - Arching	---	Failed – No arching 7.65 - Arching	---
BREW 7	1/4 3572-37-1	12	8	7.7	17.8 - No arching 8.36 - Arching	131.2 8.6	Failed – No arching 6.2 - Arching	--- 19.5
BREW 8	1/8 3572-74-2	12	8	11.6	Failed - No arching 10.56 - Arching	--- 8.9	Failed - No arching 6.5 - Arching	--- 43.9
BREW PSEAG	1/8 Catcher Retrofit B&H	12	8	12.9	22.3 - No arching 7.72 - Arching	72.9 40.2	Failed - No arching 7.7 - Arching	--- 40.3

8 DISCUSSIONS, CONCLUSIONS, AND RECOMMENDATIONS

8.1 Discussions of the results

The tests conducted by AFRL were designed to examine the effectiveness of polymer retrofits in mitigating wall disintegration and instability due to blast pressure. These tests were not designed to verify computational analytical models. The small number of tests shown in Table 7.1-1 does not lend itself to scientific statistical averages and makes it difficult to use them in verification of computational models. Running a large enough number of full-scale blast tests for dependable scientific averages are cost prohibitive. However, the availability of such data provides an opportunity for comparison and perhaps a tuning of the computational models for better results.

The test results include several areas of curiosity. In twelve of the tests the maximum wall displacement at the midpoint was greater than the wall thickness of 7.625 inches. In two cases (BREW 2 and BREW 8) the wall collapsed. Common wisdom dictates that a concrete masonry wall would collapse if the midpoint lateral displacement is greater than the wall thickness. In the other ten cases shown in Table 7.1-1 where the wall survived, the credit is attributed to the membrane retrofit. In most of these cases, the wall is no longer structurally sound but the membrane retrofit continues to hold it in place. This is one of the benefits that membrane retrofits provide toward prevention of the complete collapse of these walls.

Several of the wall tests have almost exactly the same build, charge size, and stand-off distance. The only difference is the type of polymer used in the tests. One example of this kind is the case of the two cubicles in wall test 3, in which there are no differences between the two walls, yet the midpoint displacements from the test are 4.94 inches versus 5.95 inches. Similar results are noted for wall test BREW 8 where the left wall displacement at the mid-point is 9.7 inches, versus the right wall midpoint displacement of 11.5 inches. In this test, the walls were built side by side in the same reaction structure. Another observation regarding BREW 8 test is that both walls experienced some level of collapse, and their final displaced shape points towards the blast source rather than caving into the occupied area.

The BREW PSEAG test was radically different from the other tests discussed in this report. In this test a simulated vehicle search area was set up that included two walls, one of which had a retrofit over a common CMU wall construction (catcher system). The test included multiple barriers used around the vehicle to replicate the damage incurred by the structures and barriers due to the pressure and fragmentation from explosives concealed in a vehicle. The wall deflected excessively but survived the test. The placement of the explosive charge in the vehicle and the barriers set up around the vehicle significantly alters the blast pressure experienced by the polymer retrofit CMU wall. This may potentially be the sole contributor to the differences between the maximum test displacement and those computed by analytical models shown in Table 7.1-1.

Although polymer membrane retrofits improve the structural stability of concrete masonry walls exposed to lateral blast pressure, they do not have a significant impact on

the stiffness of these walls. Every polymer retrofit used in the tests had a low modulus of elasticity and tensile strength; therefore, the discrepancies noted in the tests were most likely not caused by the use of different polymers. They may be attributed to several other factors. The charge size and stand-off distance do not always generate the same blast pressure and impulse, as shown by Connell (2002) and Thornburg (2004). This is influenced by the size of the blast source, which is not always an exact measurement, the ground conditions underneath the blast source, which may not be the same from one test to another, and finally blockage by buildings, heavy concrete partitions, temperature, humidity, or other items. The method of construction for concrete masonry walls varies from one builder and site to another. As much as these methods may be kept similar, differences creep in regarding material properties of the CMUs, mortar, outside temperature and humidity at the time of construction, the size of the gap at the top interface of the wall, etc.

The blast loads used in both the SDOF analysis and the finite element analysis were generated using the SBEDS (2006) program. The time versus pressure curve generated in this fashion is at best a good approximation, but does not match the pressure time history measured during the actual tests. This fact is shown in Chapter 7, Fig. 7.1-2 for test 1, and should be considered as one of the factors that influence the discrepancy between analysis and test results. The best approach is to digitize the test pressure time history for use in the analytical efforts; however, this is often cost prohibitive.

It is important to mention the reliability and precision of high-fidelity finite element models over approximate analytical techniques, such as the resistance-function-based SDOF approach. Although the SDOF approach is easy, fast, cost effective, and

accurate, it is no match for the level of detail high-fidelity finite element models can probe into the behavior of these complex walls. Overall deformation of the wall system, local deformations, strains, stresses, mortar to concrete masonry joints, membrane retrofit to concrete masonry attachments, and many other areas of interest can only be examined through the use of high-fidelity finite element models.

The arching resistance function SDOF analysis results agreed well (1.4% - 18.4% difference) with test results for walls #1, #2, #10, #11, #12b, BREW 1, BREW 2 (since wall collapsed), BREW 4, BREW 5, BREW 6 (although no test results were available), BREW 7, and BREW8. This is 15 wall results out of 21 walls, which indicates a success rate of over 70% in predicting the correct wall response.

The finite element analysis results agreed well (4.2% - 19.5% difference) with test results for walls #1, #2, #3, BREW 6, and BREW 7a. This is 5 wall results out of 8 walls, which indicates a success rate of over 60%. This success rate would increase significantly if finite element models were made of more of the walls.

In either of the analytical approaches, the success rate is significant when considering the discrepancies noted in the tests. Analytical simulation models using resistance functions and finite element methods use formulas, blast pressure, wall stiffness, and other parameters to compute the response. These parameters remain exactly the same from one model to another unless dictated by wall geometry, material properties, and or loading conditions. The same is not true for actual blast tests of membrane retrofit concrete masonry walls. The attempt to validate analytical results using actual wall tests that differ one from another based on factors other than the parameters used in the analysis may not be prudent in every case. It is certain to assume

the success rate of the analytical methods would increase if tests could be performed in perfect conditions such that two identical walls would produce identical results under the same exact loading conditions.

8.2 Conclusions

This research provides the formulation for the resistance of membrane retrofit concrete masonry walls to lateral uniform pressure. Resistance functions are provided for three separate cases:

1. Unreinforced concrete masonry walls with and without membrane retrofit.
2. Unreinforced concrete masonry walls with and without membrane retrofit, and with arching action.
3. Unreinforced concrete masonry walls with a membrane retrofit catcher system.

The research provides the proper formulation to cost effectively determine the response of membrane retrofit concrete masonry walls to blast and environmentally induced pressures. The results may be used in high-risk areas to enhance the construction of new buildings using unreinforced concrete masonry walls, as well as to retrofit similar walls in existing buildings or homes. For arching action to develop, care must be taken to ensure gaps are not present between the wall and its top and bottom interfaces.

The research also provides a reliable high-fidelity finite element model to be used for detailed analysis of such walls where localized deformations, high-stress areas, and a host of pertinent parameters may be examined.

8.3 Recommendations

Based on the results of this research, the following recommendations are made regarding the construction of membrane retrofit concrete masonry walls:

1. In every case possible, walls subjected to lateral pressure must be constructed without any gaps at the top and bottom supports in order to develop arching forces.
2. Metal membrane retrofits such as steel and aluminum sheets are far better choices for the construction of such walls. These retrofits increase the resistance function of concrete masonry walls to lateral pressure substantially.
3. The next choice would be the use of high stiffness, high-strength polymers if the cost is not prohibitive.
4. Care must be given to the attachment of membrane retrofits to the wall, floor, and ceiling in order to fully develop the strength of the wall system.

Although membrane retrofit concrete masonry walls have shown great results in seismic and blast tests, further studies are recommended to quantify the improvement of this system for wind conditions, as well as tests to verify the analysis results. The studies should concentrate on:

5. The application of polymer retrofit materials to concrete masonry walls: To date, there is no objective evidence that polymer retrofits lack adequate adherence to

the surface of concrete masonry. However, little research has been conducted to accurately determine the adherence of polymers to concrete masonry surfaces.

6. Application of the membrane retrofit material to the bottom and top boundaries of the wall needs to be investigated. Adequate extension and attachment of the membrane retrofit through the top and bottom supports play a major role in the structural integrity of the wall system.
7. Shock tunnel and wind tunnel tests of full-size or reduced-size membrane retrofit walls will allow for better instrumentation of the wall and membrane retrofit. The results will be used to fine-tune the current analytical models.
8. Static and dynamic tests to better define the strain for the arching ends: To date, little is published in the literature on the behavior of the arching ends of the wall system. A knowledge of the crushing behavior of the arched end while the wall experiences large deflections is important to the accuracy of the current analytical models.

LIST OF REFERENCES

Avallone, E.A. and Baumeister, T. (1987). *Mark's standard handbook for mechanical engineers,* McGraw-Hill, NewYork, N.Y.

Baker, L.R. (1980), "Lateral Loading of Masonry Panels: *Structural Design of Masonry*," Cement and Concrete Association of Australia, Sydney, Australia.

Baker L.R. (1977), "The Failure Criterion of Brickwork in Vertical Flexure." Proc., of the 6th International Symposium on Loadbearing Brickwork, London, England, 203-216.

Barbero, E. J., Davalos, J. F., Kiger, S. A., Shore, J. S. (1997). "Reinforcement with advanced composite materials for blast loads." *Proc., Structures Congress XV*, Portland, Oregon.

Baylot, J. T., Bullock, B., Slawson, T. R., Woodson, S. C. (2005). "Blast Response of Lightly Attached Concrete Masonry Unit Walls." *Journal of Structural Engineering*, ASCE, 131(8), 1186-1193.

Beshara, F.B.A. (March 1994). "Modelling of blast loading on aboveground structures-I. General phenomenology and external blast." Technical paper. *Computers and Structures* 51(5), 585-596.

Biggs (1964), *Introduction to Structural Dynamics*, McGraw-Hill Book Company, New York.

Britt, J.R., and Lumsden, M.G. (1994). *Internal blast and thermal environment from internal and external explosions: A user's guide for BLASTX Code, Version 3.0*, Science Applications International Corporation, St. Joseph, Louisiana, Report No. SAIC 405-94-2.

Broadhouse, B.J. (February 1995). *The Winfrith Concrete Model in LS-DYNA*, Structural Performance Department, AEA Technology, Winfrith Technology Centre.

Burke, L.M., Iannacchione, A.T., Barczak, T. M., Westman, E., (2004), "*Numerical Modeling for Increased Understanding of the Behavior and Performance of Coal Mine Stopping*," Virginia Tech., Blacksburg, Virginia.

Connell (2002), "Evaluation of Elastomeric Polymer for Retrofit of Unreinforced Masonry Walls Subjected to Blast," MS Thesis, University of Alabama at Birmingham, Alabama.

Crawford, J. E., Bogosian, D. D., Wesevich, J. W. (1997a). "Evaluation of the effects of explosive loads on masonry walls and an assessment of retrofit techniques for increasing their strength." *Proc., 8th International Symposium on Interaction of the Effects of Munitions with Structures*, McLean, Virginia.

Crawford, J. E., Malvar, L. J., Wesevich, J. W., Valancius, J., Reynolds, A. D. (1997b). "Retrofit of reinforced concrete structures to resist blast effects." Technical paper, Title No. 94-S34. ACI Structural Journal, 94(4), 371-377.

Davidson, J.S., Porter, J.R., Dinan, R.J., Hammons, M.I., Connell, J.D. (May 2004). "Explosive Testing of Polymer Retrofit Masonry Walls." *Journal of Performance of Constructed Facilities*, ASCE, 18(2), 100-106.

Davidson, J.S., Fisher, J.W., Hammons, M.I., Porter, J.R., Dinan, R.J. (August 2005). "Failure Mechanisms of Polymer-Reinforced Concrete Masonry Walls Subjected to Blast." *Journal of Structural Engineering*, ASCE, Vol. 131, No. 8, 1-12.

Dennis, S. T. (1999). "Masonry walls subjected to blast loading-DYNA3D analysis." U.S. Army Engineer Waterways Experiment Station, Vicksburg, Mississippi.

Dennis, S. T., Baylot, J. T., Woodson, S. C. (2000). "Response of ¼ scale concrete masonry unit (CMU) walls to blast." *Proc., ASME Pressure Vessels and Piping Conference*, Seattle, Washington.

Dharaneepathy, M.V., Keshava Rao, M.N., Santhakumar, A.R. (October 1995). "Critical distance for blast-resistant design." *Computers and Structures* 54(4). 587-595.

Dinan, R.J., Fisher, J.W., Hammons, M.I., Porter, J.R. (2003). " Failure mechanisms in unreinforced concrete masonry walls retrofitted with polymer coatings," *Proc., of the 11th International Symposium on Interaction of the Effects of Munitions with Structures*, May 5-9, 2003.

Du Bois, P.A. (2004). *Crashworthiness engineering course notes*, Livermore Software Technology Corporation, California.

Doherty, K., Griffith, M.C., Lam, N., Wilson, J. (2002). "Displacement-based Seismic Analysis for Out-of-Plane Bending of Unreinforced Masonry Walls," *Earthquake Engineering and Structural Dynamics*, 31(4), 833-850.

Drysdale, R.G., Hamid, A.A., Baker, L.R. (1994). *Masonry and Structures: Behavior and Design*, Prentice Hall, Englewood Cliffs, New Jersey.

Drysdale, R. G., Hamid A. A., Baker L. R. (1999). *Masonry structures: behavior and design*, The Masonry Society, Boulder, Colorado.

Effects of Airblast, Cratering, Ground Shock and Radiation on Hardened Structures, (1976), Air Force Systems Command Manual, AFSCM 500-6, United States Air Force, Andrews Air Force Base, Washington, DC.

Engineering Technical Letter (ETL) 02-4 (2002). "Airblast Protection Polymer Retrofit of Unreinforced Concrete Masonry Walls," HQ AFCESA/CES, Department of the Air Force, Tyndall Air Force Base, Florida.

Facility and Component Explosive Damage Assessment Program (FACEDAP), May 1994, Version 1.2, Theory Manual, Technical Report 92-2, Department of the Army, Corps of Engineers, Omaha District, Omaha.

Fintel (1974), *Handbook of Concrete Engineering*, Van Nostrand Reinhold Company, New York.

Flanagan, R.D., and Bennett, R.M. (1999). "Arching of Masonry Infilled Frames: Comparison of Analytical Methods." *Pract. Per. Struct. Des. Constr.*, 4(3), 105-110.

Gabrielsen, B. L., Wilton, C. (1973). "Shock Tunnel Tests of Preloaded and Arched Wall Panels," Report #AD-764 263 prepared for the Defense Civil Preparedness Agency, URS Research Company, Distributed by National Technical Information Service, U.S. Department of Commerce, Springfield, VA.

Gabrielsen, B. L., and Wilton, C., Kaplan, K. (1975). "Response of Arching Walls and Debris from Interior Walls Caused by Blast Loading," Final Report prepared for the Defense Civil Preparedness Agency, Scientific Services, Inc., Redwood City, CA.

Govindjee, S., Kay, G. J., Simo, J.C. (1995). "Anisotropic modelling and numerical simulation of brittle damage in concrete." *International Journal for Numerical Methods in Engineering,* 38, 3611-3633.

Gurley, C.R., and Nichols, J.S.F. (December 1982), "Earthquake Strengthening of Old Masonry with Reference to the Auckland Ferry Building," *Bulletin of the New Zealand National Society for Earthquake Engineering*, 15(4), PP 199-215.

Hamid, A.A., and Drysdale, R.G. (January 1988). "Flexural tensile strength of concrete block masonry." Technical paper. *Journal of Structural Engineering*, 114(1). 50-66.

Hill S.I. (2003). *High rate tensile tests of 2003HSD001 polyurea*, Evaluation Report UDR-TR-2003-00130, Report Submitted to Air Force Research Laboratory, Tyndall, Florida, by Structural Test Group, University of Dayton Research Institute.

Hornbostel (1978), *Construction Manual*, John Wiley and Sons, New York.

Johnson, C.F., Slawsom, T.R., Cummins, T.K., Davis, J.L. (2005). *Concrete Masonry Unit Walls Retrofitted with Elastomeric Systems for Blast Loads*, U.S. Army Engineering Research and Development Center (ERDC), Vicksburg, MS.

Kariotis, J.C., Ewing, R.D., Johnson, A.W. (1985), "Predictions of Stability for Unreinforced Brick Masonry Walls Shaken by Earthquakes." Proc. 7th International Brick Masonry Conference, Melbourne, 2, 1175-1184.

Kariotis, J.C., Ewing, R.D., Johnson, A.W., Adham, S.A. (1985). "Methodology for Mitigation of Earthquake Hazards in Unreinforced Brick Masonry Buildings." Proc., 7th International Brick Masonry Conference, Melbourne, 2, 1339-1350.

Kiger, S., and Salim, H. (1999). "Use and Misuse of Structural Damping in Blast Response Calculations," *Concrete and Blast Effects, ACI Special Publication SP-175,* 121-130.

Knox, K. J., Hammons, M. I., Lewis, T. T., Porter, J. R. (2000). Polymer materials for structural retrofit. Force Protection Branch, Air Expeditionary Forces Technology Division, Air Force Research Laboratory, Tyndall AFB, Florida.

Krauthammer, T., and Otani, R.K. (1997). "Mesh, gravity and load effects on finite element simulations of blast loaded reinforced concrete structures." Technical paper. *Computers and Structures,* 63(6), 1113-1120.

Krieg, R.D. (1972). *A Simple Constitutive Description for Cellular Concrete*, Sandia National Laboratory.

Lane, J.W. (2003) "Modeling and Design of Explosion-Resistant Steel Stud Wall System," MSCE Thesis, University of Missouri, Columbia, Missouri.

La Mendola, L.L., Papia, M., Zingone, G. (1995). "Stability of Masonry Walls Subjected to Seismic Transverse Forces," *Journal of Structural Engineering*, ASCE, 121(11), 1581-1587.

Laursen, I. Harold (1978). *Structural Analysis*, 2nd Ed., McGraw Hill, New York.

Laursen, P. T., Seible, F., Hegemeir, G. A. (1995). "Seismic retrofit and repair of reinforced concrete with carbon overlays." *Rep. No. SSRP-95/01*, Structural Systems Research Project, University of California, San Diego, California.

Len Schwer (2001) Draft, Laboratory Tests for Characterizating Geomaterials, Livermore Software Technology Corporation, Livermore, California.

Lotfi, H.R., and Shing, P.B. (1994), "Interface Model Applied to Fracture of Masonry Structures," Journal of Structural Engineering, ASCE, 120(1), 63-80.

Lourenco, P.B., Mohamad, G., and Roman, H.R., (2005) "Mechanical Behavior Assessment of Concrete Masonry Prisms Under Compression," University of Coimbra. Department of Civil Engineering, 261-268.

LS-DYNA keyword user's manual: nonlinear dynamic analysis of structures. (1999). Livermore Software Technology Corporation, Livermore, California.

LS-DYNA keyword user's and Theoretical Manuals: Version 960 (2001). Livermore Software Technology Corporation, Livermore, California.

Manual of Steel Construction: 8th Ed. (1980), American Institute of Steel Construction, Chicago, Illinoise.

Martini, K. (1996a). "Research in the out-of-plane behavior of unreinforced masonry." Ancient Reconstruction of the Pompeii Forum. School of Architecture, University of Virginia, Charlottesville, Virginia.

Martini, K. (1996b). "Finite element studies in the two-way out-of-plane behavior of unreinforced masonry," Ancient Reconstruction of the Pompeii Forum. School of Architecture, University of Virginia, Charlottesville, Virginia.

Martini, K. (1997). "Research in the Out-of-Plane Behavior of Unreinforced Masonry," Department of Architecture and Civil Engineering, University of Virginia, Charlottesville, Virginia.

Mays, G.C., Hetherington, J.G., Rose, T.A. (1998). "Resistance-Deflection Functions for Concrete Wall Panels with Openings." *J. Struct. Eng*., 124(5), 579-587.

McDowell, E.L., McKee, K.E., ASCE, A.M., Sevin, E. (1956). "Arching Action Theory of Masonry Walls", Journal of Structural Division, Proceedings of ASCE, Paper 915, 1-18.

Melis, G. (2002). "Displacement-based seismic analysis for out of plane bending of unreinforced masonry walls," Masters Dissertation, European School Of Advanced Studies in Reduction Of Seismic Risk, Rose School.

Mendola, L.L., Papia, M., Zingone, G. (1995). "Stability of Masonry Walls Subjected to Seismic Transverse Forces," *Journal of Structural Engineering*, ASCE, 121(11), 1581-1587.

Methodology for Mitigation of Seismic Hazards in Existing Unreinforced Masonry Buildings (1984), ABK A Joint Venture, El Segundo, California.

Moradi, L. (2003). "Constitutive Properties for a Single Concrete Masonry Unit (CMU) Subjected to Blast," MS Project, University of Alabama at Birmingham, Birmingham, Alabama.

Moradi, L., Davidson, J., Dinan, R. (2007), "Resistance of Membrane Retrofit Concrete Masonry Walls to Lateral Pressure", Submitted.

Moradi, L., Davidson, J., Dinan, R. (2007), "Response of Membrane Retrofit Concrete Masonry Walls to Blast Pressure", Pending submission.

Moradi, L., Davidson, J., Dinan, R. (2007), "Resistance of Membrane Catcher Retrofit Concrete Masonry Walls to Lateral Blast Pressure", Pending submission.

Paulay, T., and Priestley, M.J.N. (1992), *Seismic Design of Reinforced Concrete and Masonry Buildings*, Wiley, New York.

Priestley, M.J.N. (1985). "Seismic Behaviour of Unreinforced Masonry Walls", Bulletin of the New Zealand National Society for Earthquake Engineering, 18(2), 191-205.

Priestley, M.J.N.; and Robinson, L.M. (1986). "Discussion: Seismic Behaviour of Unreinforced Masonry Walls," *Bulletin of the New Zealand National Society for Earthquake Engineering*, 19(1), 65-75.

Purcell, M. R., Muszynski, L. C., Taun, C. Y. (1995). Explosive field tests to evaluate composite reinforcement of concrete and masonry walls, Applied Research Associates, Inc., Gulf Coast Division, Tyndall AFB, Florida.

Randers-Pehrson, G. and Bannister, K.A. (March 1997). *Airblast loading model for DYNA2D and DYNA3D*, Army Research Laboratory, ARL-TR-1310.

Roark and Young (1975). *Formulas for Stress and Strains*, 5th Ed., McGraw Hill, New York.

Schwer, L. (2001), *Laboratory tests for characterizing geomaterials*, Livermore Software Technology Corporation, Livermore, California.

Seible, F., and Karbhari, V. M. (1996). "Seismic retrofit of bridge columns using advanced composite materials." Division of Structural Engineering, University of California, San Diego, La Jolla, California.

Seide, P. (1977). "Large deflection of rectangular membranes under uniform pressure." Technical paper. *International Journal of Nonlinear Mechanics*, 12, 397-406.

Shope, R., and Frank, R. (1998). Preliminary finite element analysis of masonry walls. Applied Research Associates, Inc., Raleigh, North Carolina.

Single-Degree-of-Freedom Blast Effects Design Spreadsheets (SBEDS) (2006), U.S. Army Corps of Engineers, Protective Design Center Technical Report, PDC-TR 06-02.

Single-Degree-of-Freedom Structural Response Limits for Antiterrorism Desig, (2006), U.S. Army Corps of Engineers, Protective Design Center Technical Report, PDC-TR 06-02.

Slawson, T.R. (1995). *Wall Response to Airblast Loads: The Wall Analysis Code (WAC)*, prepared for the U.S. Army ERDC, Vickburg, MS, Contract DACA39-95-C-0009, ARA-TR-95-5208.

Slawson, T. R., Coltharp, D. R., Dennis, S. T., Mosher, R. (1999). "Evaluation of anchored fabric retrofits for reducing masonry wall debris hazard." *Proc., 9th International Symposium on Interaction of the Effects of Munitions with Structures*, Berlin-Strausberg, Federal Republic of Germany.

Sudame, S. (2004), "Development of Computational Models and Input Sensitive Study of Polymer Reinforced Concrete Masonry Walls Subjected to Blast", MS Thesis, University of Alabama at Birmingham, Birmingham, Alabama.

Taun, C. Y., Muszynski, L. C., Dass, W. C. (1995). "Explosive test of an externally-reinforced multi-story concrete structure at Eglin AFB, FL," Applied Research Associates, Inc., Gulf Coast Division, Tyndall AFB, Florida.

Thornburg, D.L. (2004), "Evaluation of Elastomeric Polymer Used for External Reinforcement of Masonry Walls Subjected to Blast," MS Thesis, University of Alabama at Birmingham, Birmingham, Alabama.

Tropical Report 08, ABK Consultants (1984), "Methodology for Mitigation of Seismic Hazards in Existing Unreinforced Masonry Buildings", El Segundo, CA.

User's Guide for the Single-Degree-of-Freedom Blast Effects Design Spreadsheets (SBEDS) (2006), U.S. Army Corps of Engineers, Protective Design Center Technical Report, PDC-TR 06-02.

Wall response to airblast loads: the wall analysis code (WAC). (1995). U.S. Army Engineer Waterways Experiment Station, Vicksburg, Mississippi.

Weeks, J., Seible, F., Hegemeir, G., Priestly, M. J. N. (1994). The U.S.-TCCMAR full-scale five-story masonry research building test: part V – repair and retest. Rep. No. SSRP-94/05, Structural Systems Research Project, University of California, San Diego.

Wesevich, J. W., and Crawford, J. E. (1996). Candidate retrofit designs for increasing the blast resistance of conventional wall panels. Technical report, TR-96-32.1, Karagozian and Case, Glendale, California.

Whiting, W. D., and Coltharp, D. R. (1996). "Retrofit measures for conventional concrete masonry unit building subject to terrorist threat." U.S. Army Engineer Waterways Experiment Station, Vicksburg, Mississippi.

Yokel, F. Y. (1971). “Stability and Load Capacity of Members with no Tensile Strength.” *Proc., American Society of Civil Engineers*, Journal of the Structural Division ST 7, 1913 – 1926.

Yokel, F. Y., and Dikkers, R. D. (1971). “Strength of load bearing masonry walls.” *Proc., American Society of Civil Engineers*, Journal of the Structural Division, 97, 1593 – 1609.

W. F. Chen (1982). *Plasticity in Reinforced Concrete*, McGraw-Hill, New York.